Spintronic materials and device
Micro-magnetics and Spintronics

Shang-Fan Lee (李尚凡)
Institute of Physics, Academia Sinica

J. J. Liang (梁君致)
Dept. of Physics, Fu Jen University

D. S. Hung(洪東興)
Dept. of Info. Telecom. Eng.
Ming Chuan University

S. Y. Huang (黃斯衍), C. Yu (于 淳),
T. W. Chiang (江典蔚), L. K. Lin (林呂圭), L. J. Chang (張良君), Faris B.
Y. C. Chiu (邱昱哲), Y. H. Chiu (邱亦欣)

Intrinsic spin-dependent thermal transport

S. Y. Huang, W. G. Wang, S. F. Lee, J. Kwo, and C. L. Chien

PRL **107**, 216604 (2011)

Supported by the US NSF grant DMR 05-20491 and the Taiwan NSC grant 99-2911-I-007-510

outline

- Giant Magnetoresistance, Tunneling Magnetoresistance
- Spin Transfer Torque
- Micro and nano Magnetics
- Pure Spin current (no net charge current)
  - Spin Hall, Inverse Spin Hall effects
  - Spin Pumping effect
  - Spin Seebeck effect

Spintronics :

Electronics with electron spin as an extra degree of freedom
Generate, inject, process, and detect spin currents

•Generation: ferromagnetic materials, spin Hall effect, spin pumping effect etc.

•Injection: interfaces, heterogeneous structures, tunnel junctions

•Process: spin transfer torque

•Detection: Giant Magnetoresistance, Tunneling MR

科學月刊 **38**, 898 (2007).
物理雙月刊 **30**, 116 (2008).
科學人 **87**, 82 (2009).

鐵磁性元素 : 鐵 Fe, 鈷 Co, 鎳 Ni, 釓 Gd, 鏑 Dy,
錳 Mn, 鈀 Pd ??

Elements with ferromagnetic properties

合金, alloys

錳氧化物 MnOx

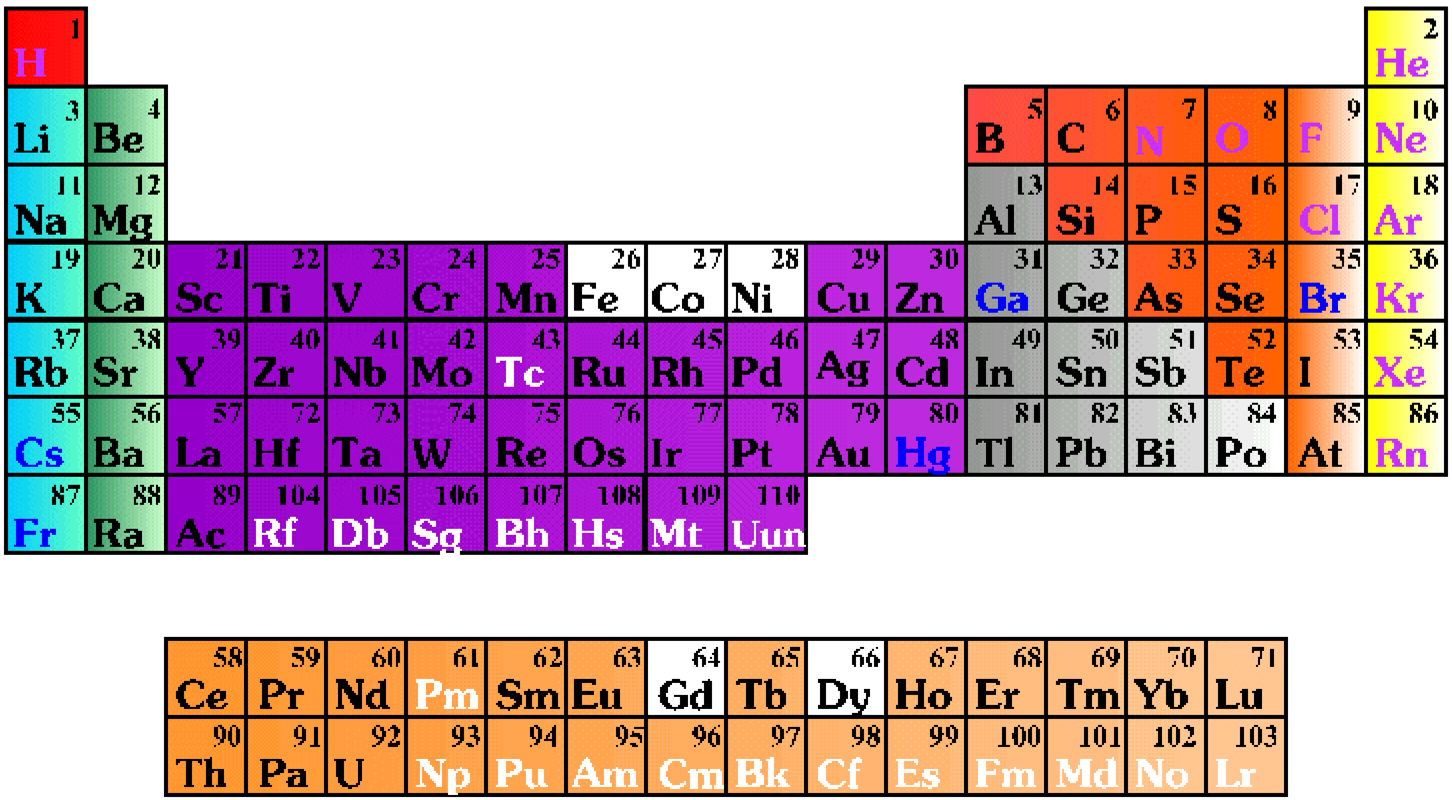

Solar system

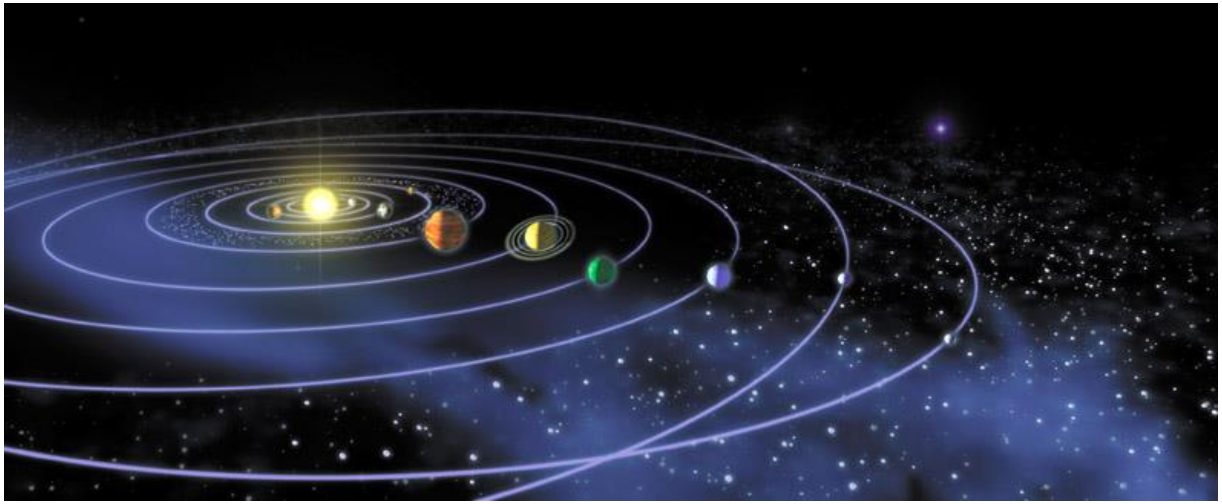

s, p electron orbital

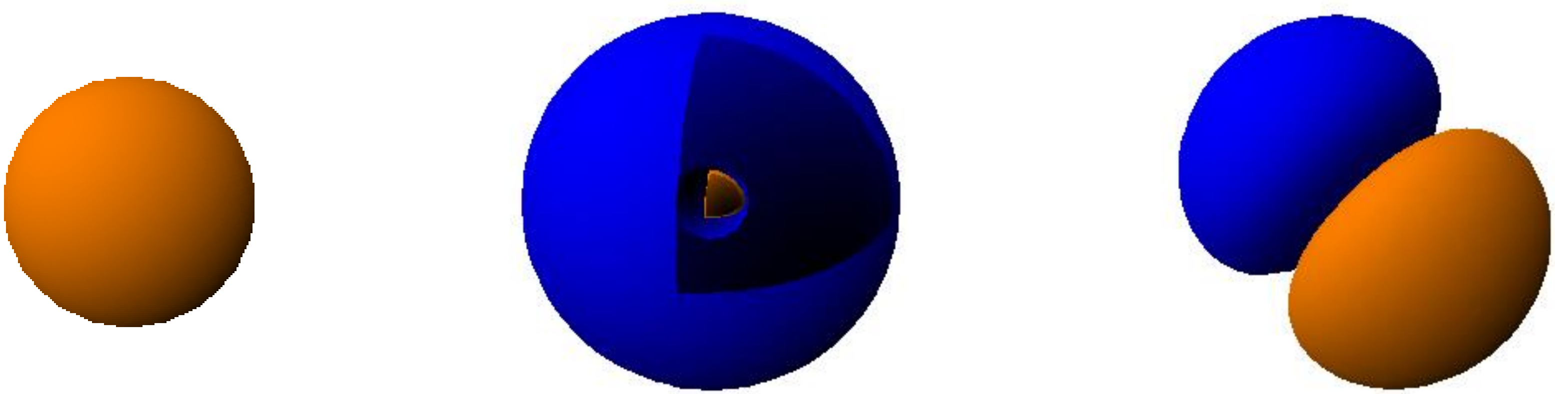

Orbital viewer

3d transition metals:

Mn atom has 5 d↑ electrons

Bulk Mn is NOT magnetic.

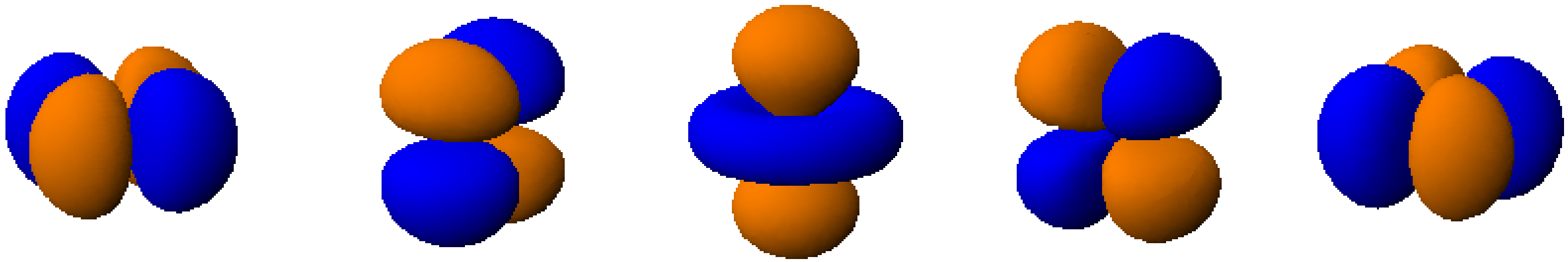

3d electron distribution in real space

Co atom has 5 d↑electrons and 2 d↓ electrons

Bulk Co is magnetic.

Stoner criterion for ferromagnetism:

$I\,N(E_F) > 1$, I is the Stoner exchange parameter and $N(E_F)$ is the density of states at the Fermi energy.

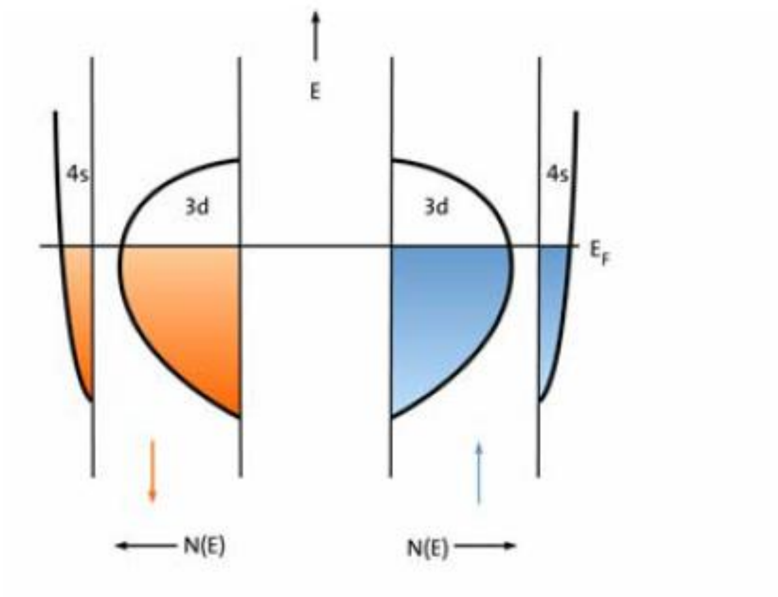

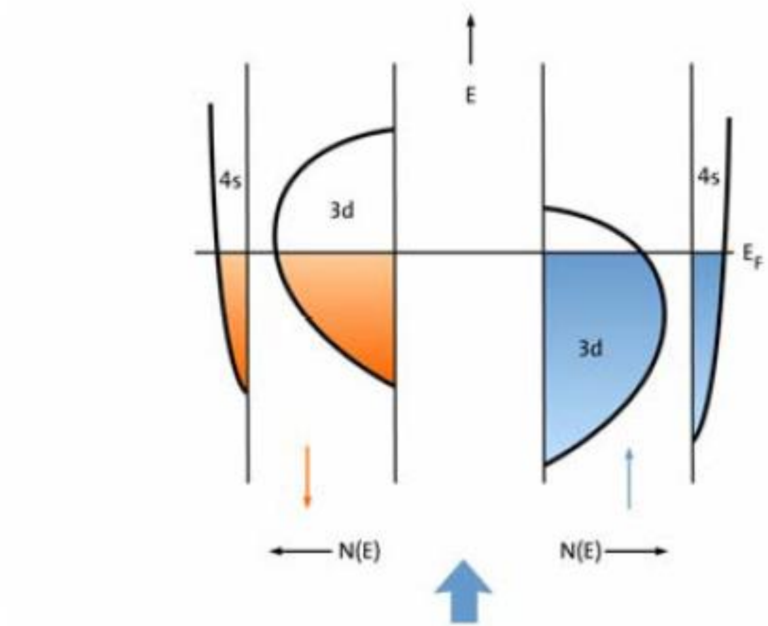

For the non-magnetic state there are identical density of states for the two spins.

For a ferromagnetic state, N↑ > N↓. The polarization is indicated by the thick blue arrow.

Schematic plot for the energy band structure of 3d transition metals.

RKKY (*Ruderman-Kittel-Kasuya-Yosida*) interaction

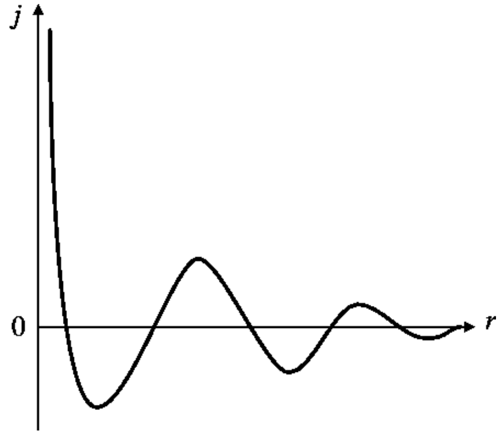

coupling coefficient

$$j\left(\boldsymbol{R}_l - \boldsymbol{R}_{l'}\right) = 9\pi \left(\frac{j^2}{\epsilon_F}\right) F\left(2k_F\left|\boldsymbol{R}_l - \boldsymbol{R}_{l'}\right|\right)$$

$$F(x) = \frac{x\cos x - \sin x}{x^4}$$

Magnetic coupling in superlattices

- Long-range incommensurate magnetic order in a Dy-Y multilayer

  M. B. Salamon, Shantanu Sinha, J. J. Rhyne, J. E. Cunningham, Ross W. Erwin, Julie Borchers, and C. P. Flynn, Phys. Rev. Lett. **56**, 259 - 262 (1986)

- Observation of a Magnetic Antiphase Domain Structure with Long-Range Order in a Synthetic Gd-Y Superlattice

  C. F. Majkrzak, J. W. Cable, J. Kwo, M. Hong, D. B. McWhan, Y. Yafet, and J. V. Waszczak,C. Vettier, Phys. Rev. Lett. **56**, 2700 - 2703 (1986)

- Layered Magnetic Structures: Evidence for Antiferromagnetic Coupling of Fe Layers across Cr Interlayers

  P. Grünberg, R. Schreiber, Y. Pang, M. B. Brodsky, and H. Sowers, Phys. Rev. Lett. **57**, 2442 - 2445 (1986)

Magnetic coupling in multilayers

- **Long-range incommensurate magnetic order in a Dy-Y multilayer**
  M. B. Salamon, Shantanu Sinha, J. J. Rhyne, J. E. Cunningham, Ross W. Erwin, Julie Borchers, and C. P. Flynn, Phys. Rev. Lett. 56, 259 - 262 (1986)
- **Observation of a Magnetic Antiphase Domain Structure with Long- Range Order in a Synthetic Gd-Y Superlattice**
  C. F. Majkrzak, J. W. Cable, J. Kwo, M. Hong, D. B. McWhan, Y. Yafet, and J. V. Waszczak,C. Vettier, Phys. Rev. Lett. 56, 2700 - 2703 (1986)
- **Layered Magnetic Structures: Evidence for Antiferromagnetic Coupling of Fe Layers across Cr Interlayers**
  P. Grünberg, R. Schreiber, Y. Pang, M. B. Brodsky, and H. Sowers, Phys. Rev. Lett. 57, 2442 - 2445 (1986)

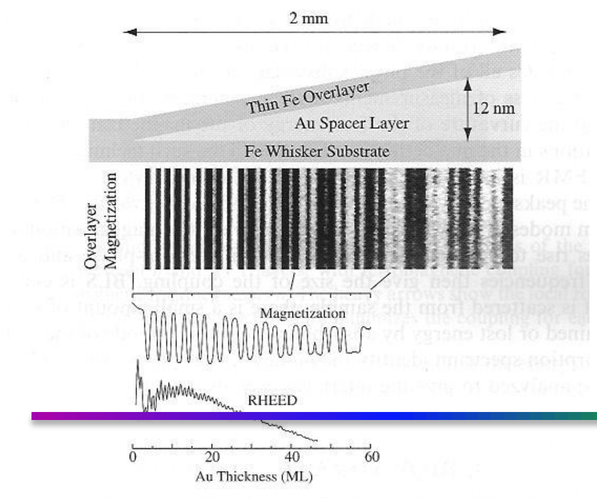

Coupling in wedge-shaped

Fe/Cr/Fe

Fe/Au/Fe

Fe/Ag/Fe

J. Unguris, R. J. Celotta, and D. T. Pierce

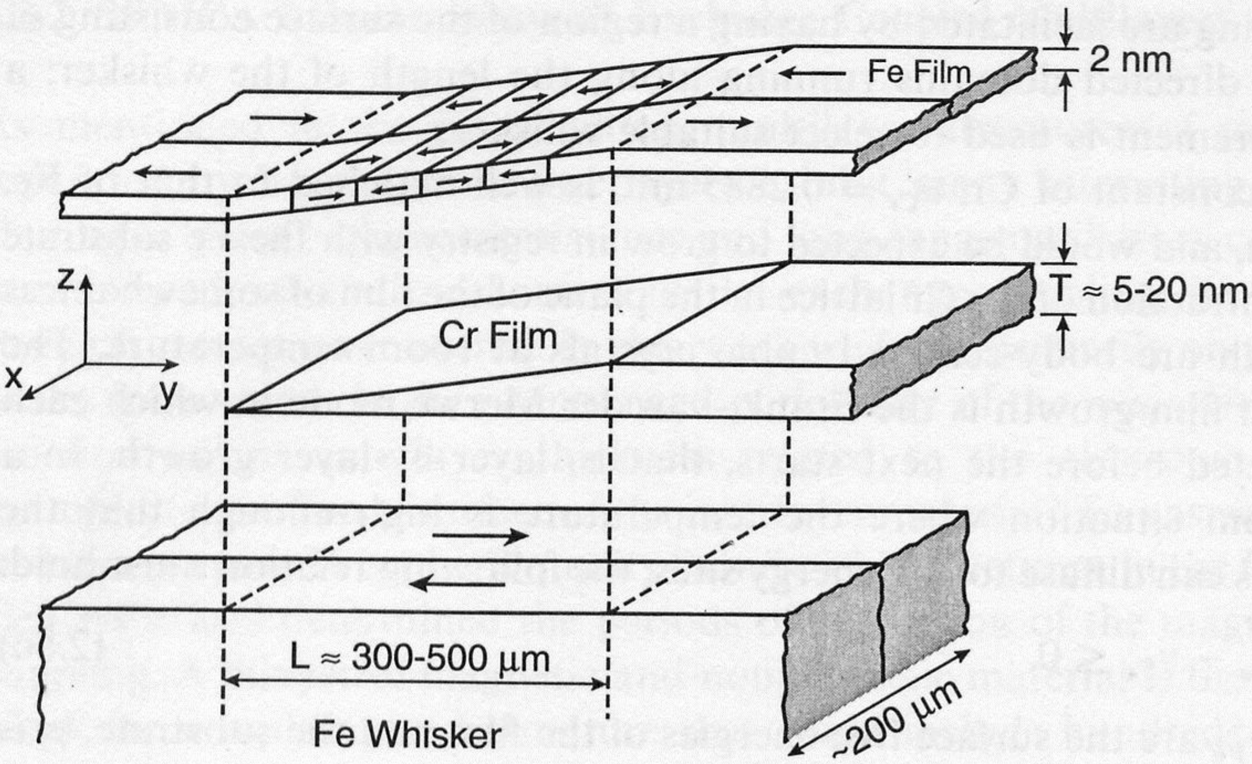

Fig. 2.41. A schematic expanded view of the sample structure showing the Fe(0 0 1) single-crystal whisker substrate, the evaporated Cr wedge, and the Fe overlayer. The arrows in the Fe show the magnetization direction in each domain. The *z*-scale is expanded approximately 5000 times. (From [2.206])

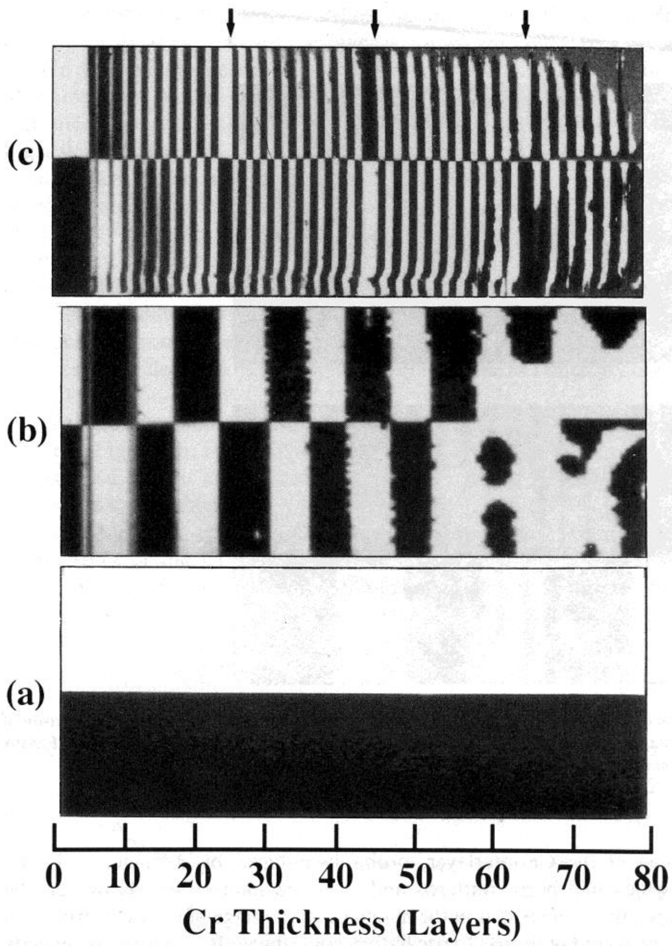

Fig. 2.43. SEMPA image of the magnetization M_y (axes as in Fig. 2.41) showing domains in (**a**) the clean Fe whisker, (**b**) the Fe layer covering the Cr spacer layer evaporated at 30 °C, and (**c**) the Fe layer covering a Cr spacer evaporated on the Fe whisker held at 350 °C. The scale at the bottom shows the increase in the thickness of the Cr wedge in (**b**) and (**c**). The arrows at the top of (**c**) indicate the Cr thicknesses where there are phase slips. The region of the whisker imaged is about 0.5 mm long

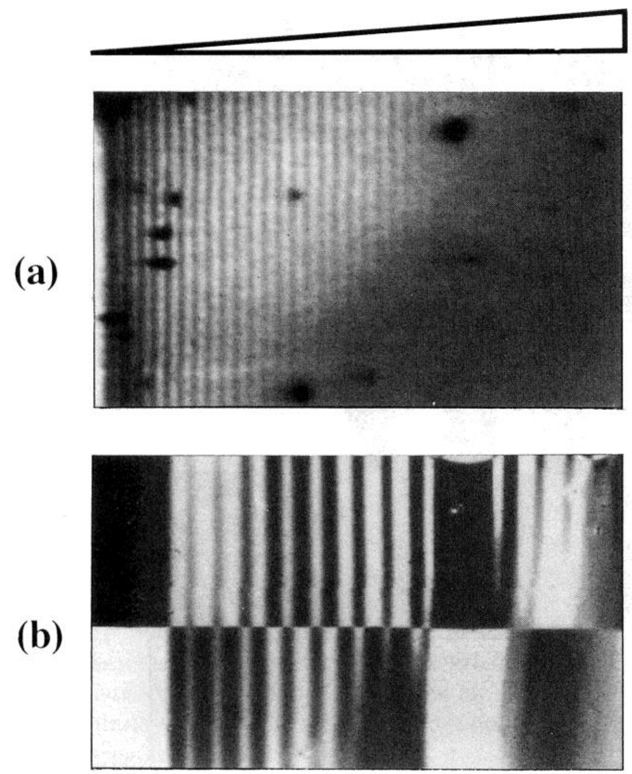

Fig. 2.44. The effect of roughness on the inertlayer exchange coupling is shown by a comparison of (**a**) the oscillations of the RHEED intensity along the bare Cr wedge with (**b**) the SEMPA magnetization image over the same part of the wedge

Oscillatory magnetic coupling in multilayers

Ru interlayer has the largest coupling strength

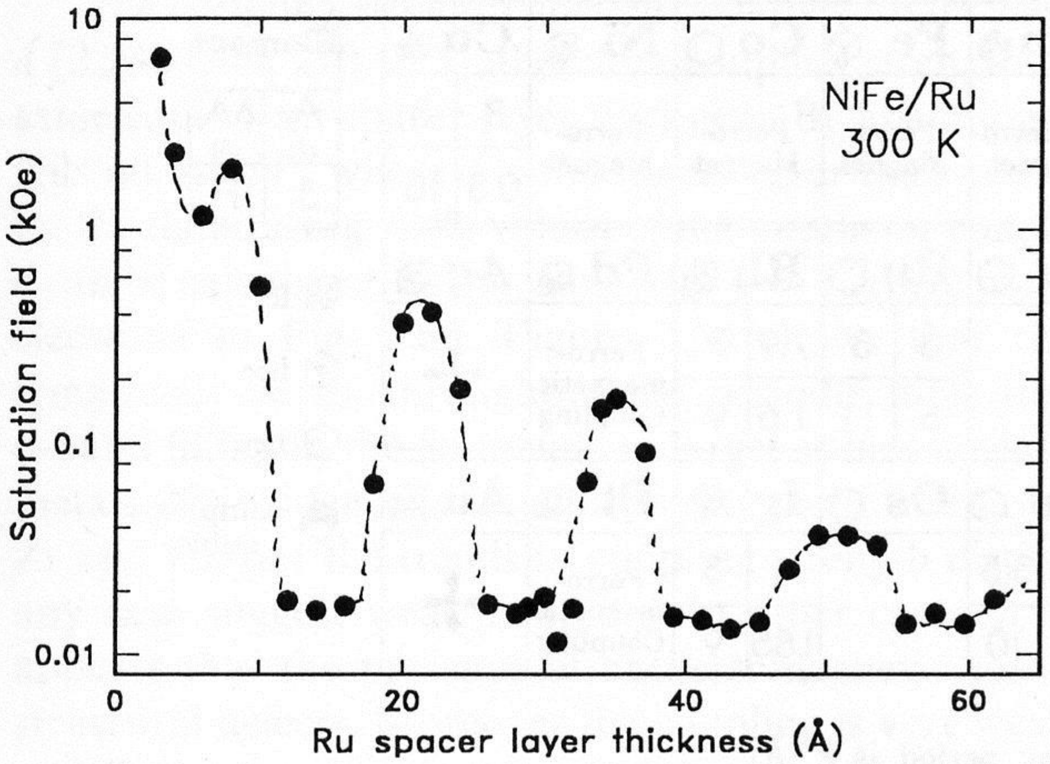

Fig. 2.58. Dependence of saturation field on Ru spacer layer thickness for several series of $Ni_{81}Fe_{19}$/Ru multilayers with structure, 100 Å Ru/[30 Å $Ni_{81}Fe_{19}/Ru(t_{Ru})]_{20}$, where the topmost Ru layer thickness is adjusted to be $\simeq$25 Å for all samples

Spin-dependent conduction in Ferromagnetic metals (Two-current model)

First suggested by Mott (1936)
Experimentally confirmed by I. A. Campbell and A. Fert (~1970)

At low temperature

$$\rho = \frac{\rho_{\uparrow}\rho_{\downarrow}}{\rho_{\uparrow} + \rho_{\downarrow}}$$

At high temperature

$$\rho = \frac{\rho_{\uparrow}\rho_{\downarrow} + \rho_{\uparrow\downarrow}(\rho_{\uparrow} + \rho_{\downarrow})}{\rho_{\uparrow} + \rho_{\downarrow} + 4\rho_{\uparrow\downarrow}}$$

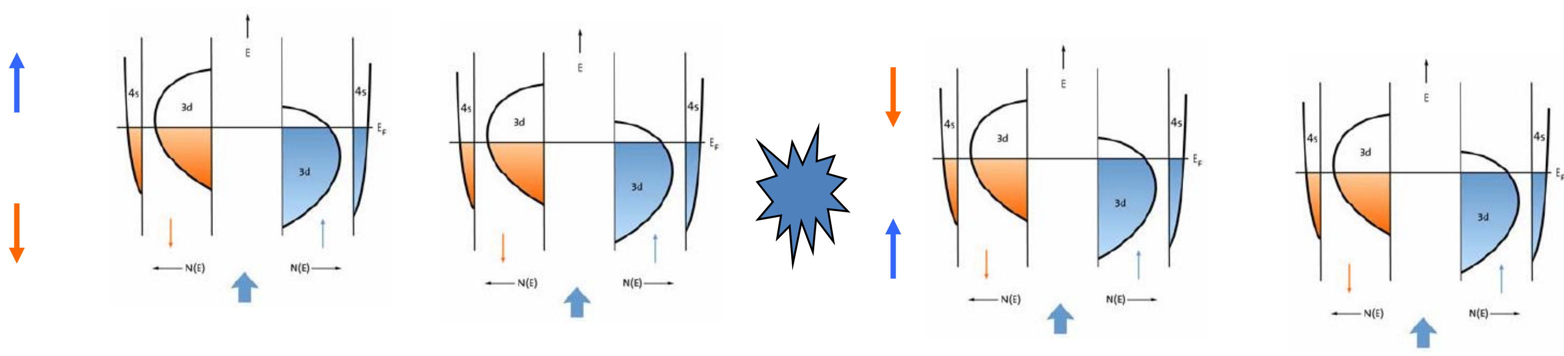

Spin mixing effect equalizes two currents

Two Current Model

***s* electrons carry the electric current**

resistivity (spin-dependent *s* → *d* scattering)

$$R^{s} = \mathrm{const.}\ N_d^{s}$$

number of empty *d* states

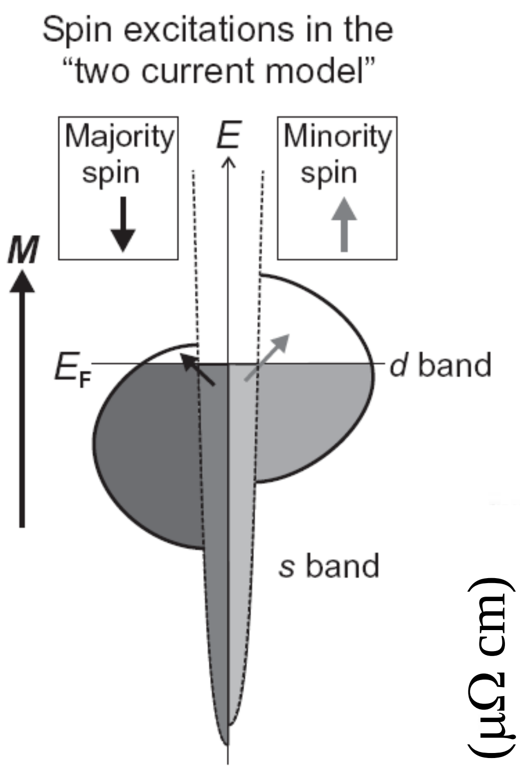

spin selective scattering

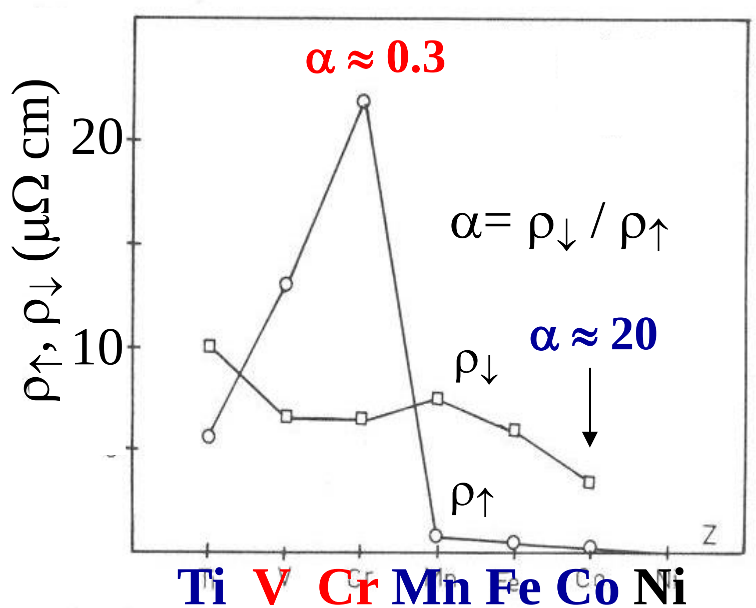

element	$N_h^{d\ a}$	$\lvert \boldsymbol{m} \rvert$ $[\mu_B]$	$R^{\ b}$ $[\Omega\,\mathrm{m}]$
Fe (bcc)	3.90	2.216	9.71×10^{-8}
Co (hcp)	2.80	1.715	6.25×10^{-8}
Ni (fcc)	1.75	0.616	6.84×10^{-8}
Cu (fcc)	0.50	–	1.68×10^{-8}

A. Fert, I.A. Campbell, PRL **21**, 1190 (1968)

outline

- Giant Magnetoresistance, Tunneling Magnetoresistance
- Spin Transfer Torque
- Micro and nano Magnetics
- Pure Spin current (no net charge current)
    - Spin Hall, Inverse Spin Hall effects
    - Spin Pumping effect
    - Spin Seebeck effect

2007 Nobel prize in Physics

2007年諾貝爾物理獎得主 左 亞伯・費爾(Albert Fert)與右彼得・葛倫貝格(Peter Grünberg)

(圖片資料來源：Copyright © Nobel Web AB 2007/ Photo: Hans Mehlin)

Giant Magnetoresistance
Tunneling Magnetoresistance

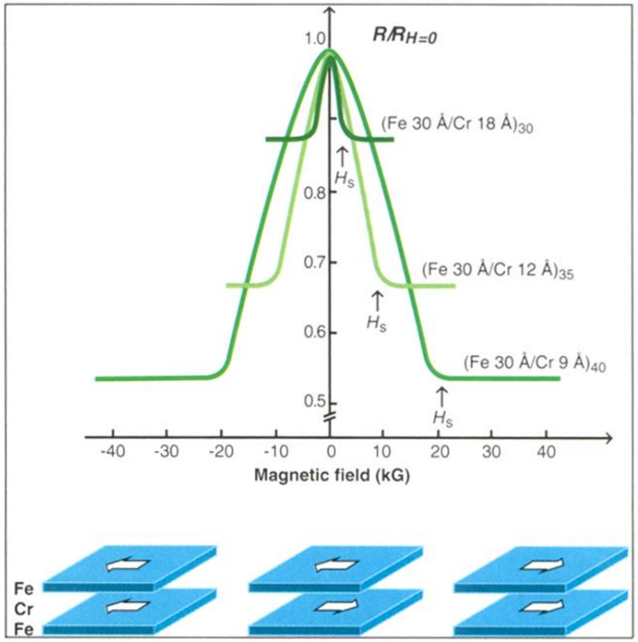

Discovery of Giant MR -- Two-current model combines with magnetic coupling in multilayers

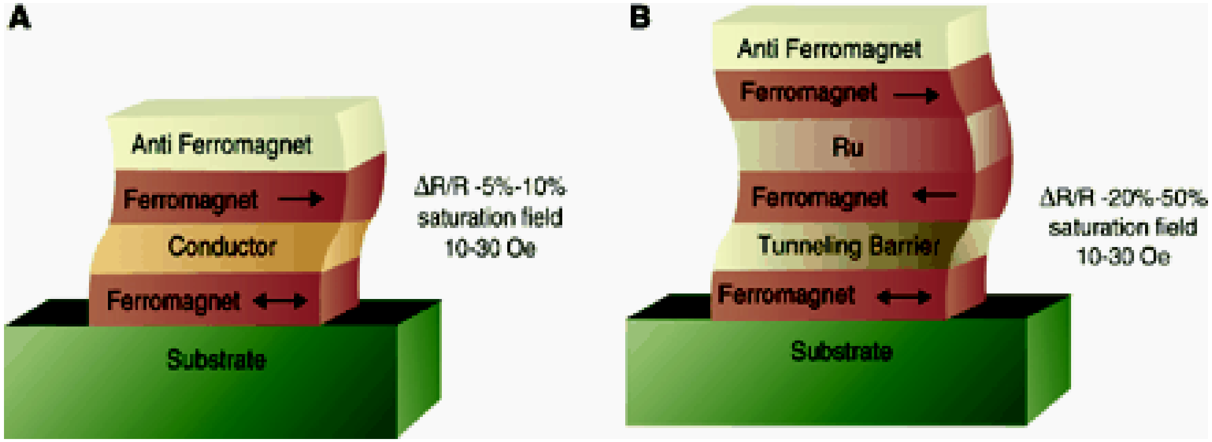

Spin-dependent transport structures. (A) Spin valve. (B) Magnetic tunnel junction. (from Science)

Moodera's group, PRL **74**, 3273 (1995)

Fert's group, PRL **61**, 2472 (1988)

Miyazaki's group, JMMM **139**, L231(1995)

Transport geometry

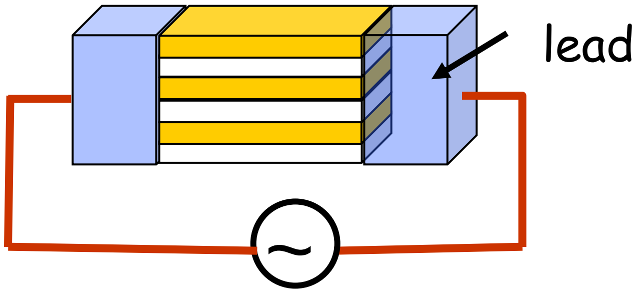

CIP geometry

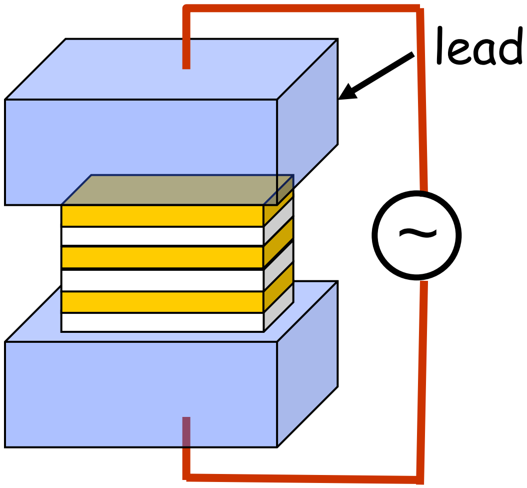

CPP geometry

- In metallic multilayers, CIP resistance can be measured easily, CPP resistance needs special techniques.
- From CPP resistance in metallic multilayers, one can measure interface resistances, spin diffusion lengths, and polarization in ferromagnetic materials, etc.

Valet and Fert model of (CPP-)GMR

Based on the Boltzmann equation

A semi-classical model with spin taken into consideration

$$j_{+(-)} = \frac{1}{e\rho_{+(-)}} \frac{\partial \mu_{+(-)}}{\partial x}$$

$$j_+ + j_- = j_e$$

$$\frac{\partial (j_+ - j_-)}{\partial x} = \frac{2eN(E_F)\Delta\mu}{\tau_{sf}}$$

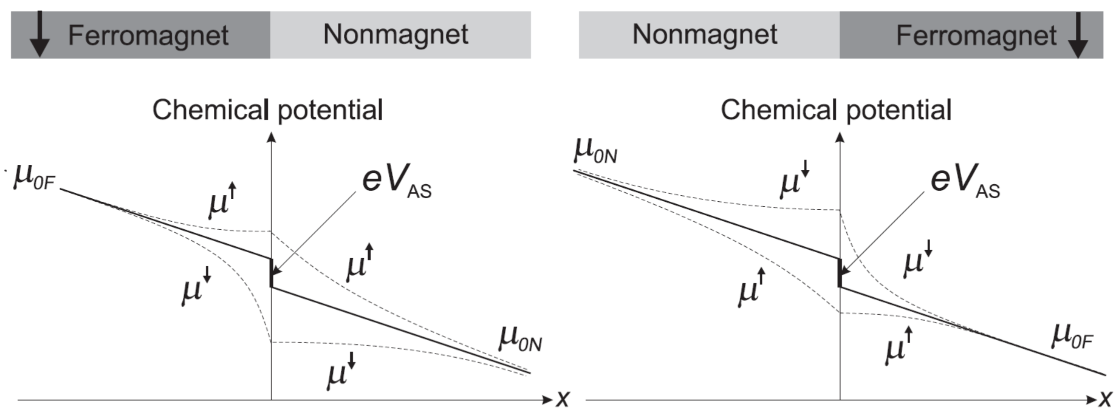

$$\frac{\partial^2 \mu_{+(-)}}{\partial z^2} = \frac{\mu_{+(-)}}{l_{sf}^2} \qquad l_{sf}^F = \left[\lambda_{sf}^F / 3(\lambda_\uparrow^{-1} + \lambda_\downarrow^{-1})\right]^{1/2}, \quad l_{sf}^N = \left[\lambda_{sf}^N \lambda / 6\right]^{1/2}$$

Spin accumulation at the interface is important

Spin diffusion length, instead of mean free path, is the dominant physical length scale

Spin valve –
a sandwich structure
with a free ferromagnetic layer (F) and a fixed F layer pinned by an antiferromagnetic (AF) layer

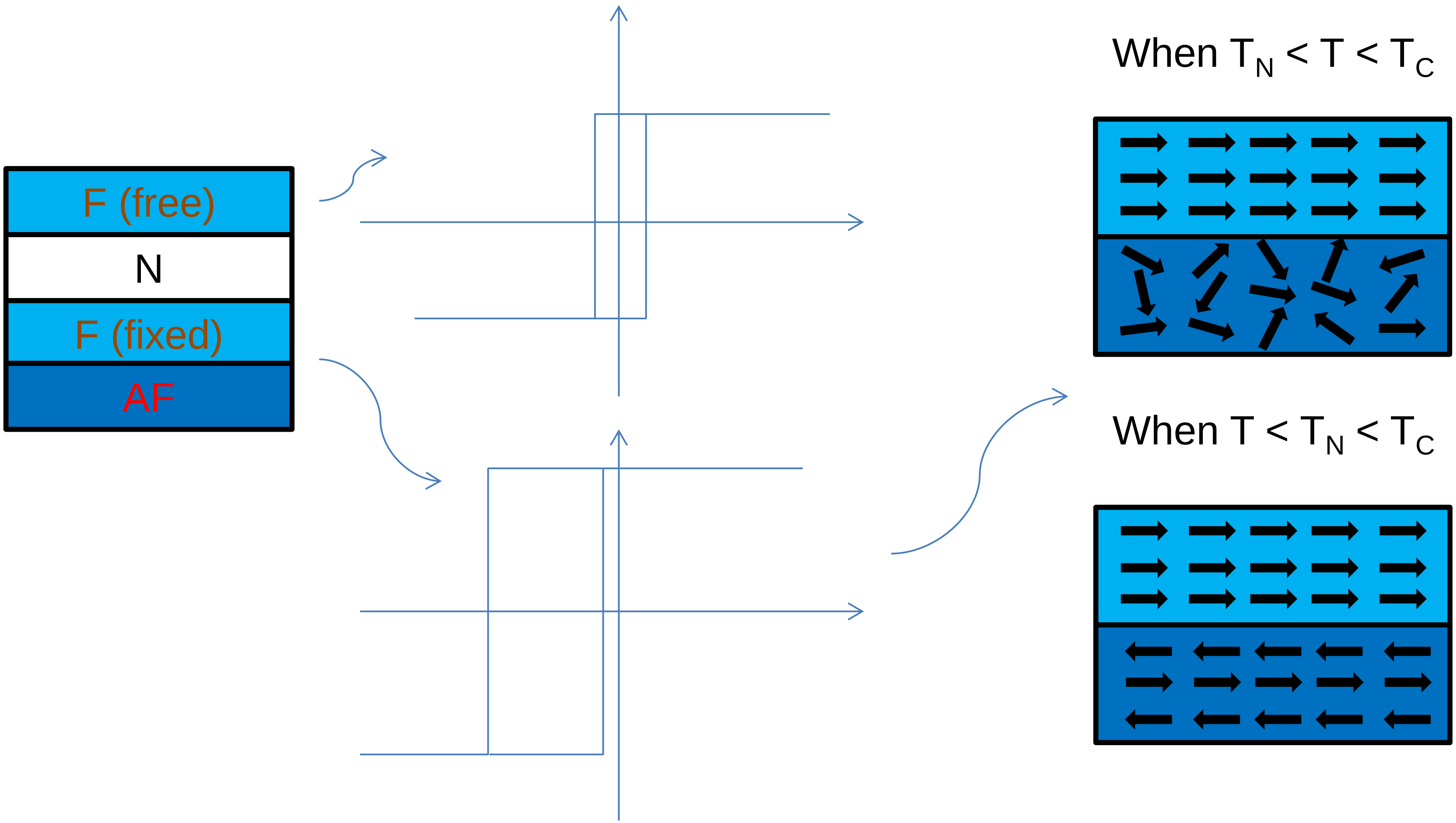

outline

- Giant Magnetoresistance, Tunneling Magnetoresistance
- Spin Transfer Torque
- Micro and nano Magnetics
- Pure Spin current (no net charge current)
    - Spin Hall, Inverse Spin Hall effects
    - Spin Pumping effect
    - Spin Seebeck effect

Spin Transfer Torque

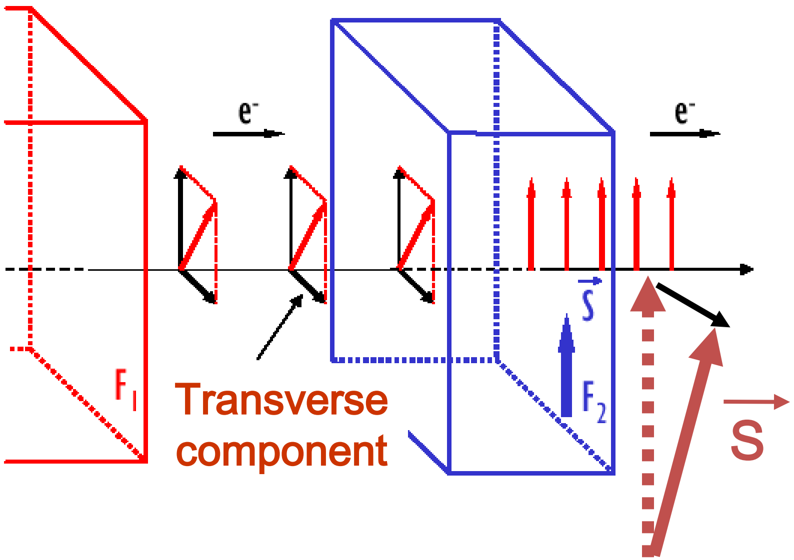

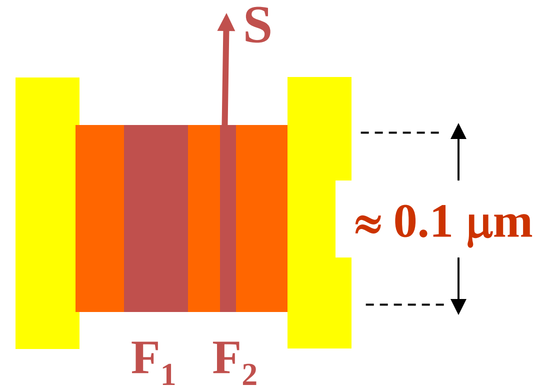

In a trilayer, current direction determines the relative orientation of F_1 and F_2

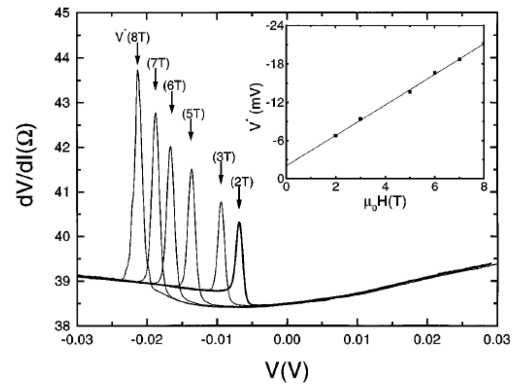

FIG. 1. The point contact $dV/dI(V)$ spectra for a series of magnetic fields (2, 3, 5, 6, 7, and 8 T) revealing an upward step and a corresponding peak in dV/dI at a certain negative bias voltage $V^*(H)$. The inset shows that $V^*(H)$ increases linearly with the applied magnetic field H.

Tsoi et al. PRL **61**, 2472 (1998)

The transverse spin component is lost by the conduction electrons, transferred to the global spin of the layer $\vec{S}$

$$\dot{S}_{1,2} = (I_e g/e)\hat{s}_{1,2} \times (\hat{s}_1 \times \hat{s}_2)$$

Slonczewski JMMM **159**, L1 (1996)

Modified Landau-Lifshitz-Gilbert (LLG) equation

$$\frac{dm}{dt} = -\gamma m \times H_{eff} + \alpha m \times \frac{dm}{dt} + \frac{\gamma \hbar P I}{2e\mu_0 M_S V}(m \times \sigma \times m)$$

Experimantally determined current density ~10^{10}-10^{12}A/m^2

Spin Transfer Torque

Landau-Lifshitz-Gilbert equation with Spin Transfer Torque terms

Current induced domain wall motion

Passing spin polarized current from Domain A to Domain B⇒B switches

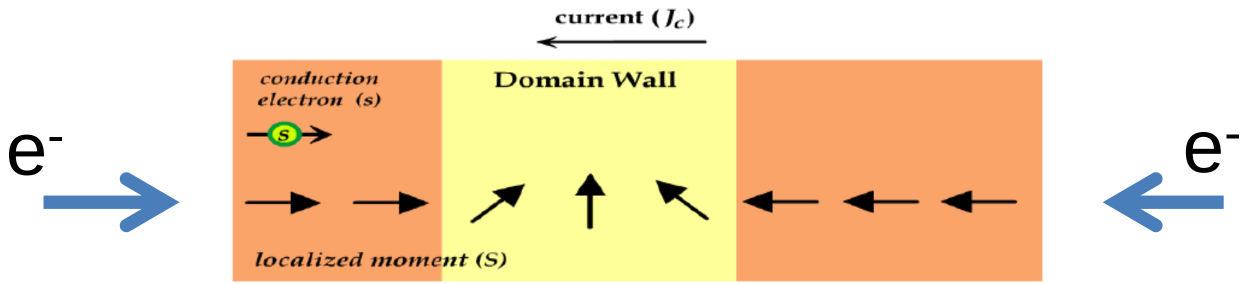

Domain A **Domain B**

$$\frac{\partial \vec{M}}{\partial t} = -\gamma \vec{M} \times \vec{H}_{eff} + \frac{\alpha}{M_s} \vec{M} \times \frac{\partial \vec{M}}{\partial t} + \vec{\mathrm{T}}_{STT}$$

Berger, *JAP* **55**, 1954 (1984)
Tatara *et. al*., *PRL* **92**, 086601 (2004)
Zhang *et. al.*, *PRL* **97**, 127204 (2004)
Thiaville *et. al.*, *Europhys. Lett*. **69**, 990 (2005)
Stiles *et. al.*, *PRB* **75**, 214423 (2007)

Spin Transfer Torque

Landau-Lifshitz-Gilbert equation with Spin Transfer Torque terms

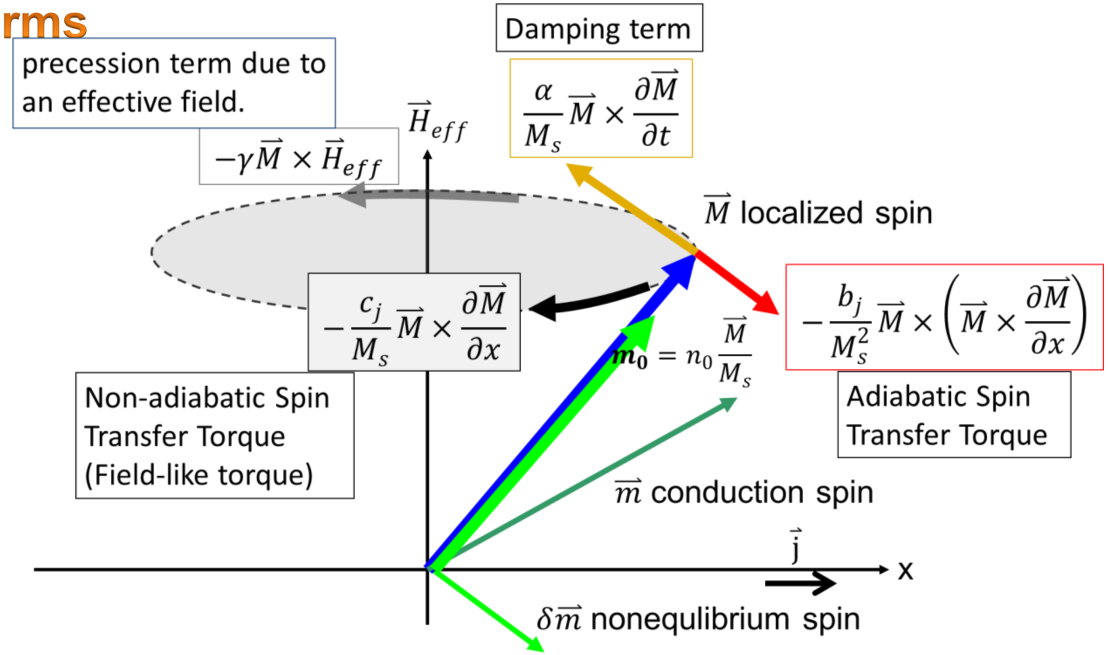

Damping term

Adiabatic Spin Transfer Torque

$$\frac{\partial\vec{M}}{\partial t} = \underline{-\gamma\vec{M}\times\vec{H}_{eff}} + \frac{\alpha}{M_s}\vec{M}\times\frac{\partial\vec{M}}{\partial t} - \frac{b_j}{M_s^2}\vec{M}\times\left(\vec{M}\times\frac{\partial\vec{M}}{\partial x}\right) - \underline{\frac{c_j}{M_s}\vec{M}\times\frac{\partial\vec{M}}{\partial x}} \qquad (2.17$$

Precessional term due to an effective field.

Non-adiabatic Spin Transfer Torque

Industrial applications

Read head in hard drives

MRAM

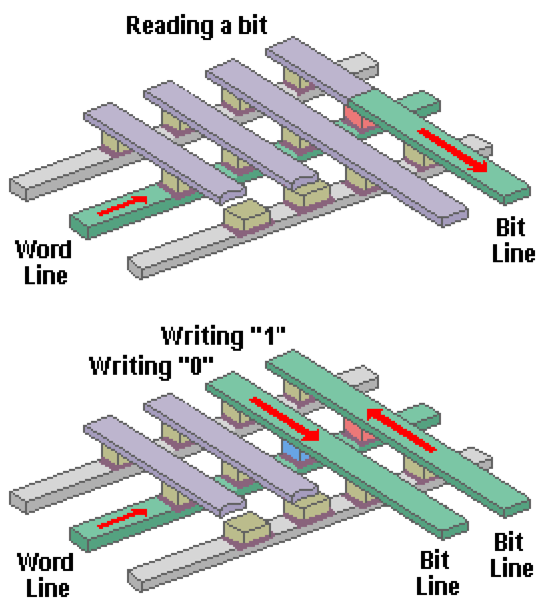

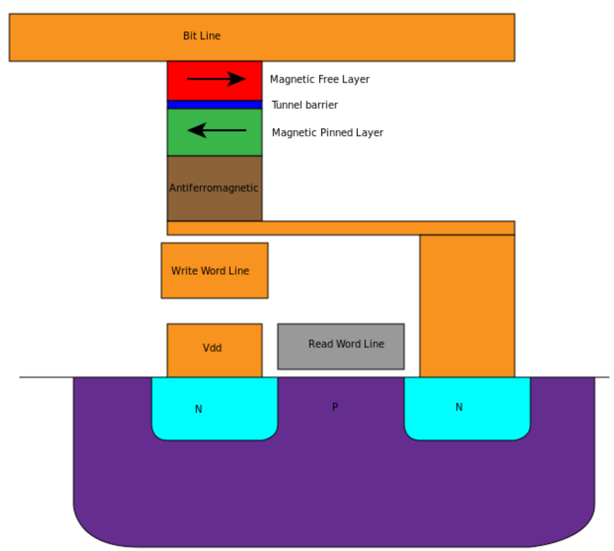

Application of Spin Transfer Torque

Magnetic Domain-Wall Racetrack Memory

Dr. Stuart S. P. Parkin Science **320**, 190 (2008)

A novel three-dimensional spintronic storage class memory

Magnetic nanowires: information stored in the domain walls

- Immense storage capacity of a hard disk drive

- High reliability and performance of solid state memory (DRAM, FLASH, SRAM...)

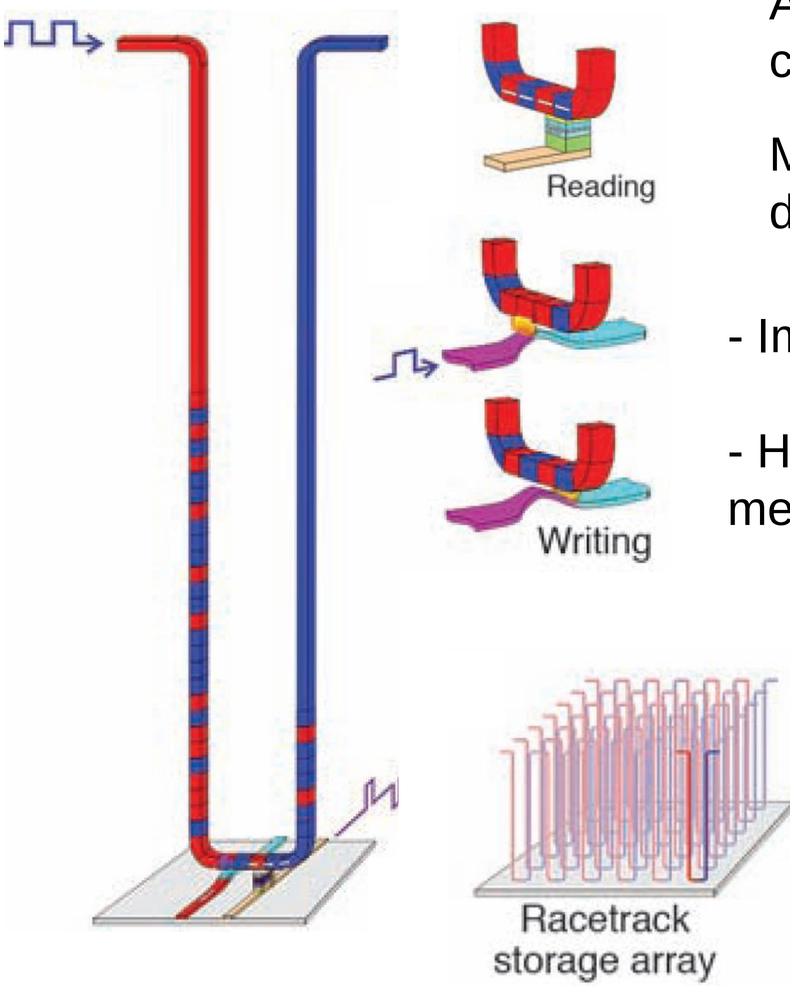

→ **Understanding of current induced domain wall (DW) motion**

Application of Spin Transfer Torque

Domain Wall Structures in Permalloy Nanowires

(a)

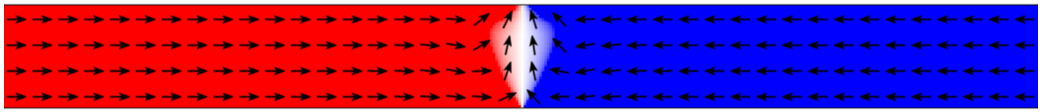

Transvers DW

(b)

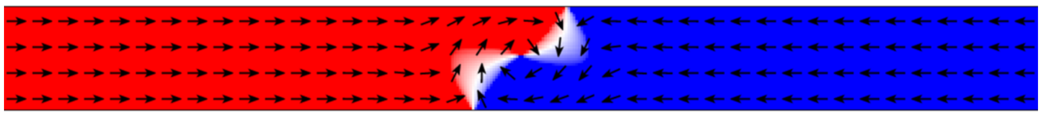

Vortex DW

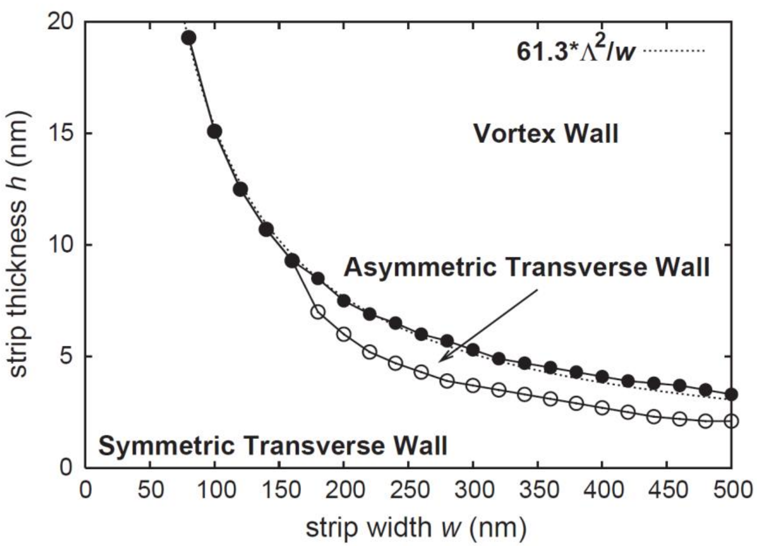

J. Magn. Magn. Mater. **290**, 750 (2005)

DW traps

protrusion

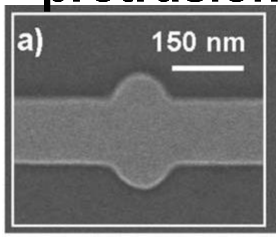

notch

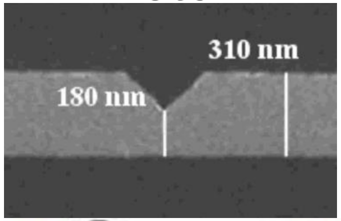

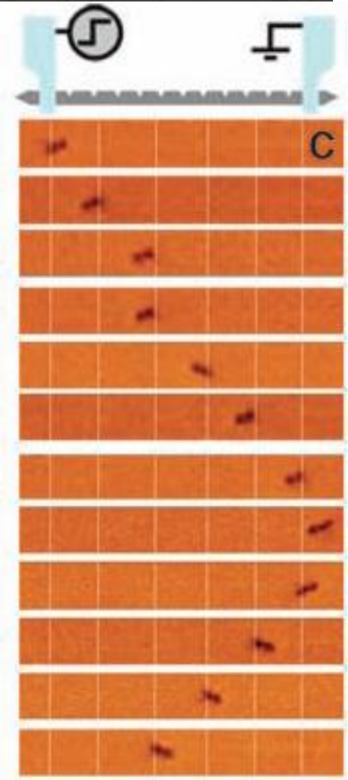

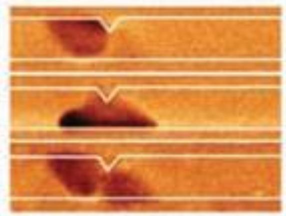

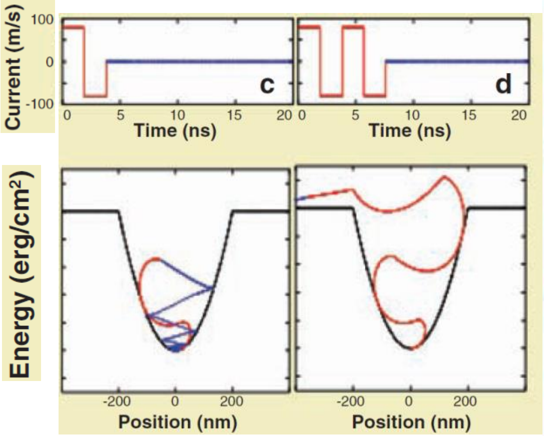

Application of Spin Transfer Torque

DW Oscillators

$j_W < j_a < j_{dep}$

e^- → ← H

Walker breackdown

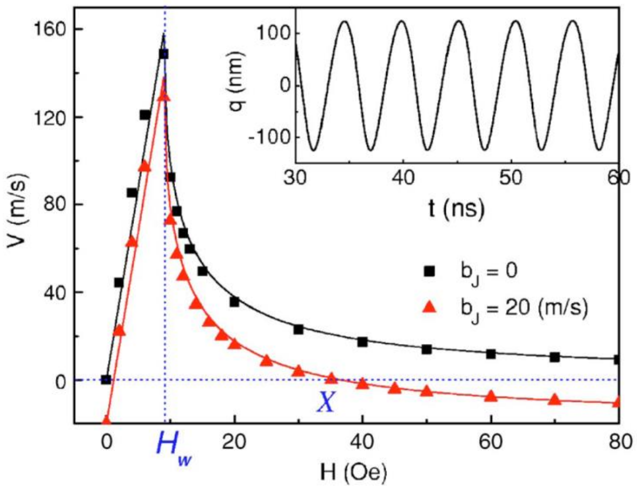

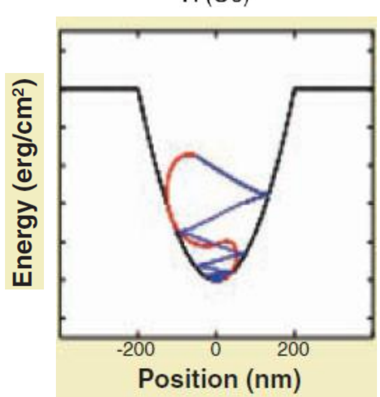

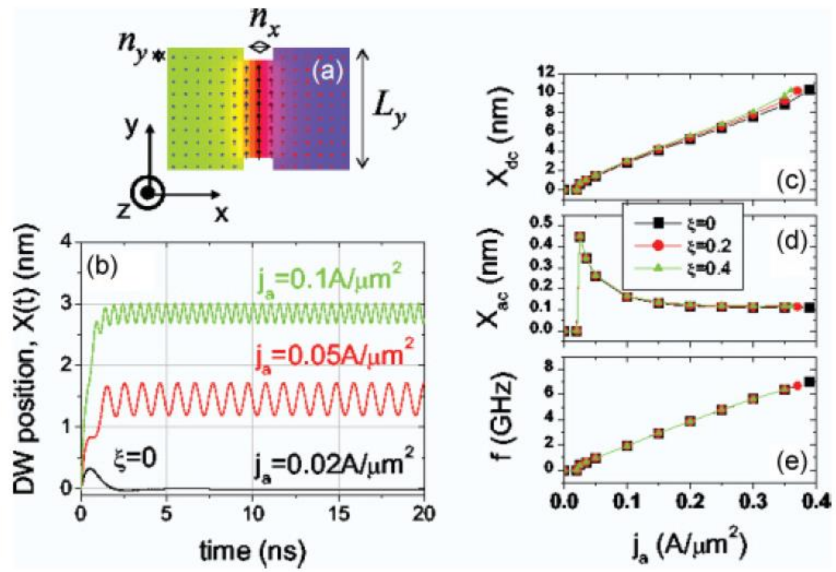

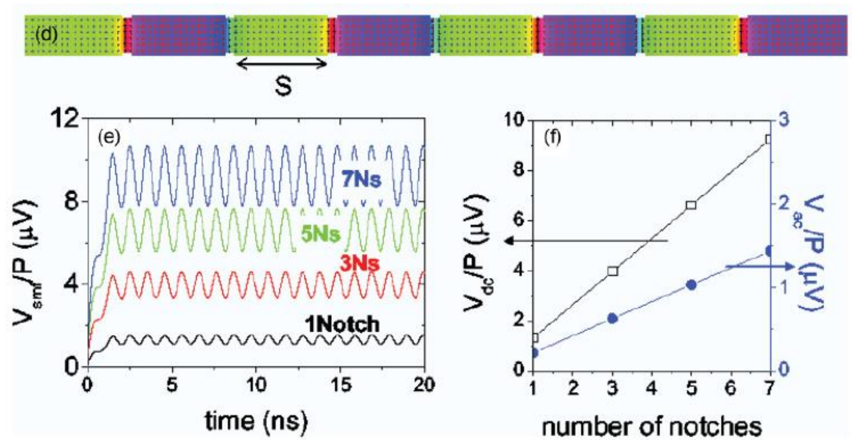

PHYSICAL REVIEW B **83**, 174444 (2011)
Appl. Phys. Lett. **90**, 142508 (2007)

Application of Spin Transfer Torque

AC Current-Induced DW Resonance

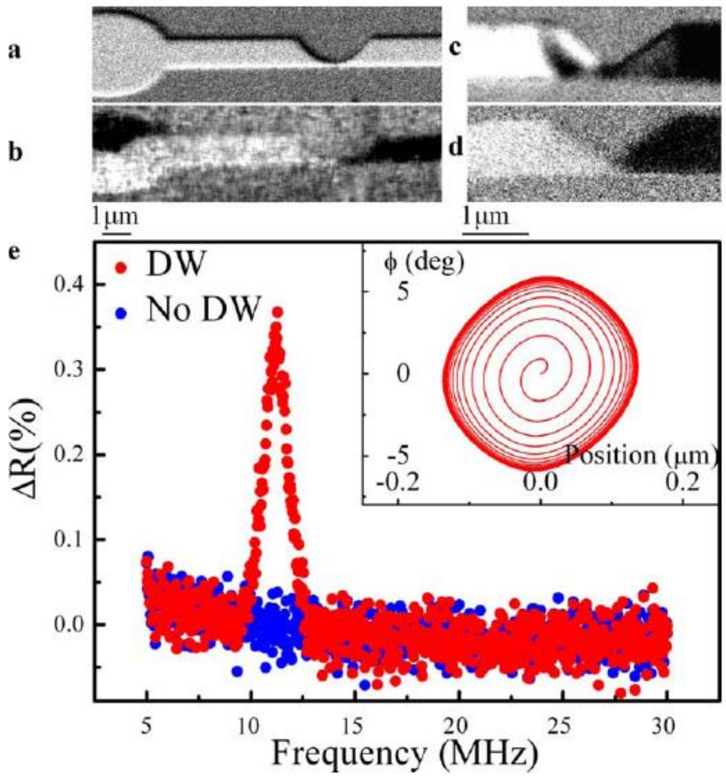

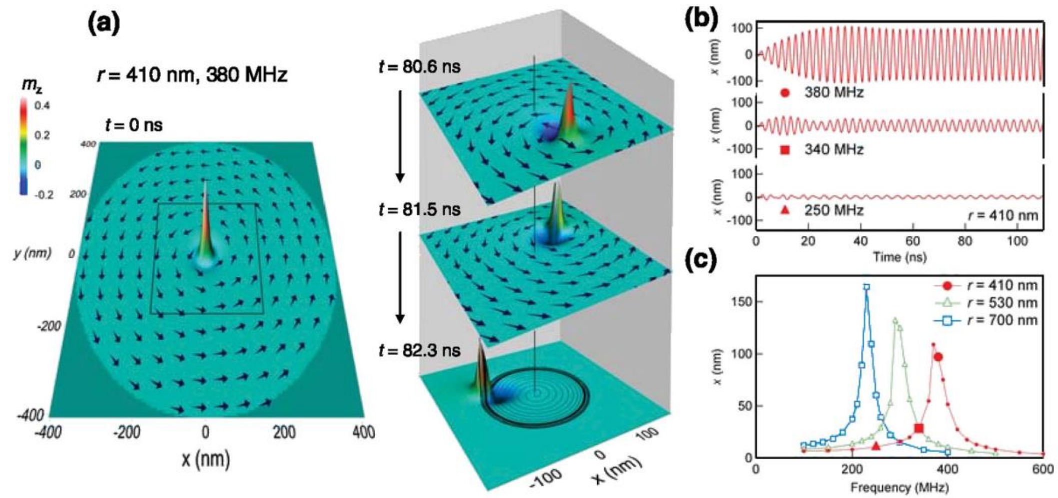

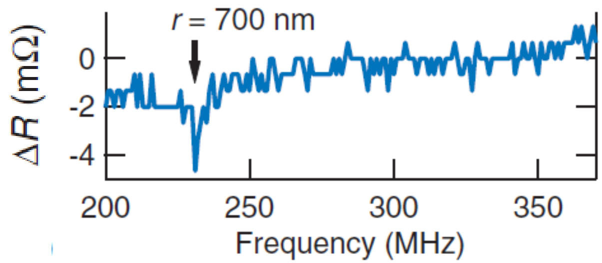

PRB **81**, 060402 (2010), PRL **97**, 107204 (2006)

Application of Spin Transfer Torque

Radio-Frequency DW Oscillators

AC

DC

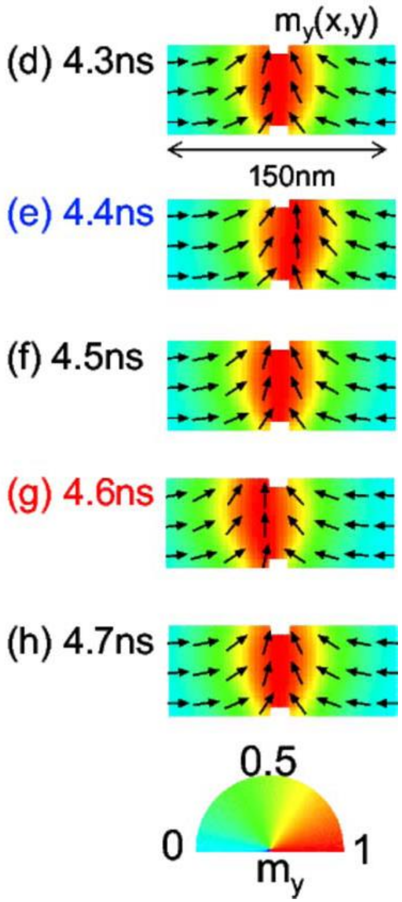

CPP-nanopillar

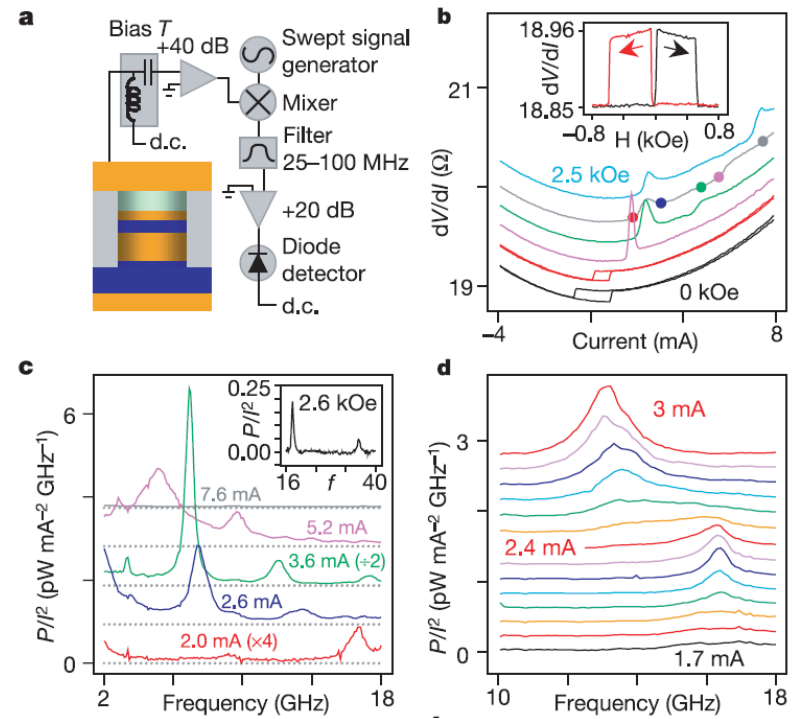

Nature **425**, 380 (2003)

Our works

Superconductor/ferromagnet proximity effect, inverse proximity effect

Magnetic nanostructures

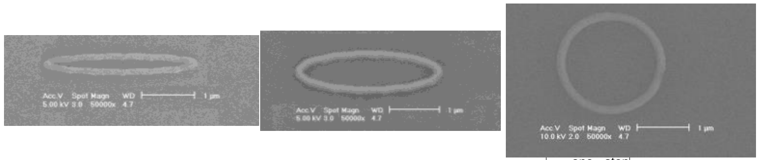

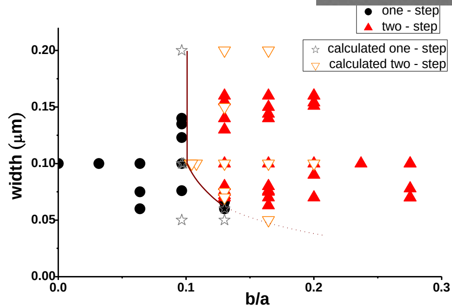

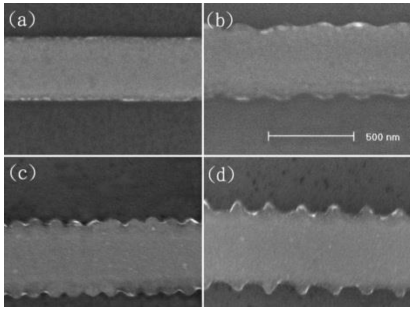

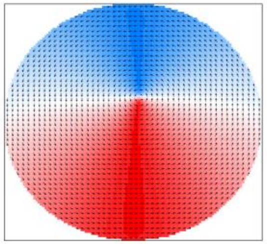

- “Quantitative analysis of magnetization reversal in submicron S-patterned structures with narrow constrictions by magnetic force microscopy”. APL **86**, 053111 (2005).
- “Observation of Room Temperature Ferromagnetic Behavior in Cluster Free, Co doped HfO_2 Films”. APL **91**, 082504 (2007).
- “Variation of magnetization reversal in pseudo-spin-valve elliptical rings”. APL **94**, 233103 (2009).
- “Compensation between magnetoresistance and switching current in Co/Cu/Co spin valve pillar structure”. APL **96**, 093110 (2010).
- “Exchange bias in spin glass (FeAu)/NiFe thin films”. APL **96**, 162502 (2010).
- “Demonstration of edge roughness effect on the magnetization reversal of spin valve submicron wires”. APL **97**, 022109 (2010).

outline

- Giant Magnetoresistance, Tunneling Magnetoresistance
- Spin Transfer Torque
- Micro and nano Magnetics
- Pure Spin current (no net charge current)
    - Spin Hall, Inverse Spin Hall effects
    - Spin Pumping effect
    - Spin Seebeck effect

Nano Magnetism

Vortex induced by dc current in a circular magnetic spin valve nanopillar

L. J. Chang and S. F. Lee

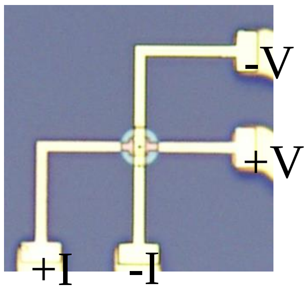

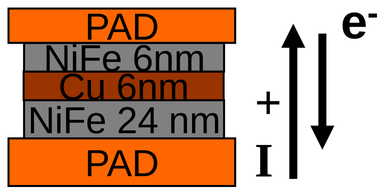

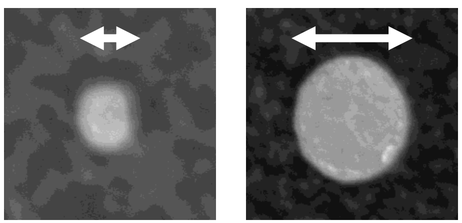

90 nm   380 nm

oommf

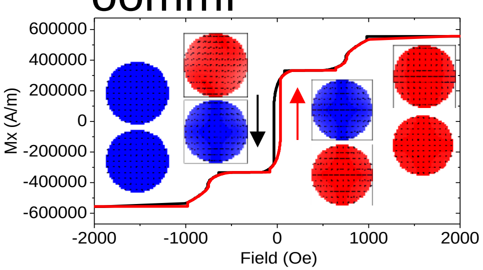

D = 90 nm

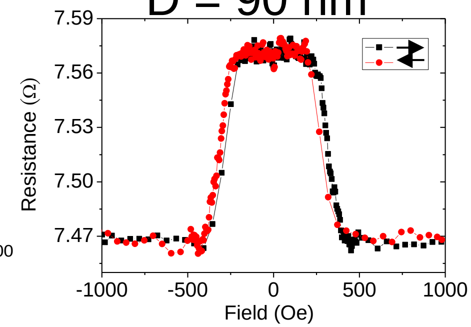

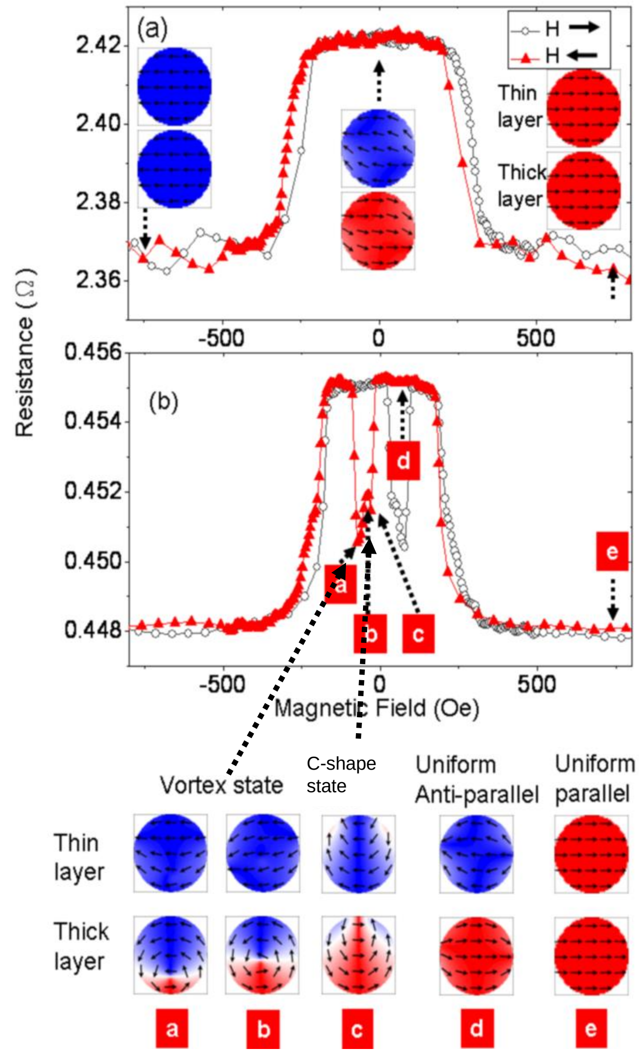

D = 160 nm

D = 380 nm

Current driven vortex nucleation

D = 160 nm H = 0 Oe

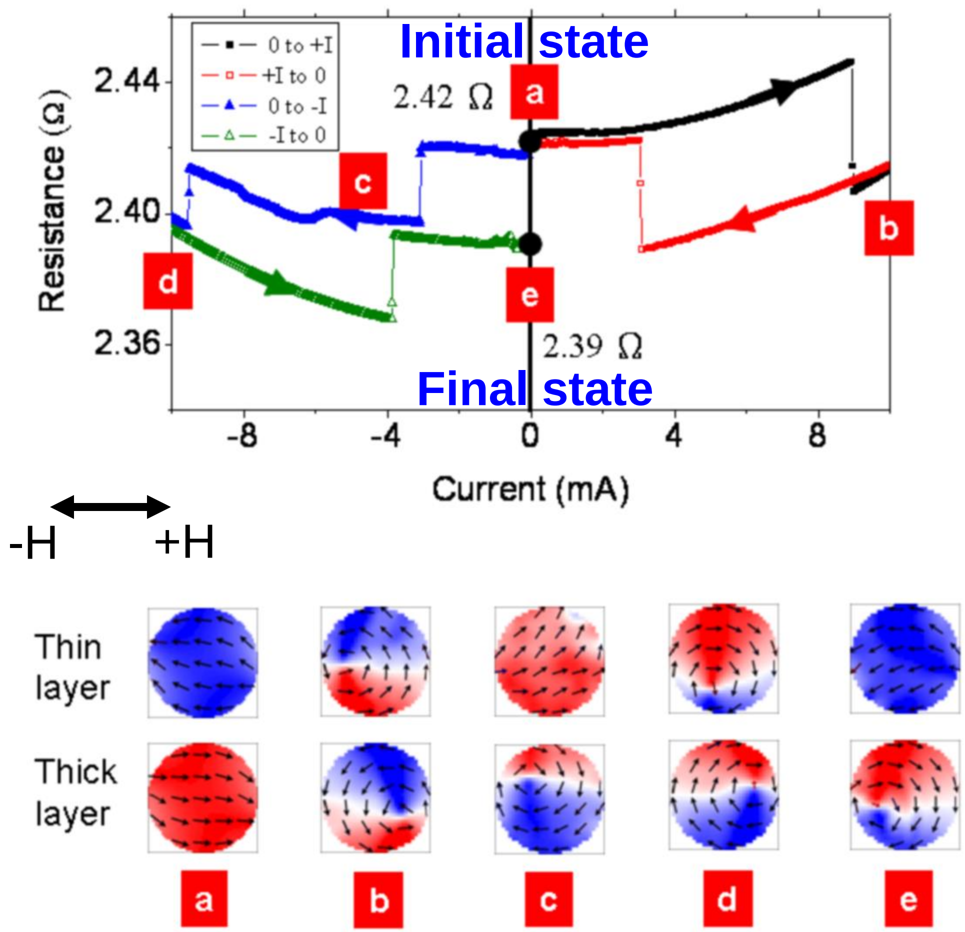

Other research interest include superconductor-magnetic material proximity effect, Ferromagnetic Resonance etc.

Domain wall oscillation in a trapping potential

Theoretical Backgrounds

Resonant DW induced by AC spin-polarized current in Ferromagnetic strips

DW dynamics equation

$$(1+\alpha^2)m\frac{d^2x}{dt^2} = F_p(x) + F_f + F_s + F_d$$

where $\mathrm{m} = \frac{2(\mu_0 L_y L_z)}{\gamma_0^2 (N_z - N_y)\Delta_0}$ is the effective DW mass (kg), and the other variables are listed below.

L_y : width of wire (m)

L_z : thickness of wire (m)

μ_0 : permeability ($4\pi \times 10^{-7}$ $\mathrm{VsA^{-1}m^{-1}}$)

γ_0 : electron gyromagnetic ratio (2.2×10^5 $\mathrm{Vs^2m^{-1}kg^{-1}}$)

N_z, N_y : transverse demagnetizing factors

Δ_0 : DW width (m)

x : DW position (m)

Theoretical Backgrounds

Resonant DW induced by AC spin-polarized current in Ferromagnetic strips

pinning force $$F_p(x) = -\frac{\partial V_{pin}(x)}{\partial x} = \begin{cases} -K_N x & (|x| \le L_N) \\ 0 & (|x| > L_N) \end{cases}$$

L_N : length of pinning potential (m)

where K_N (N/m) is the elastic constant of the DW trap

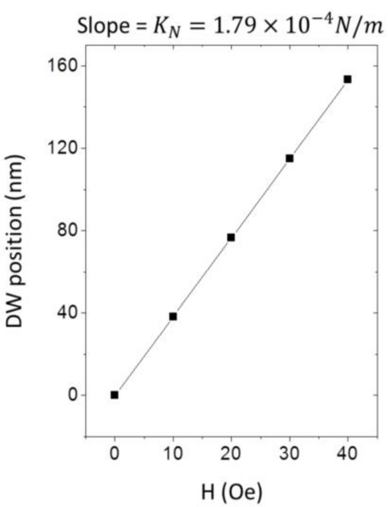

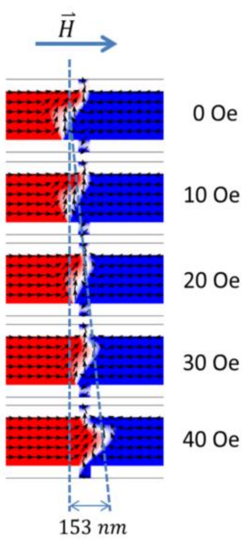

K_N =1.79×10^{-4} N/m.
$m = 5.25 \times 10^{-25}$kg

$$f_r = \frac{1}{2\pi}\sqrt{\frac{K_N}{m}} = \frac{1}{2\pi}\sqrt{\frac{1.79 \times 10^{-4} N/m}{5.25 \times 10^{-25} kg}}$$
$$= 2.93\text{GHz}$$

Theoretical Backgrounds

Resonant DW induced by AC spin-polarized current in Ferromagnetic strips

friction force $$F_f = -\left[\alpha m \omega_d \left(1+\frac{\omega_r^2}{\omega_d^2}\right)\right]\frac{dx(t)}{dt} = -b\,\frac{dx(t)}{dt}$$

$\omega_d = \gamma_0 M_s (N_z - N_y)$: angular frequency of magnetization oscillations around the demagnetizing field inside the wall.

$\omega_r = 2\pi f_r$: angular frequency of free harmonic oscillator.

$$b = \left[\alpha m \omega_d \left(1+\frac{\omega_r^2}{\omega_d^2}\right)\right] \Rightarrow \frac{b}{m} = \alpha \omega_d \left(1+\frac{\omega_r^2}{\omega_d^2}\right)$$

$$\omega_d = \gamma_0 M_s (N_z - N_y) = \frac{2(\mu_0 L_y L_z)}{\gamma_0 m \Delta_0} M_s = \frac{2[4\pi\times10^{-7}(VsA^{-1}m^{-1})\cdot 400\times10^{-9}(m)\cdot 12\times10^{-9}(m)]}{2.2\times10^5(Vs^2m^{-1}kg^{-1})\cdot 5.25\times10^{-25}(kg)\cdot 100\times10^{-9}(m)}\cdot$$

$$8.6\times10^5\left(\frac{A}{m}\right) = 8.97\times10^{11}(s^{-1})$$

$$\Rightarrow \frac{b}{m} = \alpha\omega_d\left(1+\frac{\omega_r^2}{\omega_d^2}\right) \sim \alpha\omega_d = 0.01\times 8.97\times10^{11}(s^{-1}) = 8.97\times10^{9}(s^{-1})$$

Theoretical Backgrounds

Resonant DW induced by AC spin-polarized current in Ferromagnetic strips

static driving force $$F_s = F_H + F_j = m\omega_d\left(\gamma_0\Delta_0 H_a - c_j\right)$$

$c_j = \xi b_j$ ： non-adiabatic STT term

time-varying contribution $$F_d = F_{H_a} + F_{j_a} = m\left[\alpha\gamma_0\Delta_0\frac{\partial H_a}{\partial t} - (1+\alpha\xi)\frac{\partial b_j}{\partial t}\right]$$

$b_j = j_a(t)\frac{\mu_B P}{eM_s(1+\xi^2)}$ ： adiabatic STT term

$j_a(t) = jcos(2\pi f_j t)$ ： AC current dencity

Theoretical Backgrounds

Resonant DW induced by AC spin-polarized current in Ferromagnetic strips

zero external field $H_a = 0$
zero non-adiabatic STT term $c_j = 0$.

$$(1+\alpha^2)m\frac{d^2x}{dt^2} + b\frac{dx(t)}{dt} + K_N x = m(1+\alpha\xi)\frac{j\mu_B P}{eM_s(1+\xi^2)}2\pi f_j \sin(\omega_j t)$$

set $x(t) = A\cos(\omega_j t) + B\sin(\omega_j t)$

$$\frac{dx(t)}{dt} = -A\omega_j\, sin(\omega_j t) + B\omega_j\, cos(\omega_j t)$$

$$\frac{d^2x}{dt^2} = -A\omega_j^2\cos(\omega_j t) - B\omega_j^2\, sin(\omega_j t)$$

Theoretical Backgrounds

Resonant DW induced by AC spin-polarized current in Ferromagnetic strips

$$\begin{bmatrix} [K_N - (1+\alpha^2)m\omega_j^2] & (b\omega_j) \\ (-\omega_j t) & [K_N - (1+\alpha^2)m\omega_j^2] \end{bmatrix} \begin{bmatrix} A \\ B \end{bmatrix} = \begin{bmatrix} 0 \\ m(1+\alpha\xi)\dfrac{j\mu_B P}{eM_s(1+\xi^2)}\omega_j \end{bmatrix}$$

$$\Rightarrow \mathrm{A} = \frac{m(1+\alpha\xi)\dfrac{j\mu_B P}{eM_s(1+\xi^2)}\omega_j \cdot (b\omega_j)}{[K_N - (1+\alpha^2)m\omega_j^2]^2 + (b\omega_j)^2}$$

$$\mathrm{B} = \frac{-m(1+\alpha\xi)\dfrac{j\mu_B P}{eM_s(1+\xi^2)}\omega_j \cdot [K_N - (1+\alpha^2)m\omega_j^2]}{[K_N - (1+\alpha^2)m\omega_j^2]^2 + (b\omega_j)^2}$$

Then the particular solution is：

$$x(t) = \sqrt{A^2 + B^2}\cos\left(\omega_j t - \delta\right)$$

δ：Phase between the applied current $j_a(t)$ and the DW position $x(t)$ in the stationary regime.

$\delta = \tan^{-1}\left(\frac{B}{A}\right)$

$$A_r = \sqrt{A^2 + B^2}$$

$$= \sqrt{\frac{\left(m(1+\alpha\xi)\frac{j\mu_B P}{eM_s(1+\xi^2)}\omega_j\right)^2 \cdot \left\{\left[K_N - (1+\alpha^2)m\omega_j^2\right]^2 + \left(b\omega_j\right)^2\right\}}{\left\{\left[K_N - (1+\alpha^2)m\omega_j^2\right]^2 + \left(b\omega_j\right)^2\right\}^2}}$$

$$= \frac{j\mu_B P}{eM_s(1+\xi^2)}\sqrt{\frac{(1+\alpha\xi)^2\omega_j^2}{\left[\omega_r^2 - (1+\alpha^2)\omega_j^2\right]^2 + \left(\frac{b}{m}\right)^2\omega_j^2}}$$

$$A_r = \frac{j\mu_B P}{eM_s}\sqrt{\frac{\omega_j^2}{\left[\omega_r^2-(1+\alpha^2)\omega_j^2\right]^2+\left(\frac{b}{m}\right)^2\omega_j^2}} =$$

$$\frac{5\times10^{12}(A/m^2)\cdot9.274\times10^{-24}(Am^2)\cdot0.4}{1.602\times10^{-19}(C)\cdot8.6\times10^{5}(A/m)}\sqrt{\frac{\omega_j^2}{[(2\pi\times2.93\times10^{9}(s^{-1}))^2-\omega_j^2]^2+(8.97\times10^{9}(s^{-1}))^2\cdot\omega_j^2}}$$

$$= 1.34\times10^{2}(m/s)\sqrt{\frac{\omega_j^2}{[(2\pi\times2.93\times10^{9}(s^{-1}))^2-\omega_j^2]^2+(8.97\times10^{9}(s^{-1}))^2\cdot\omega_j^2}}$$

We set the AC current density $j = 5\times10^{12}(A/m^2)$, Bohr magneton $\mu_B = 9.274\times10^{-24}(Am^2)$, spin polarization $P = 0.4$, electron charge $e = 1.602\times10^{-19}$C, width of DW $\Delta_0 = 100(nm)$, NiFe saturation magnetization $M_s = 8.6\times10^{5}(A/m)$.

Since the DW resonate with the applied AC current, $\omega_r = \omega_j$. Therefore:

$$\Rightarrow\ 1.34 \times 10^2 \left(\frac{m}{s}\right) \sqrt{\frac{\omega_j^2}{[(2\pi \times 2.93 \times 10^9 (s^{-1}))^2 - \omega_j^2]^2 + \left(8.97 \times 10^9 (s^{-1})\right)^2 \cdot \omega_j^2}}$$

$$= 1.34 \times 10^2 \left(\frac{m}{s}\right) \times \frac{1}{8.97 \times 10^9 (s^{-1})} = 14.9 \times 10^{-9} (m)$$

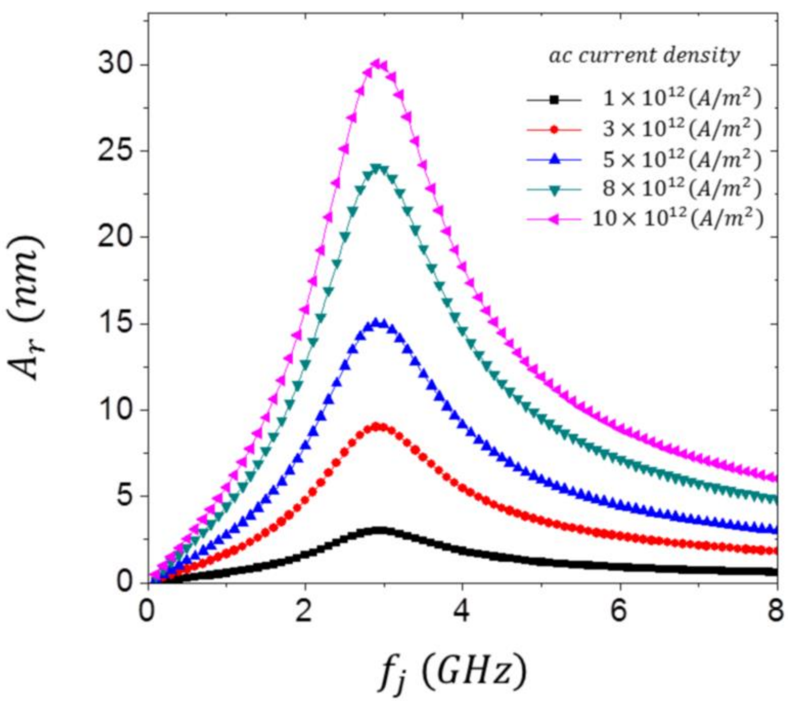

Amplitude of stationary DW oscillations as a function of the frequency of the AC current f_j for $H = 0$ mT, $\xi = 0$, which are given by Eq. (2.37) for five different values of j.

Experiment Methods

four point probe measurement circuit

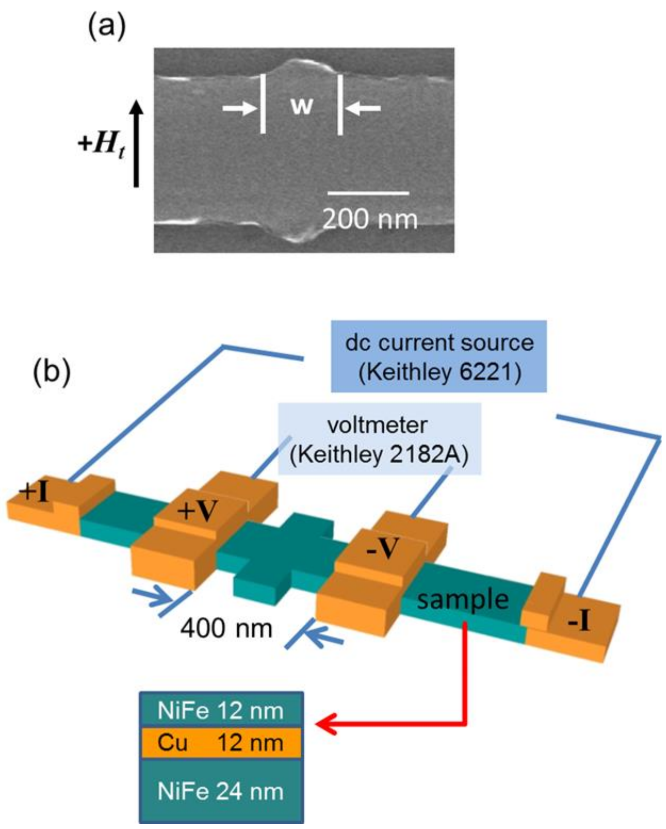

high frequency measurements circuit

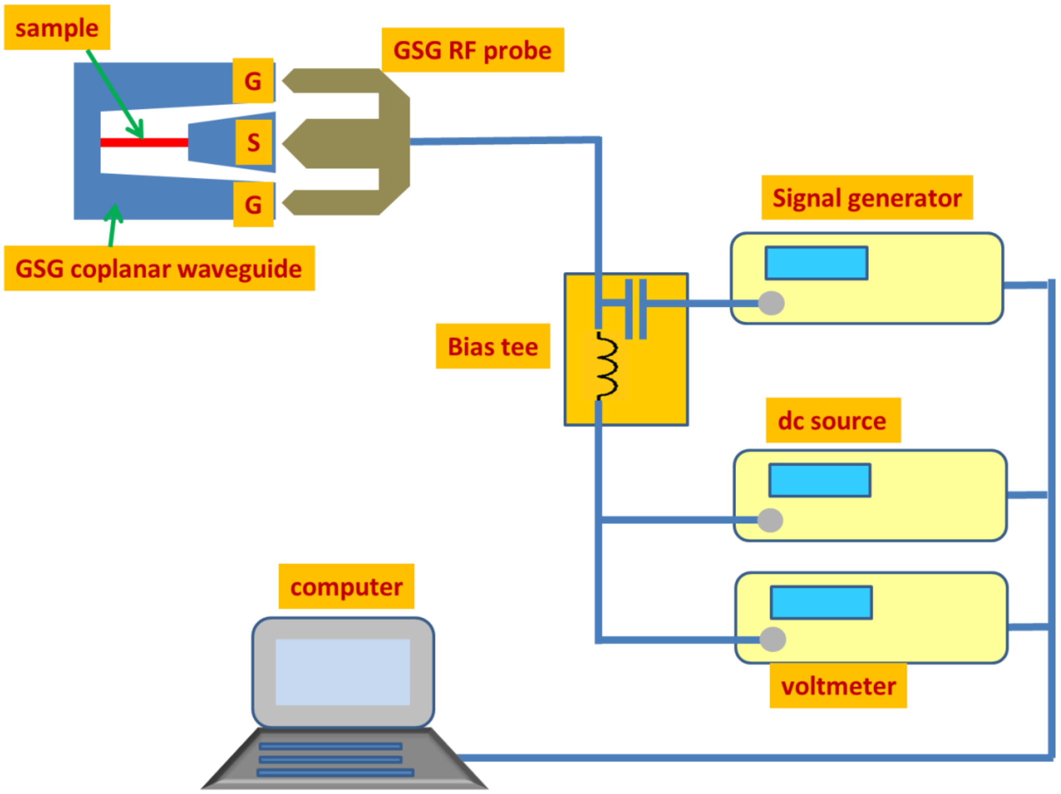

Measurement and simulation results

AC current induced localized domain wall oscillators in NiFe/Cu/NiFe submicron wires

Nucleation of Pinned anti-parallel transverse DW

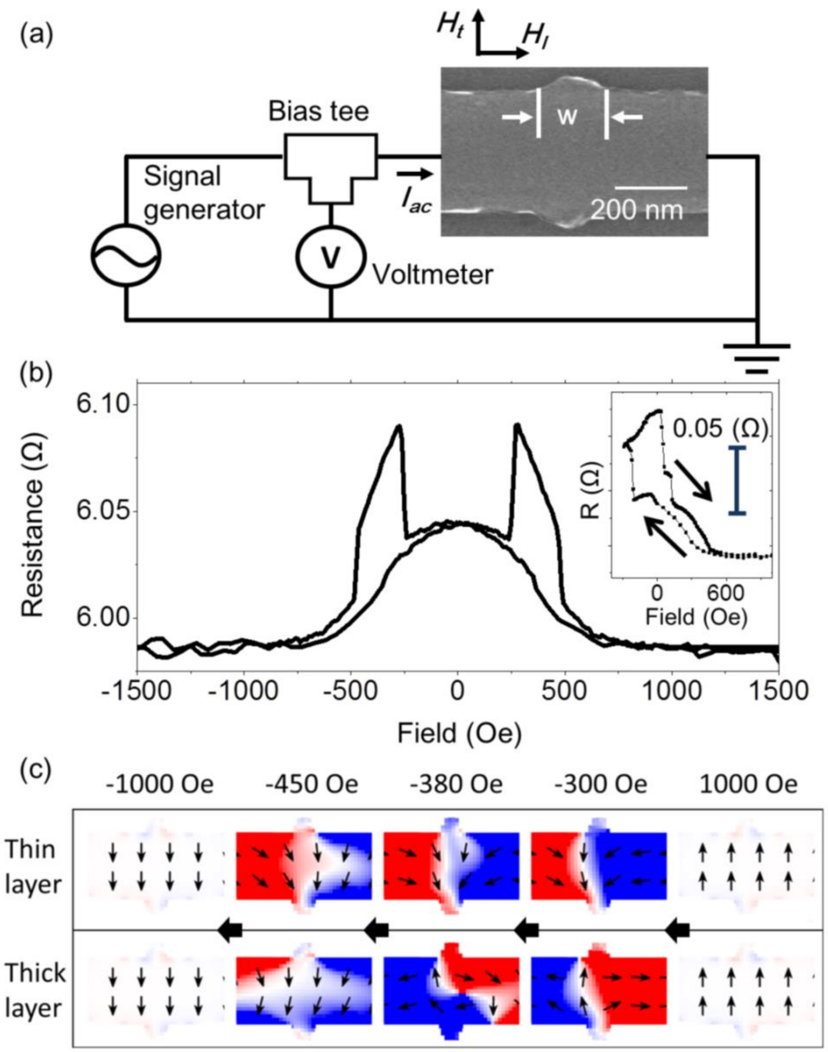

Measurement and simulation results

AC current induced localized domain wall oscillators in NiFe/Cu/NiFe submicron wires

DW resonators for frequency-selective operation

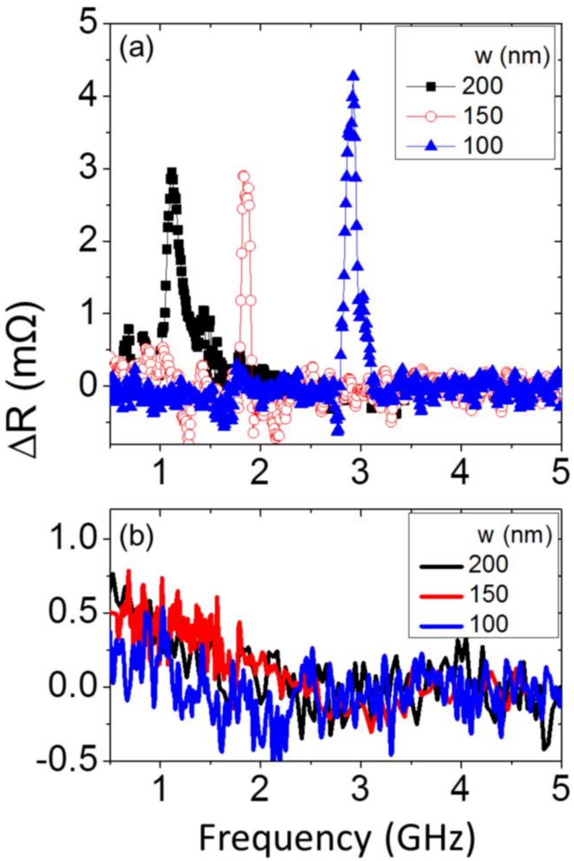

(a) Experimental measurement of the ac current induces resonance excitation of pinned DW trapped at the protrusion. Resistance change as a function of ac excitation current frequency for the submicron wires containing artificial symmetric protrusions with three different widths of protrusion w = 200, 150, and 100 nm. (b) The response curve measured at the saturation field with a uniform state of submicron wires (without DW). The ΔR is observed unchanged with frequency for each of the samples.

Measurement and simulation results

AC current induced localized domain wall oscillators in NiFe/Cu/NiFe submicron wires

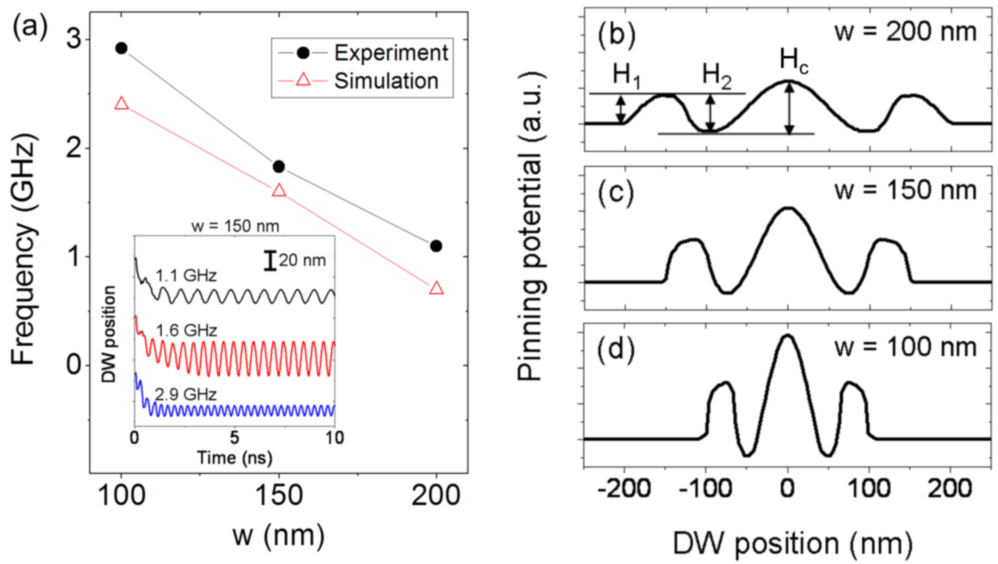

Resonance frequency of pinned DW dependence on the width of trap w, the solid circles and the open triangles indicate the experiment and simulation results respectively. The inset shows the simulated time evolutions of the DW motion with w = 150 nm. (b)-(d) Potential landscape of pinned DW from micromagnetic simulation with three different width of protrusion w = 200, 150, 100 nm.

Measurement and simulation results

Reversible domain wall motion induced by dc current in NiFe/Cu/NiFe submicron wires

Current in-plane

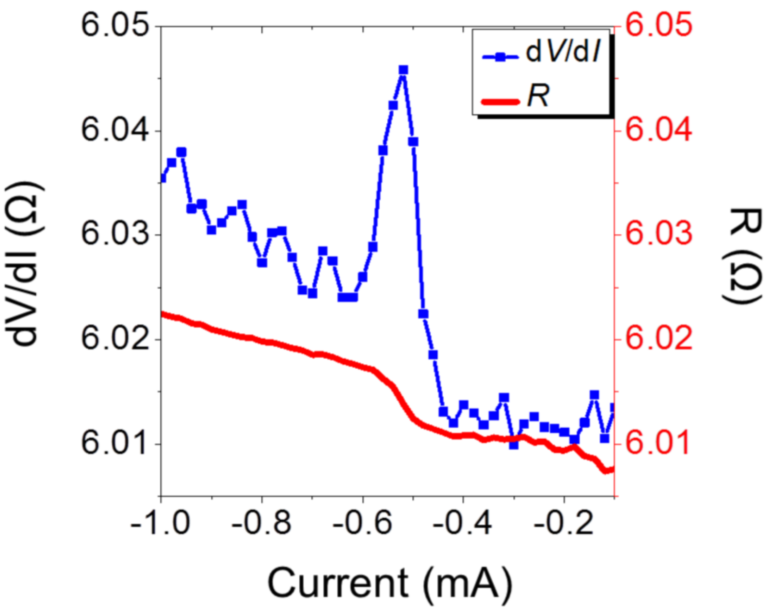

nano-pillar

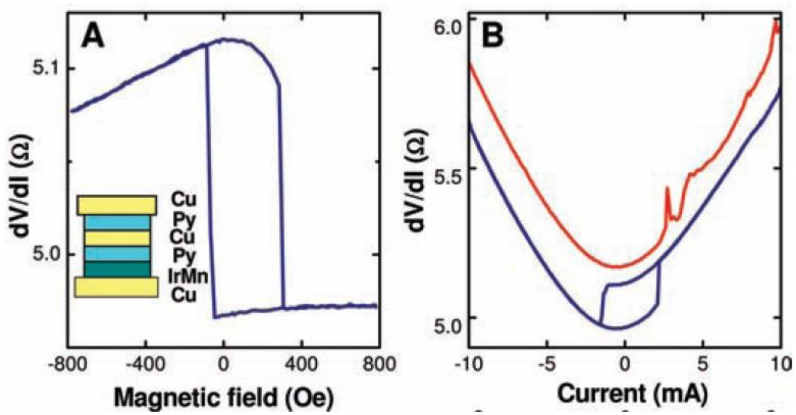

point contact

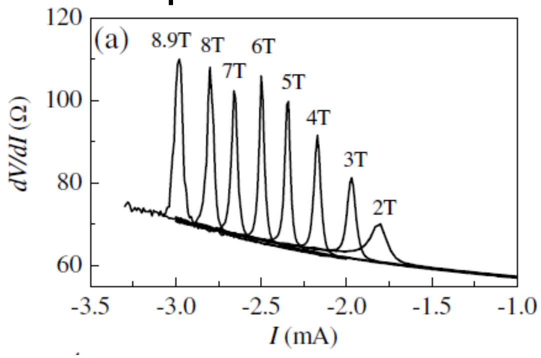

Science **307**, 228 (2005)
PRL **97**, 107204 (2006)

Measurement and simulation results

Reversible domain wall motion induced by dc current in NiFe/Cu/NiFe submicron wires

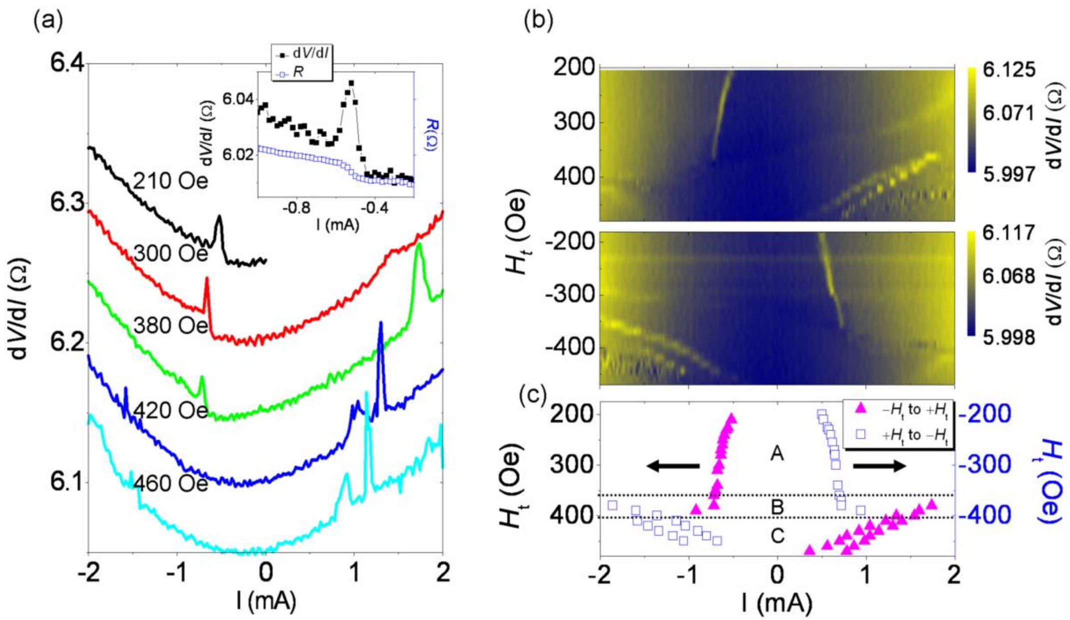

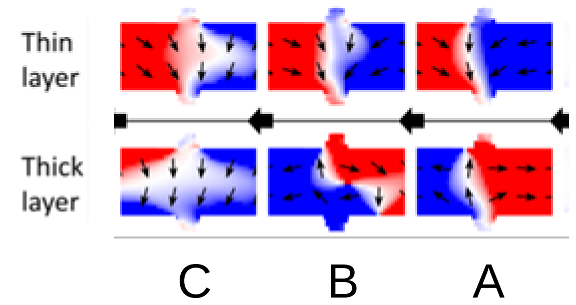

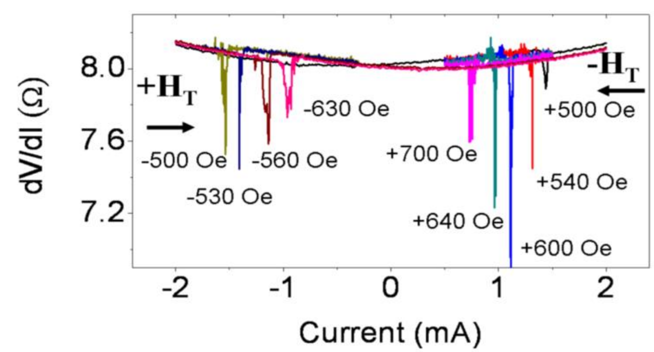

Differential resistance vs. current density at different external transverse fields H_t, enlarged in the inset for V/I vs. j at H_t = 210 Oe. (b) Map of dV/dI versus transverse field and dc current. (c) Critical current I_c vs. H_t.

Measurement and simulation results

Reversible domain wall motion induced by dc current in NiFe/Cu/NiFe submicron wires

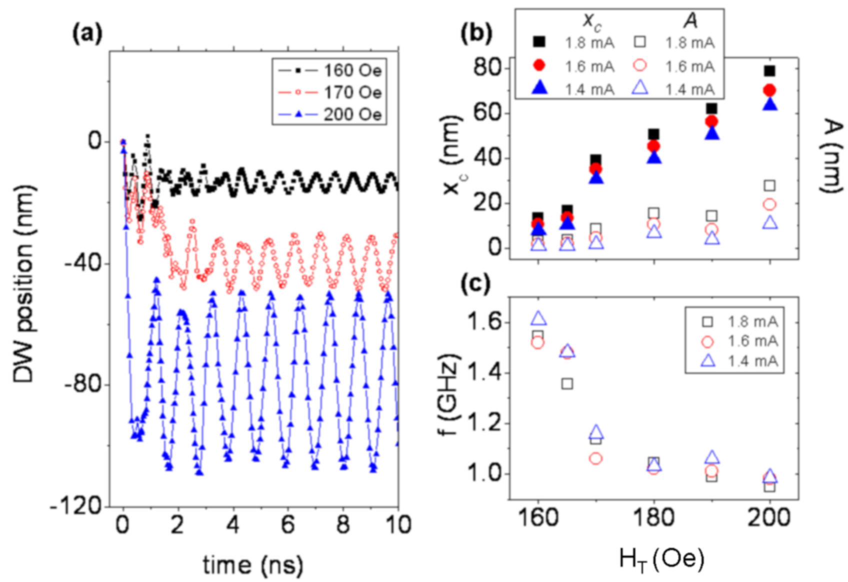

Simulation results of DW position as a function of time under fixed dc current density of 9.7×10^6 A/cm^2 with variation of external transverse field H_t. (b) central position x_c, amplitude A, and (c) frequency of the oscillator vs. H_t with different dc current.

Measurement and simulation results

Reversible domain wall motion induced by dc current in NiFe/Cu/NiFe submicron wires

Series of submicron wires with serial DW traps of artificial symmetric protrusions

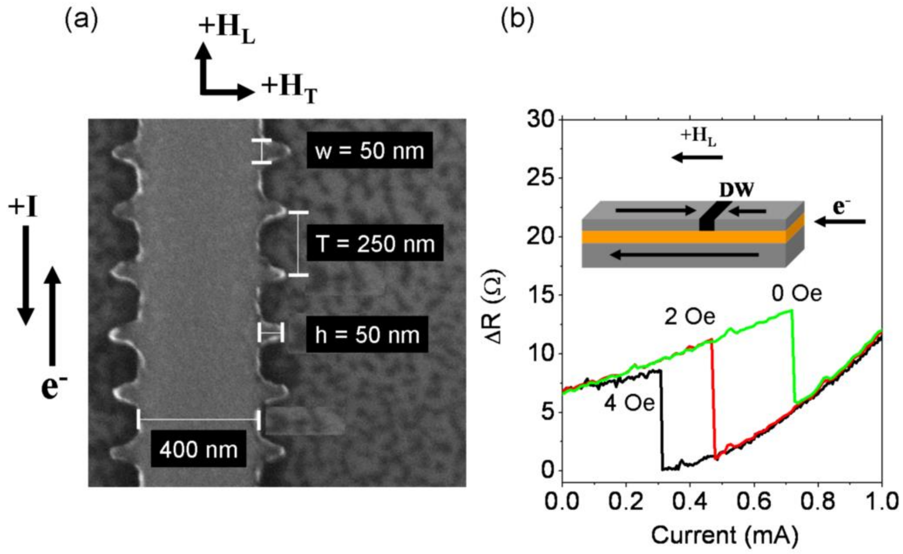

A Scanning electron microscope image of a typical serial-DW-trap sample with the protrusions 50 nm in width and height. The period was 250 nm on either side of the wire. Magnetic field and current directions are specified. (b) Schematic diagram of the sample and the irreversible resistance change from anti-parallel state to parallel state for H_L = 0 (green solid line), 2 (red dash line), and 4 (black dotted line) Oe.

Measurement and simulation results

Reversible domain wall motion induced by dc current in NiFe/Cu/NiFe submicron wires

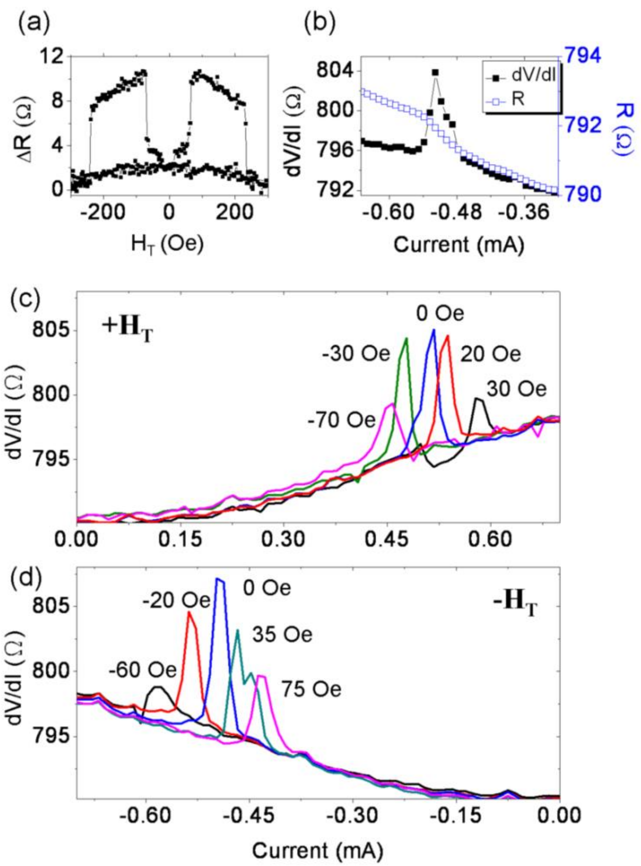

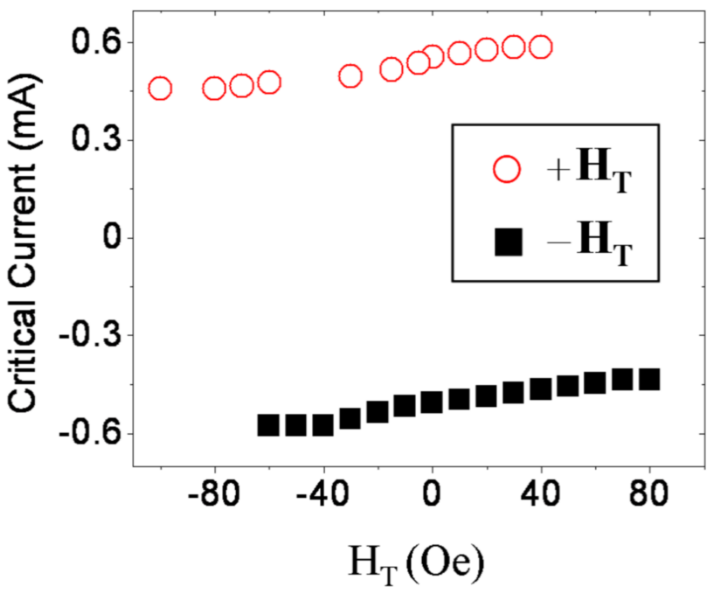

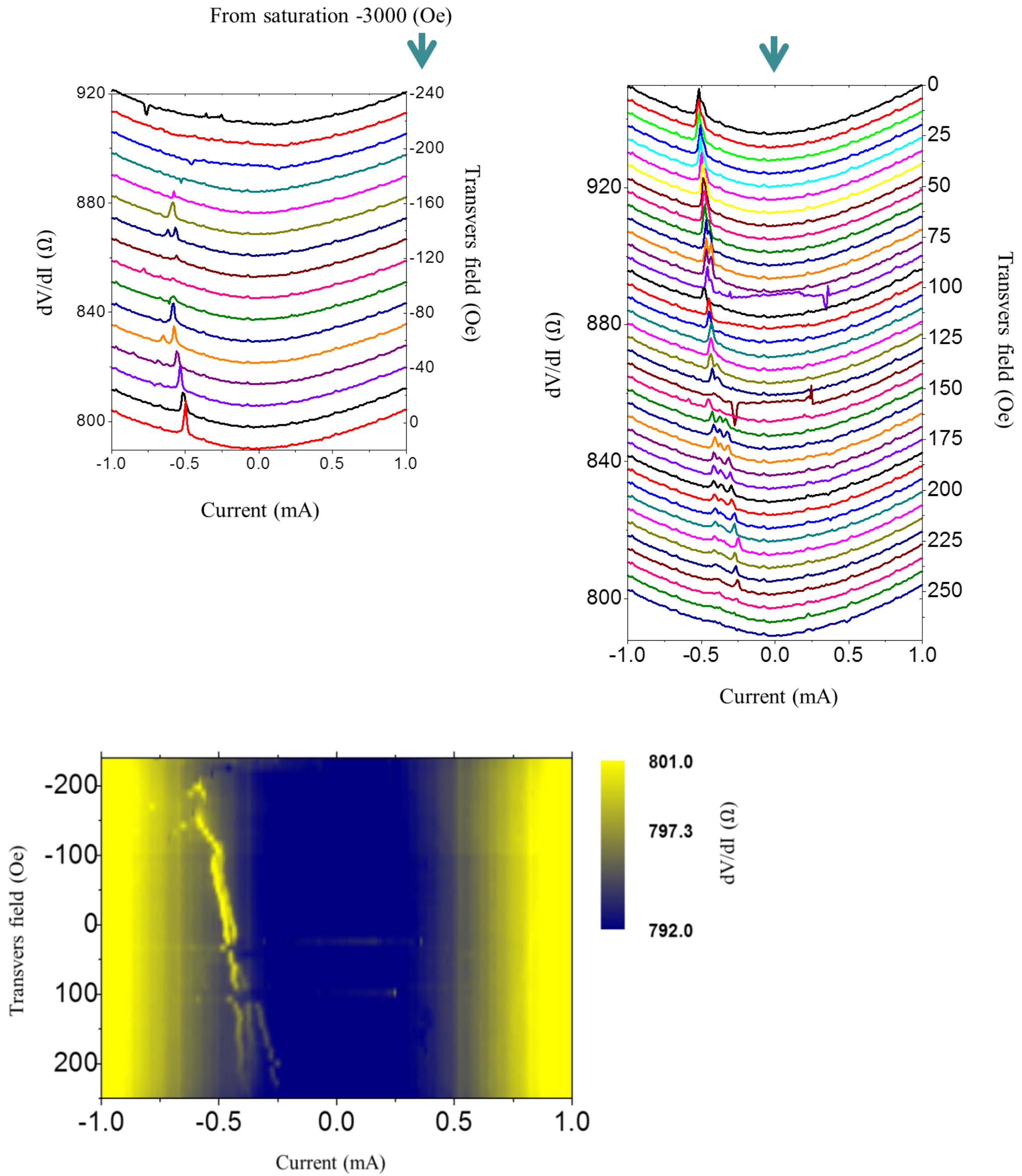

From saturation -3000 (Oe)
dV/dI (Ω)
920
880
840
800
-1.0
-0.5
0.0
0.5
1.0
Current (mA)
Transvers field (Oe)
-240
-200
-160
-120
-80
-40
0
25
50
75
100
125
150
175
200
225
250
Transvers field (Oe)
-200
-100
0
100
200
801.0
797.3
792.0
dV/dI (Ω)

Summary

- DW oscillation with resonance frequency as high as 2.92 GHz and the resonance frequency can be tuned by the width of protrusion.

- The higher resonance frequency for the narrow trap is due to the steeper potential landscape which enhances the restoring force on the pinned DW.

- For the domain wall oscillations induced by injection of a dc current investigated, the observed peak in *dV/dI* associated with the reversible change of magnetoresistance is attributed to the reversible motion of the DW.

outline

- Giant Magnetoresistance, Tunneling Magnetoresistance
- Spin Transfer Torque
- Micro and nano Magnetics
- Pure Spin current (no net charge current)
    - Spin Hall, Inverse Spin Hall effects
    - Spin Pumping effect
    - Spin Seebeck effect

Spin Hall effect

Spin Hall Effect: Electron flow generates transverse spin current

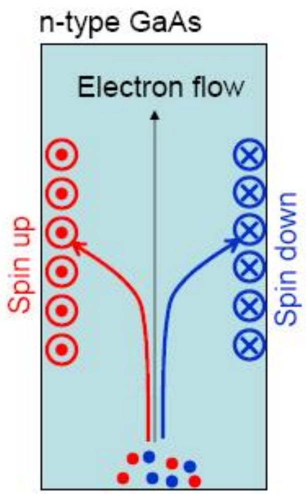

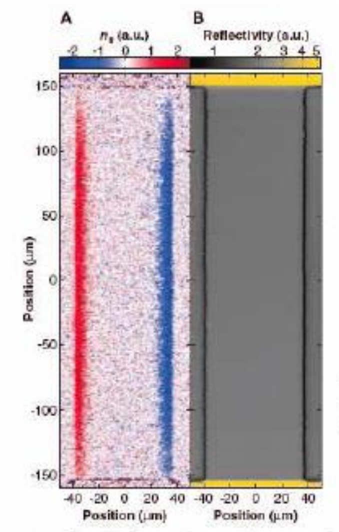

SHE observed in GaAs using Kerr effect to measure spin

Kato et.al. (Awschalom), Science 306, 1910 (2004)

Now observed at room temperature in ZnSe

M. I. Dyakonov and V. I. Perel, *JETP* **13** 467 (1971)

J. E. Hirsch, *Phys. Rev. Lett.* **83** 1834 (1999)

Guo *et al*, PRL **100** 096401 (2008)

The Intrinsic SHE is due to topological band structures

Berry curvature

$$\dot{\vec{r}} = \frac{1}{\hbar}\frac{\partial \varepsilon_n(\vec{k})}{\partial \vec{k}} + \frac{e}{\hbar}\vec{E}\times\vec{\Omega}(\vec{k})$$

The extrinsic SHE is due to asymmetry in electron scattering for up and down spins. – spin dependent probability difference in the electron trajectories

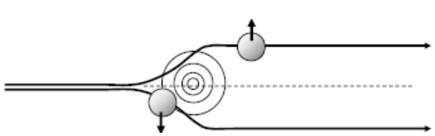

Side jump

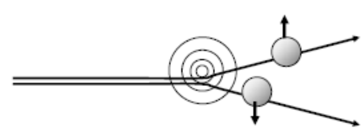

Skew scattering

Inverse Spin Hall effect

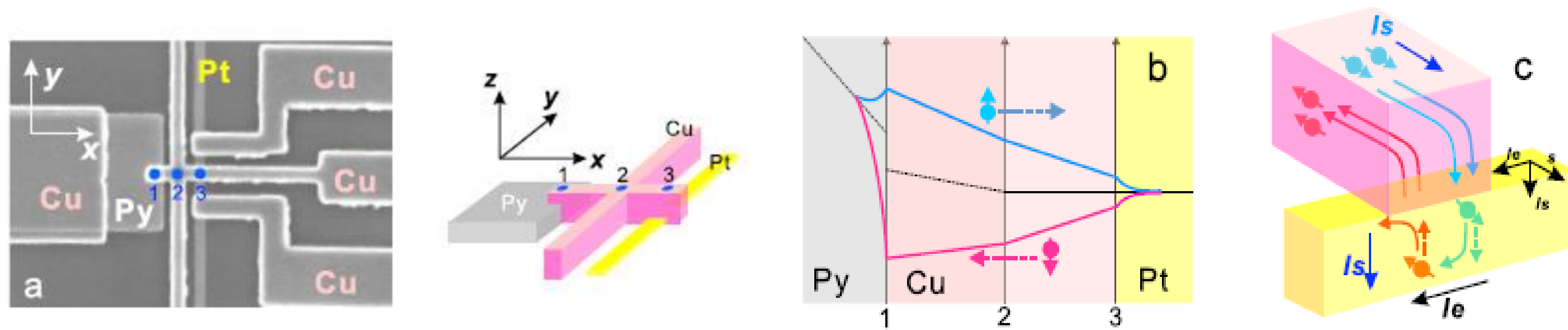

FIG. 1 (color online). (a) Scanning electron microscope (SEM) image of the fabricated spin Hall device together with a schematic illustration of the fabricated device. (b) Schematic spin dependent electrochemical potential map indicating spin accumulation in Cu and Pt induced by the spin injection from the Py pad. Dashed line represents the equilibrium position. (c) Schematic illustration of the charge accumulation process in the Pt wire, where I_S and I_e denote injected pure spin current and induced charge current, respectively. (d) Spin dependent electrochemical potential map for the charge to spin-current conversion and (e) corresponding schematic illustration.

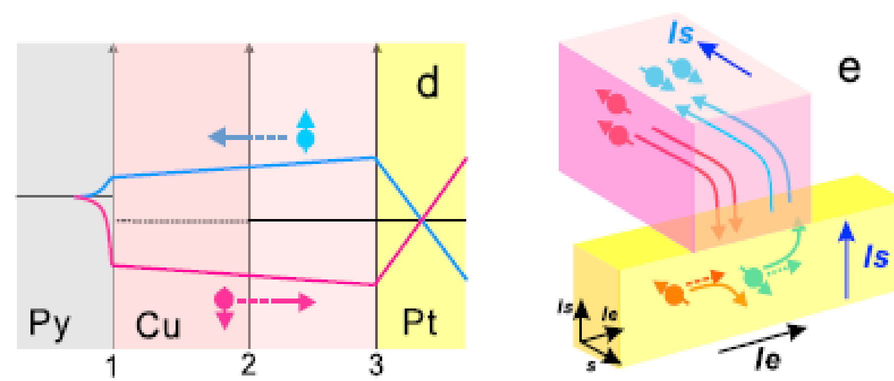

Kimura *et al*, PRL **98**, 156601 (2007)

Guo *et al*, PRL **100** 096401 (2008)

Spin Pumping

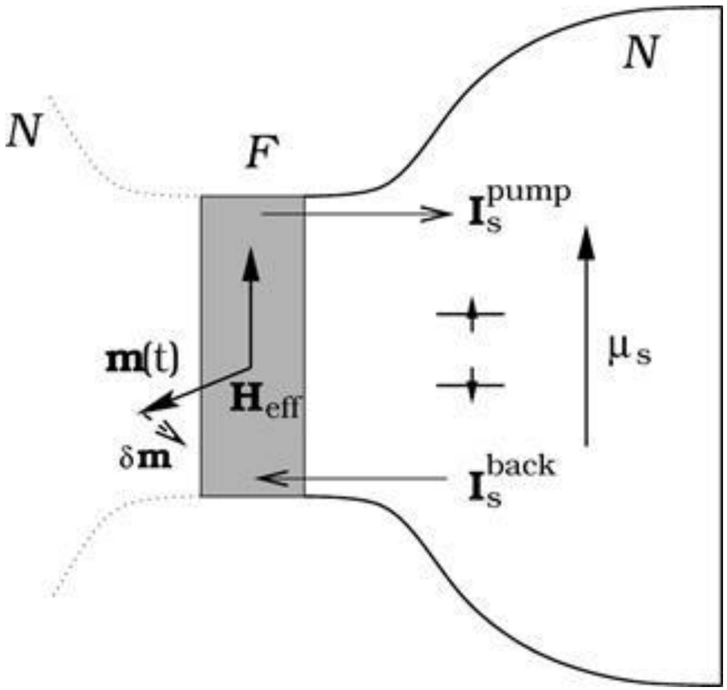

A ferromagnetic film *F* sandwiched between two nonmagnetic reservoirs *N*. For simplicity of the discussion in this section, we mainly focus on the dynamics in one (right) reservoir while suppressing the other (left), e.g., assuming it is insulating. The spin-pumping current $\mathbf{I}_s$ and the spin accumulation μ_s in the right reservoir can be found by conservation of energy, angular momentum, and by applying circuit theory to the steady state $\mathbf{I}_s^{pump} = \mathbf{I}_s^{back}$.

$$\mathbf{I}_s^{pump} = \frac{\hbar}{4\pi}\left(A_r \mathbf{m} \times \frac{d\mathbf{m}}{dt} - A_i \frac{d\mathbf{m}}{dt}\right).$$

Tserkovnyak *et al*, PRB **66**, 224403 (2002)

Combining Spin Pumping and Inverse Spin Hall Effect

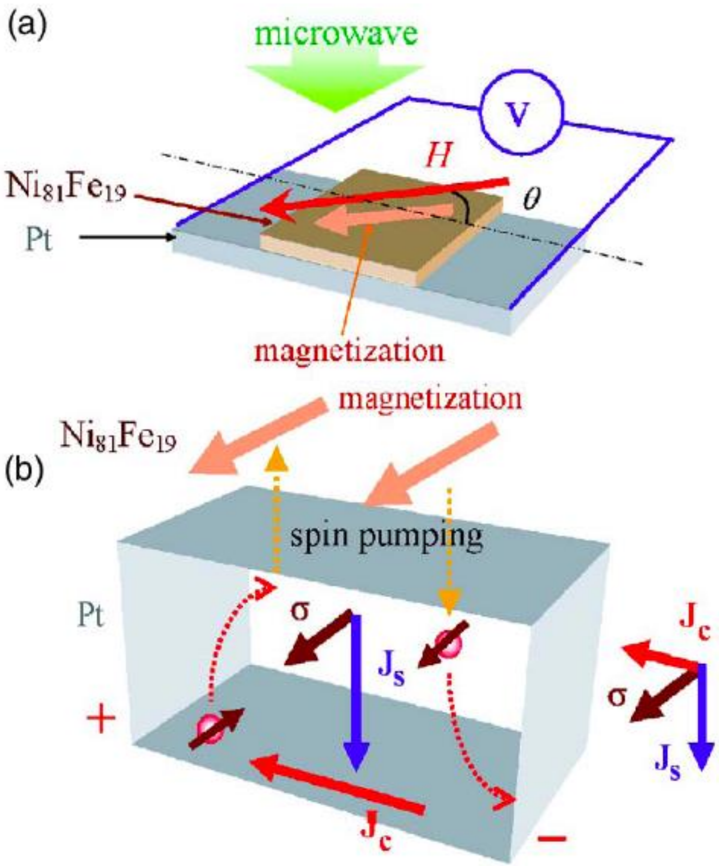

FMR

⇓

Spin Current

in adjacent

normal metal

⇓

Transverse

Charge Current

The spin-orbit interaction bends these two electrons in the same direction and induces a charge current transverse to Js,

$$\mathbf{J}_c = D_{\mathrm{ISHE}} \mathbf{J}_s \times \boldsymbol{\sigma}.$$

The surface of the Py layer is of a 1×1 mm^2 square shape. Two electrodes are attached to both ends of the Pt layer.

Saitoh *et al*, APL **88**, 182509 (2006)

Kimura *et al*, PRL **98**, 156601 (2007)

Combining Spin Pumping and Inverse Spin Hall Effect

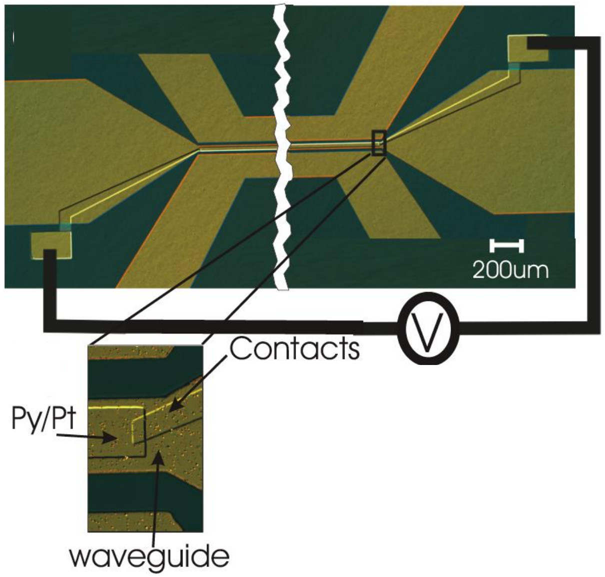

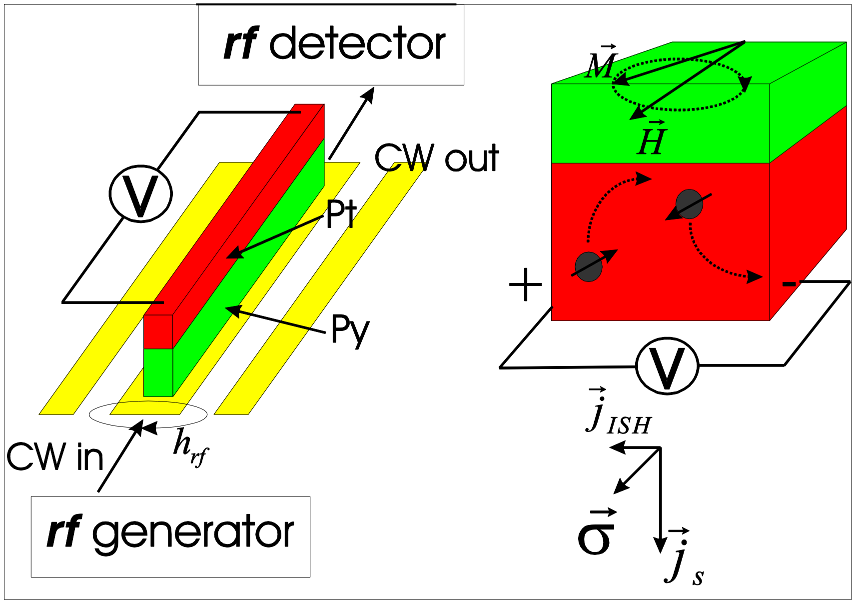

- **Use Spin Pumping to Generate Pure Spin Current**
- **Quantify Spin Current from FMR**
- **Measured Voltage Directly Determines Spin Hall Conductivity**
- **Key Advantage: Signal Scales with Device Dimension**

Mosendz *et al*, PRL **104**, 046601 (2010)

Determine Spin Hall Angle for Many Materials

$$\gamma = \frac{\sigma_{SH}}{\sigma_c}$$

$\longleftarrow$ **spin Hall conductivity**

$\longleftarrow$ **charge conductivity**

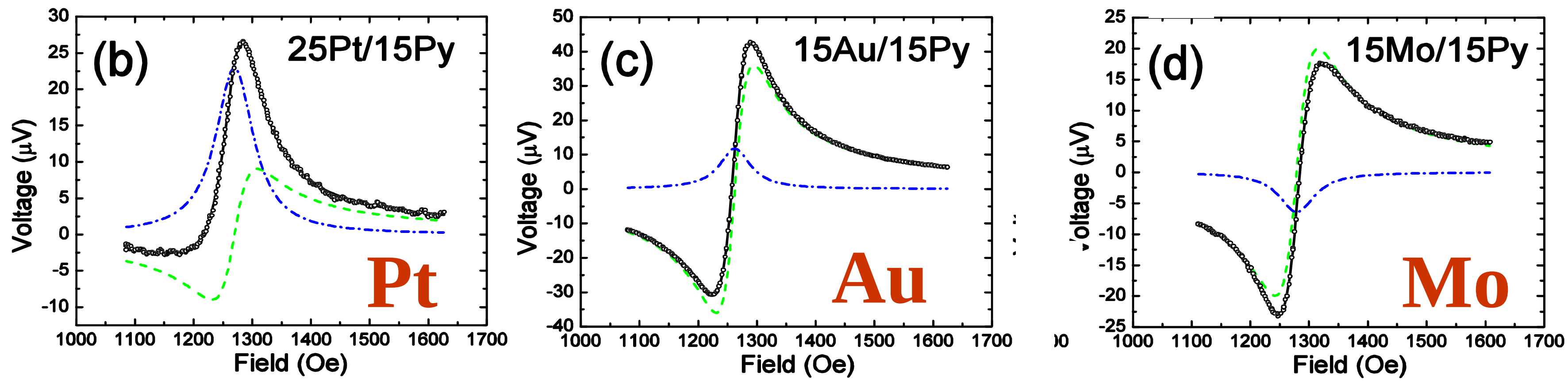

γ = 0.0120±0.0001 **γ = 0.0025±0.0006** **γ = -0.00096±0.00007**

$$V_{\mathrm{AMR}} = I_{\mathrm{rf}}^{m} \frac{R_{\mathrm{wg}}}{R_S} \Delta R_{\mathrm{AMR}} \frac{\sin(2\theta)}{2} \frac{\sin(2\alpha)}{2} \cos\varphi_0,$$

$$V_{\mathrm{ISH}} = -\frac{\gamma g_{\uparrow\downarrow} e L \lambda_{\mathrm{sd}} \omega}{2\pi\sigma_N t_N} \sin\alpha \sin^2\theta \tanh\left(\frac{t_N}{2\lambda_{\mathrm{sd}}}\right).$$

Hoffmann *et al*

Spin Seebeck effect

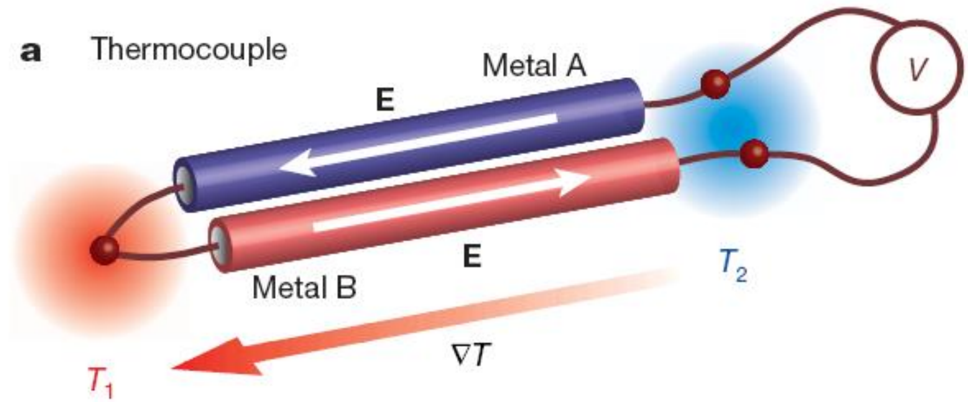

$$\delta V = S\delta T$$

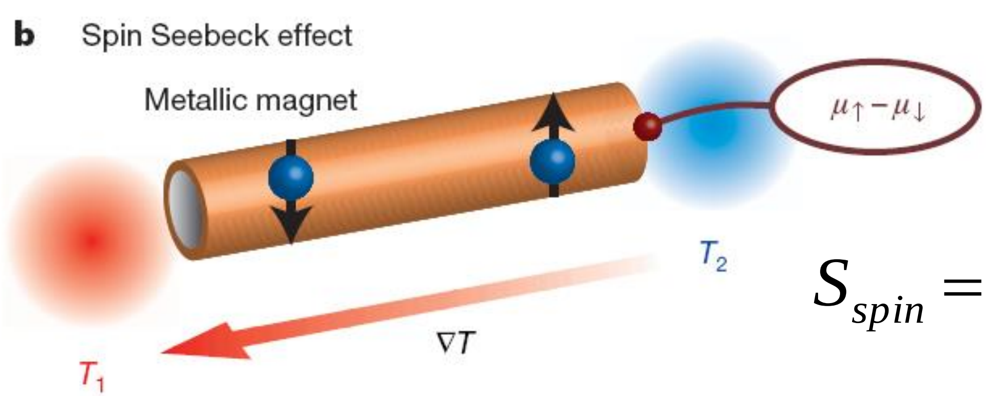

$$\delta V_{spin} = S_{spin}\delta T$$

$$S_{spin} = (1/e)[\partial \mu^c{}_\uparrow / \partial T - \partial \mu^c{}_\downarrow / \partial T]$$

Uchida *et al.*, Nature **455**, 778 (2008)

Spin Seebeck effect

In a ferromagnetic metal, **up- spin and down-spin conduction** electrons have **different scattering rates and densities**, and thus have different Seebeck coefficients.

$$j_s = j_\uparrow - j_\downarrow = (\sigma_\uparrow S_\uparrow - \sigma_\downarrow S_\downarrow)(-\nabla T)$$

This **spin current** flows **without accompanying charge currents** in the open-circuit condition, and the up-spin and down-spin currents flow **in opposite directions** along the temperature gradient

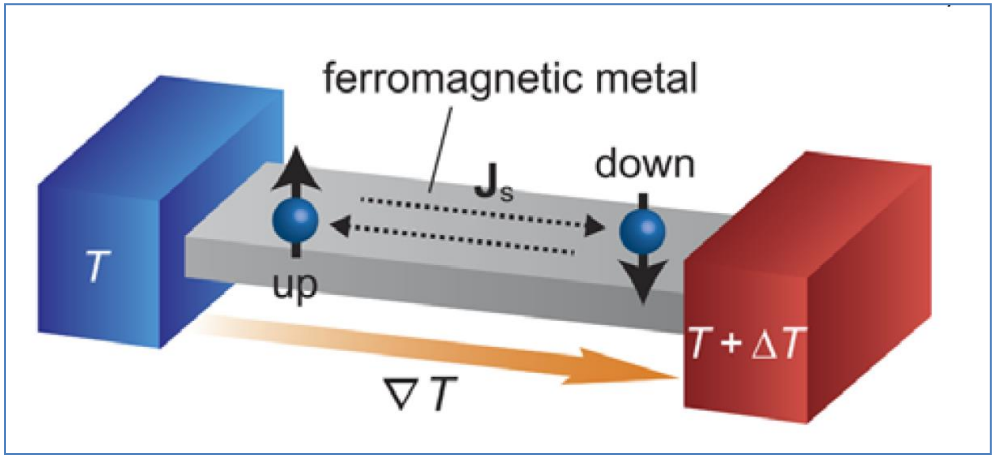

How to detect j_s?

Inverse Spin Hall Effect coverts j_s into j_c

Solid State Communications **150**, 524 (2010)

Detection of Spin Current by Inverse Spin Hall Effect

The ISHE converts a spin current into an **electromotive force** E_{SHE} by means of spin–orbit scattering.

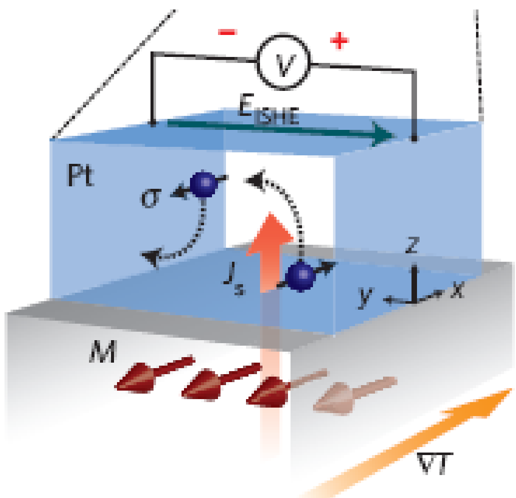

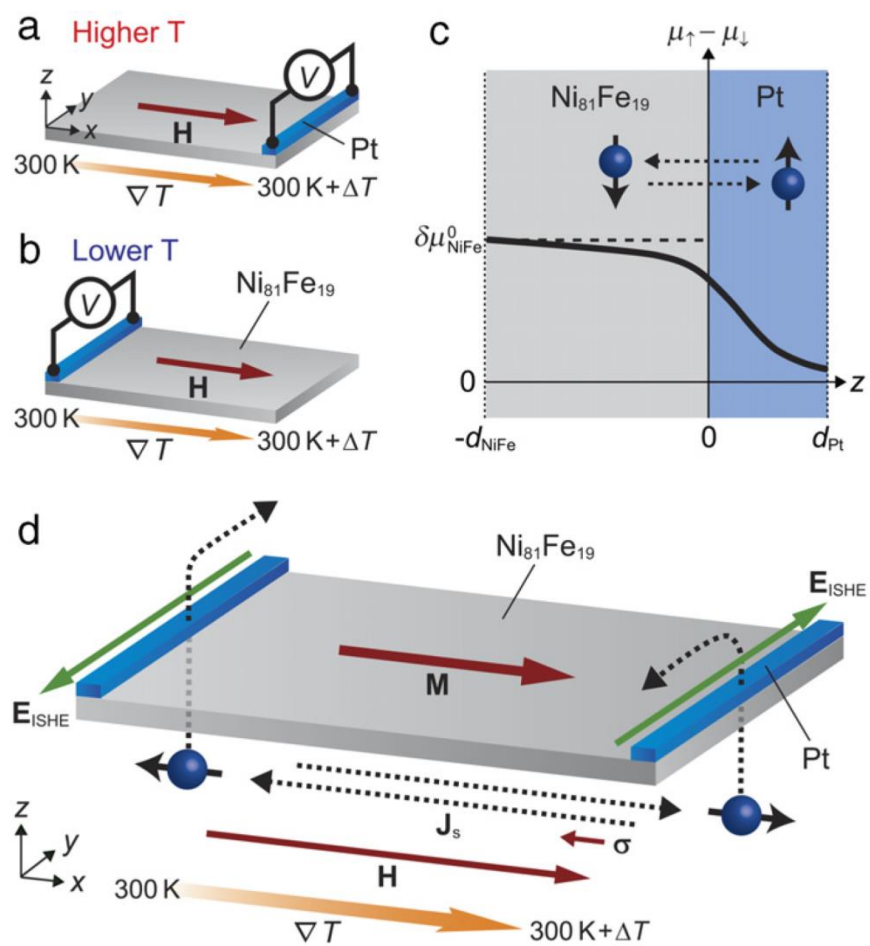

$$E_y = E_{SHE} = D_{ISHE} J_S \times \sigma$$

A spin current carries a spin-polarization vector σ along a spatial direction J_S.

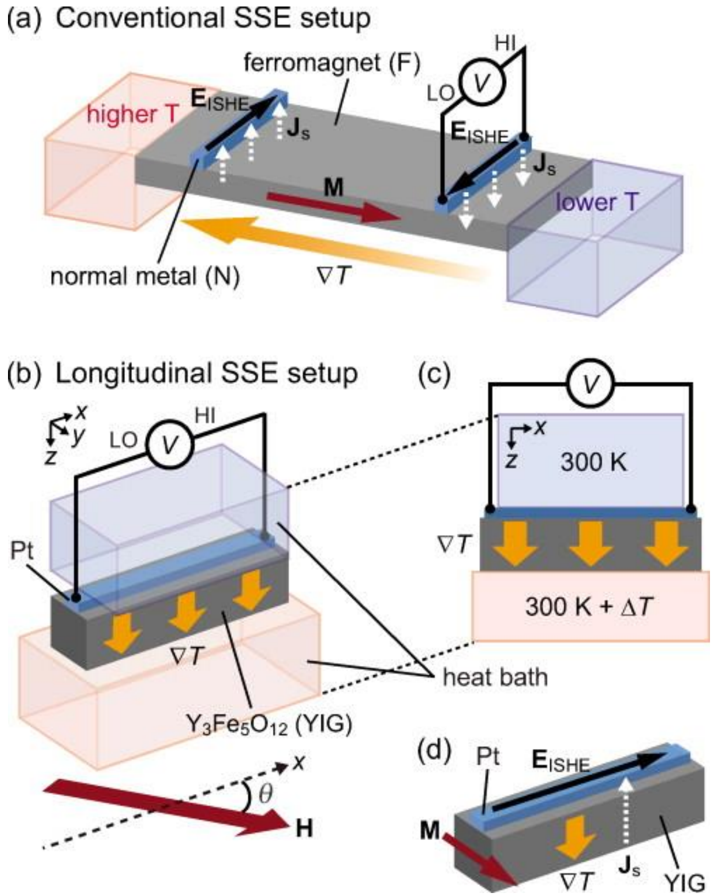

(a) A schematic of the conventional setup for measuring the ISHE induced by the SSE. Here, ∇T, M, Js, and EISHE denote a temperature gradient, the magnetization vector of a ferromagnet (F), the spatial direction of the spin current flowing across the F/no...

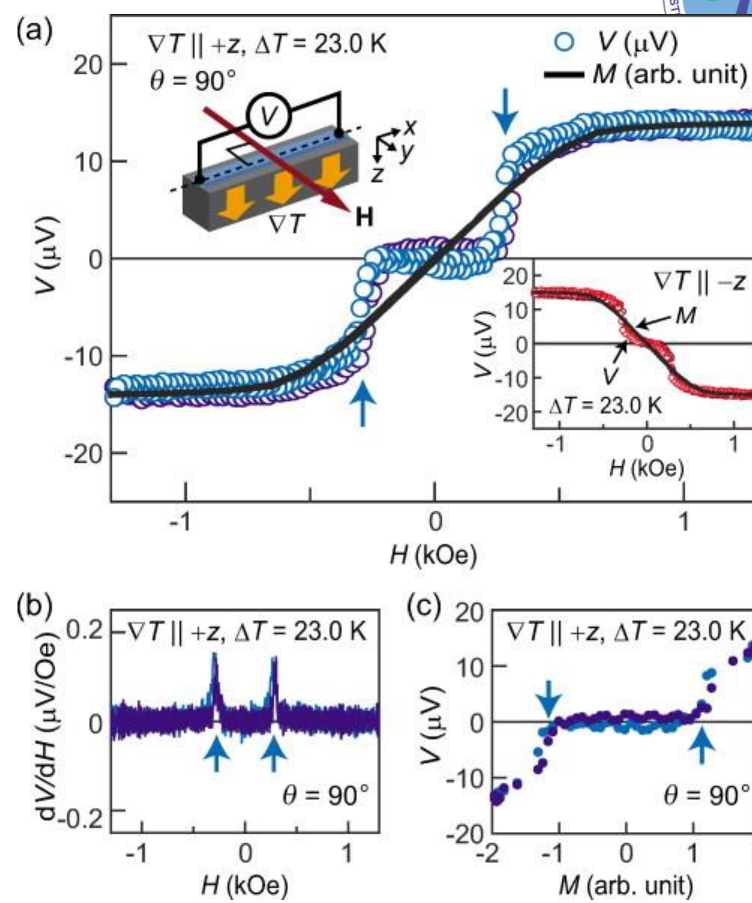

(a) Comparison between the H dependence of V at ΔT = 23.0 K in the YIG/Pt system and the magnetization M curve of the YIG. During the V measurements, ∇T was applied along the +z direction [the −z direction for the inset to (a)] and H was applied along the...

Uchida et al, APL 97, 172505 (2010)

Thermoelectric effect:

The thermoelectric effect is the direct conversion of temperature differences to electric voltage and vice-versa.

Seebeck effect (1821):

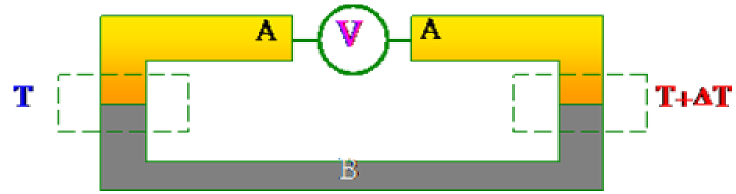

$\Delta T \rightarrow V$

Peltier effect (1823):

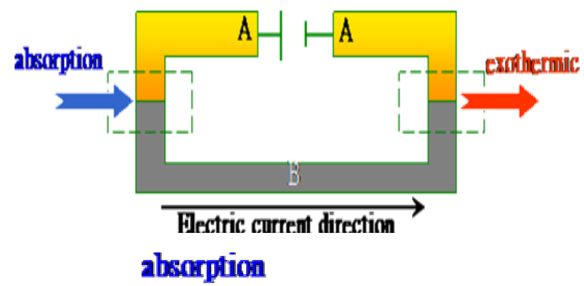

$I \rightarrow Q$

Thomson effect (1851):

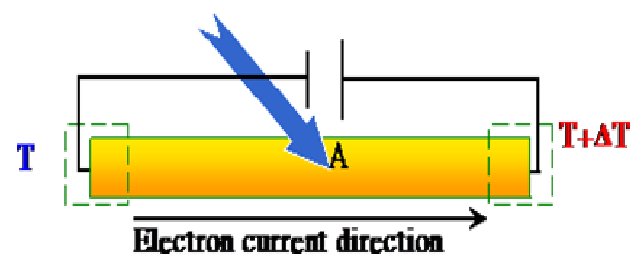

$I + \Delta T \rightarrow Q$

Nernst effect：

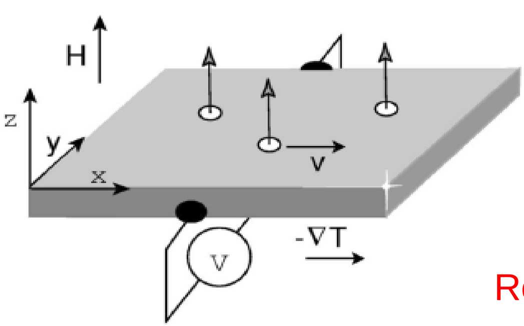

When a sample is subjected to a magnetic field and a temperature gradient normal (perpendicular) to each other, an electric field will be induced normal to both.

Ref: http://web.nchu.edu.tw/~lschang/Thermoelectric.htm

Mystery 1:
Transmission of Spin Current in Metal and Insulator

Over macroscopic distance (mm's >> spin diffusion length) without dissipation ?

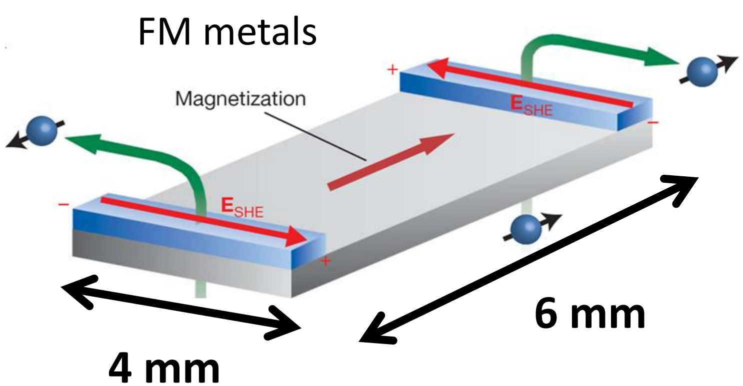

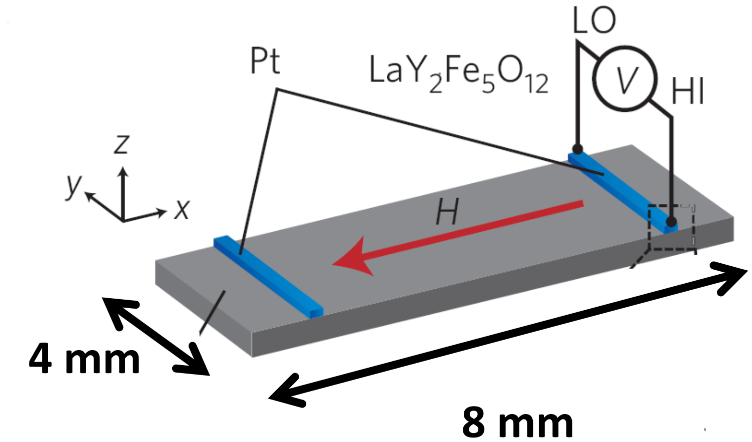

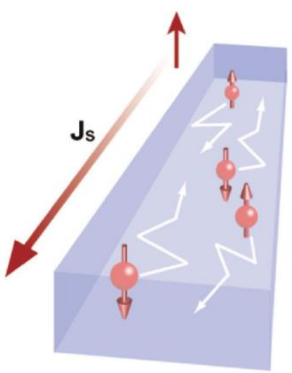

Conduction-electron spin current

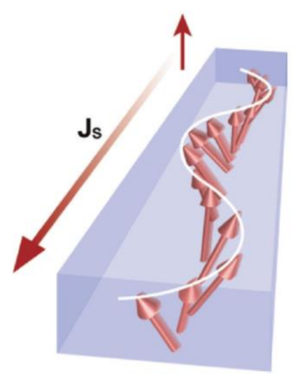

Spin-wave spin current

Resolution: Transmission of spin currents by magnons (spin waves) in either FM metals or FM insulators

Uchida *et al*., Nature **455**, 778 (2008); Nature Mater. **9**,894 (2010), Kajiwara *et al*., Nature 464, 262 (2010)

Mystery 2:
Spin Seebeck effect in broken FM semiconductor

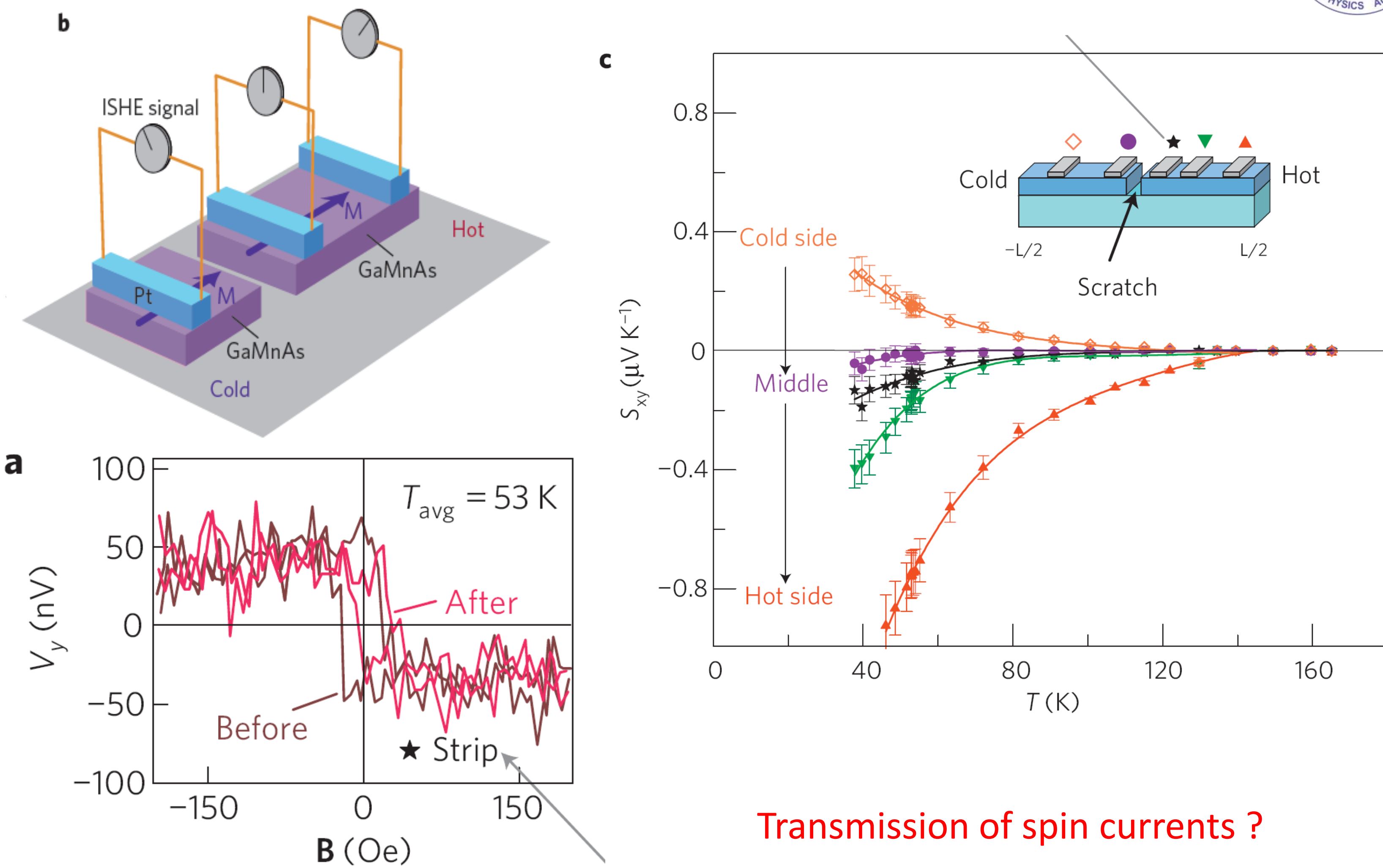

Transmission of spin currents ?

Jaworski *et al.*, Nature Materials **9**, 898 (2010)

Intrinsic Caloritronic effects (not substrate dominated) ?

Intrinsic spin Seebeck effect ?

Intrinsic spin-dependent thermal transport ?

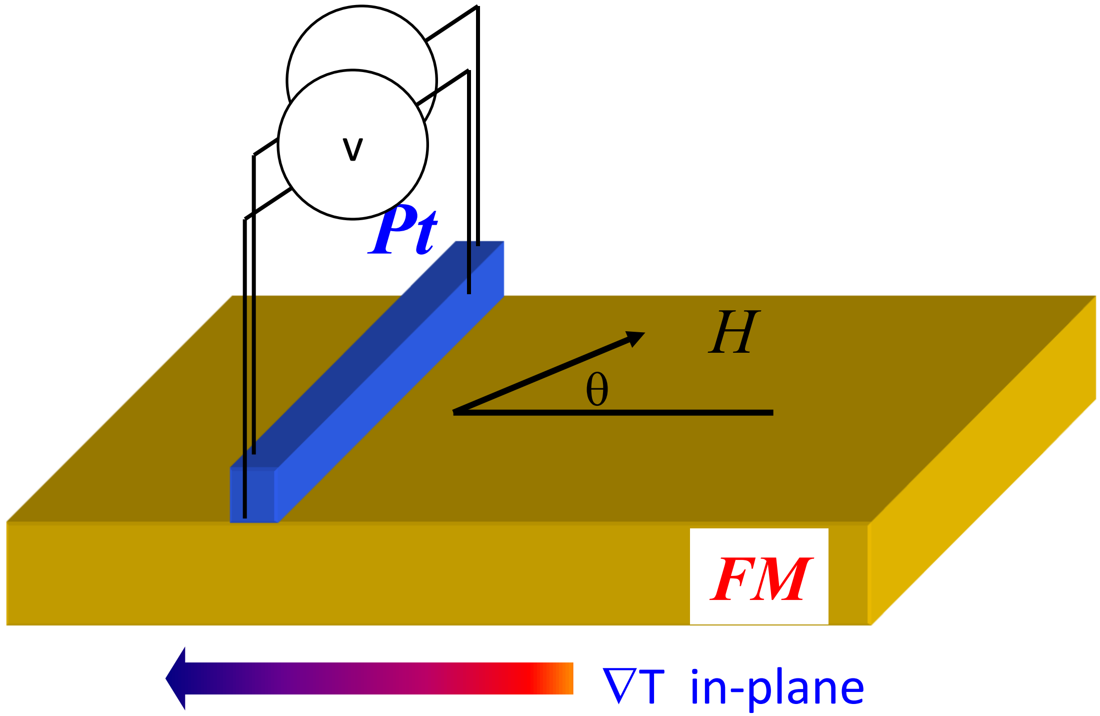

Huang, Wang, Lee, Kwo, and CLC,

"Intrinsic spin-dependent thermal transport," PRL **107**, 216604 (2011).

Spin-Dependent Thermal Transport

Longitudinal thermal voltage V_x

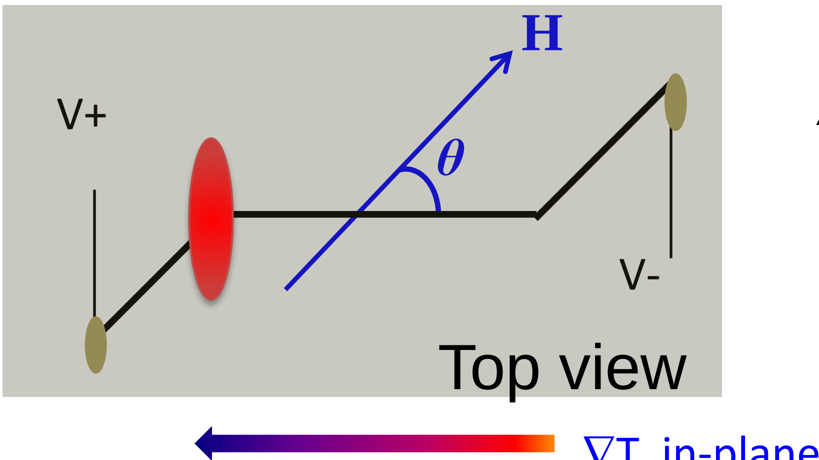

Transverse thermal voltage V_y

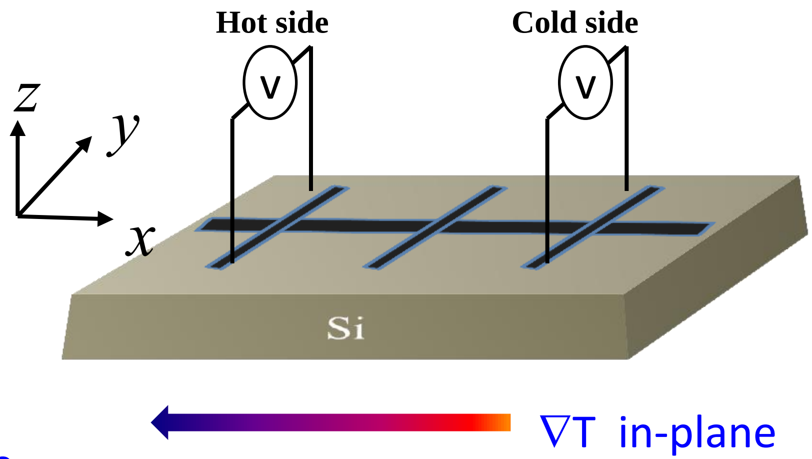

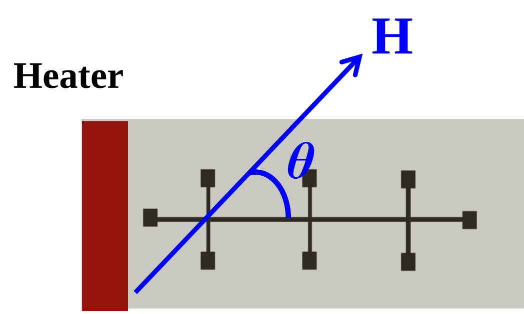

Patterned Py wire on Si substrate

Width: 50-100 μm, Thickness: 20-300 nm

Length: 5 mm   Heater power: 1W

$$V_{th} = V_o + \Delta V_{th}(H,\theta)$$

Angular and Field dependence of $\Delta V_{th}(H,\theta)$?

Consistent, Robust, but Strange $\Delta V_{th}(H,\theta)$ Results

Asymmetric in H

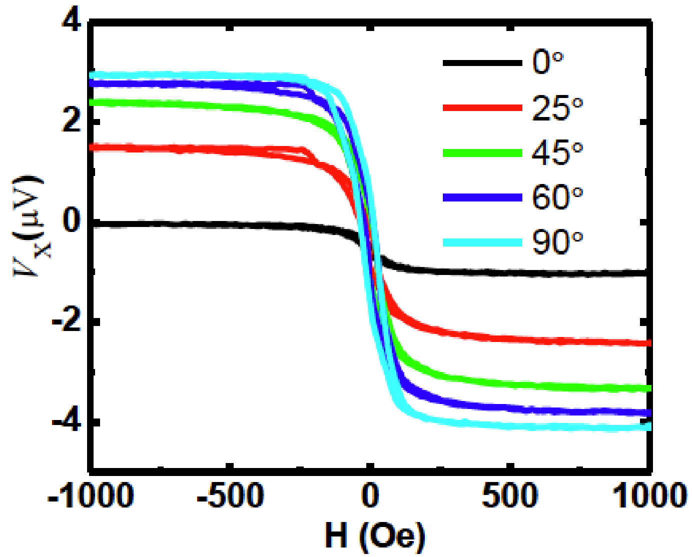

$\Delta V \propto \sin\theta$

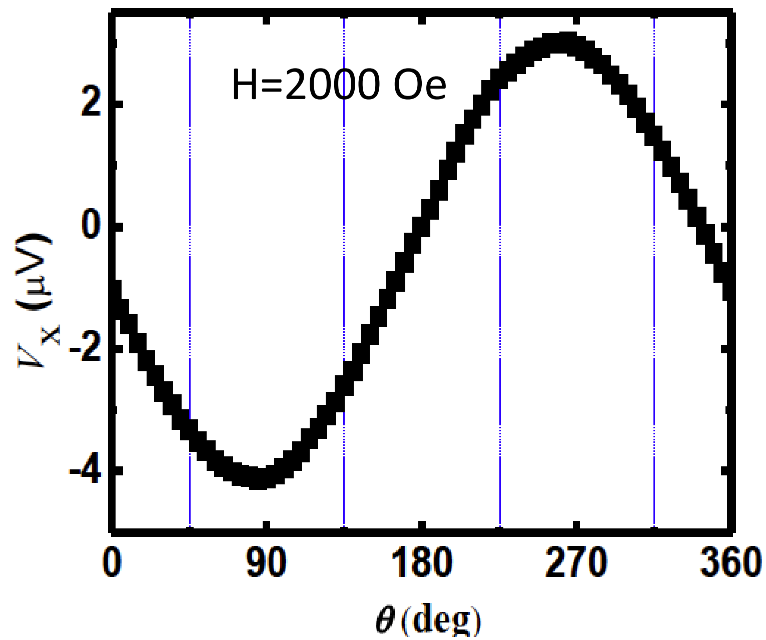

But this is physically impossible !

e.g., ***opposite*** signals at θ = 90° and θ = 270° .

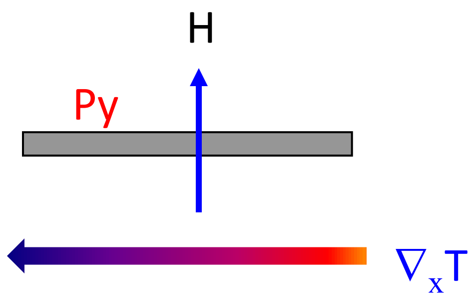

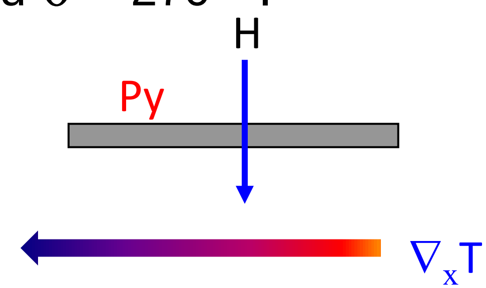

Reversed ∇T, *Same ΔV* !!

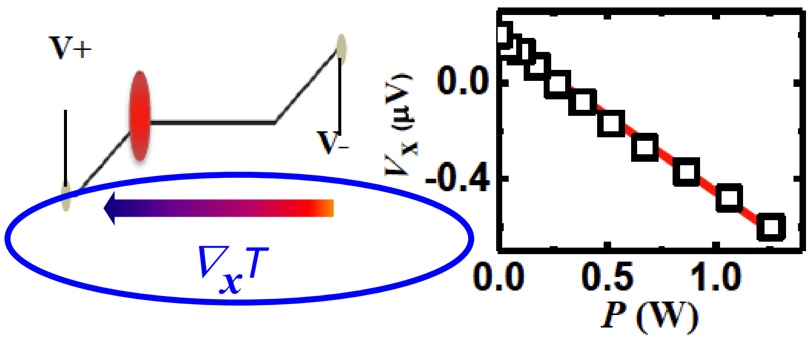

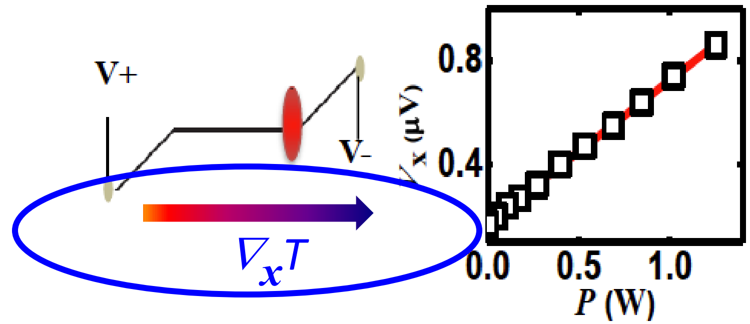

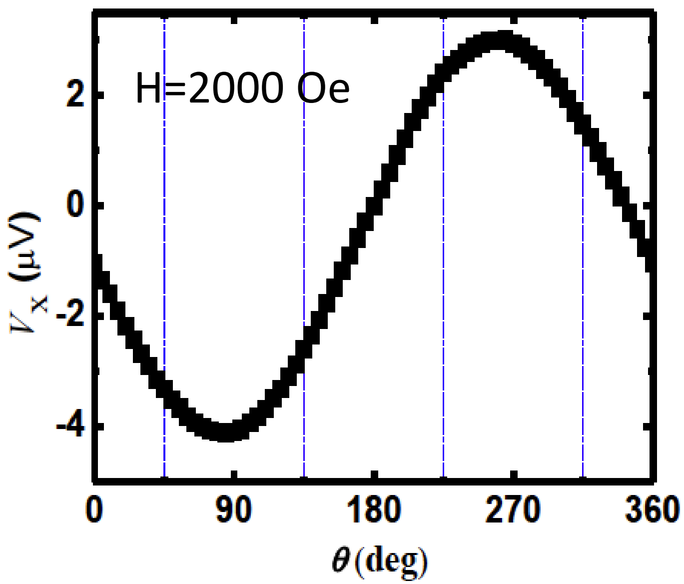

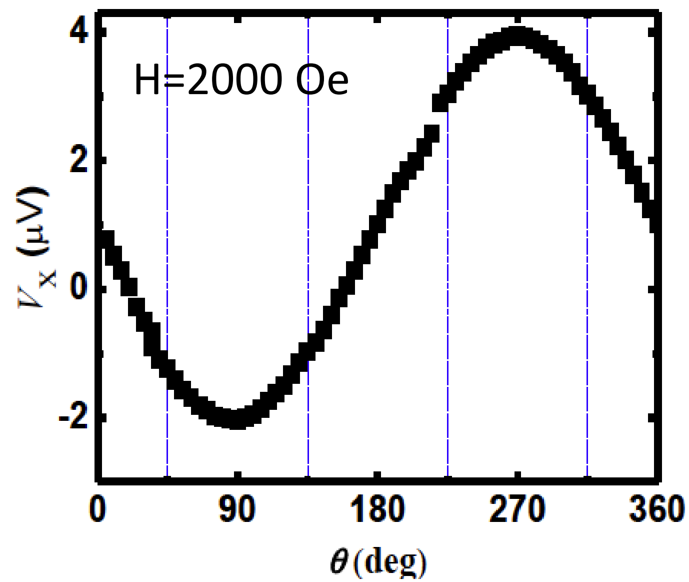

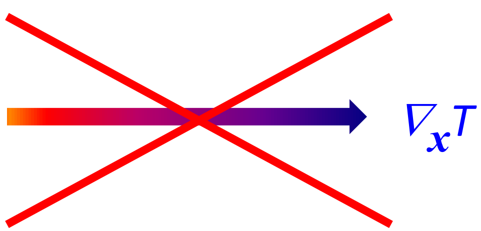

Effective ∇T is not in-plane !

Out-of-plane $\nabla_z T$!!

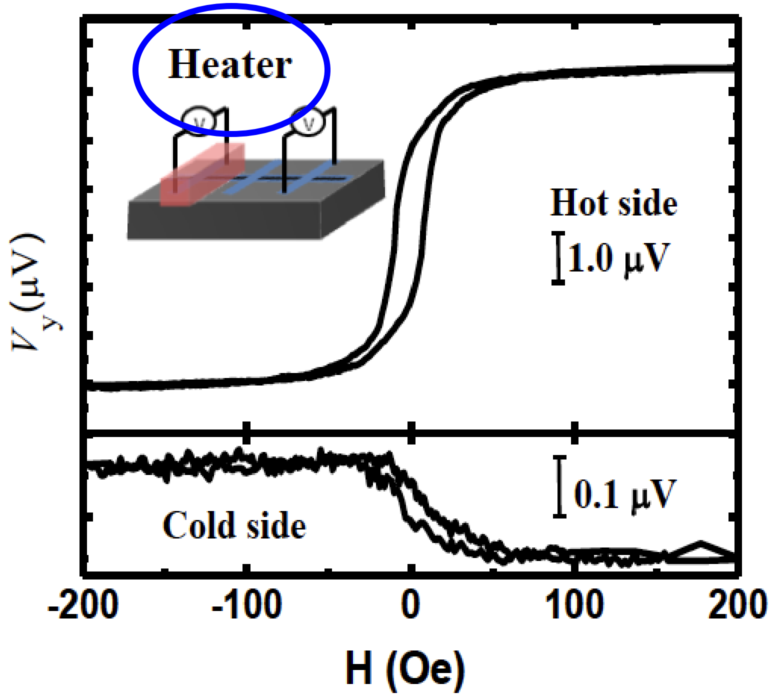

Sign change

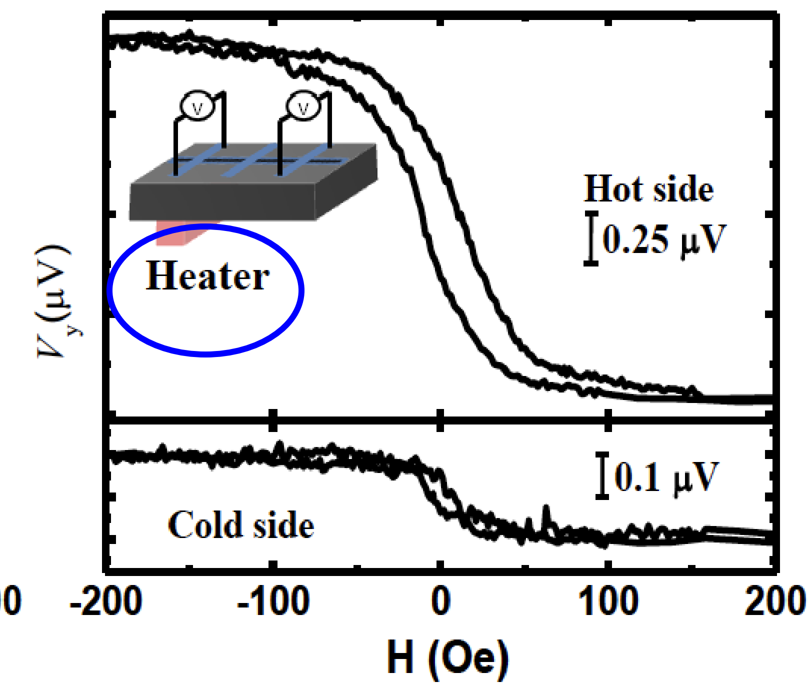

No sign change

This is **anomalous Nernst effect** with perpendicular $\nabla_z T$!!

$\nabla_z T \odot$

(Top view)

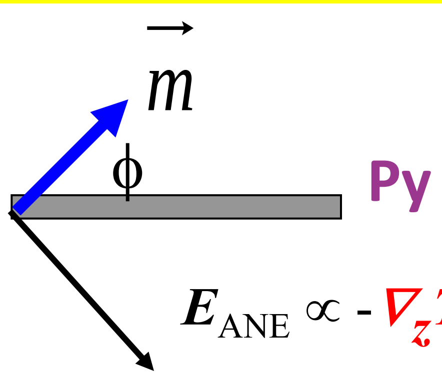

$E_{ANE} \propto -\nabla_z T \times \vec{m}$

$$E_{ANE} \propto -\nabla_z T \times \vec{m}$$

Projection along Py wire direction: $\sin\phi$

Only $\nabla_z T$!!

Uniform Heating from substrate

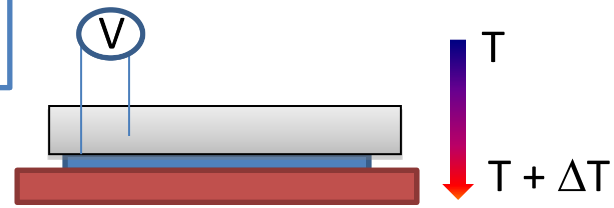

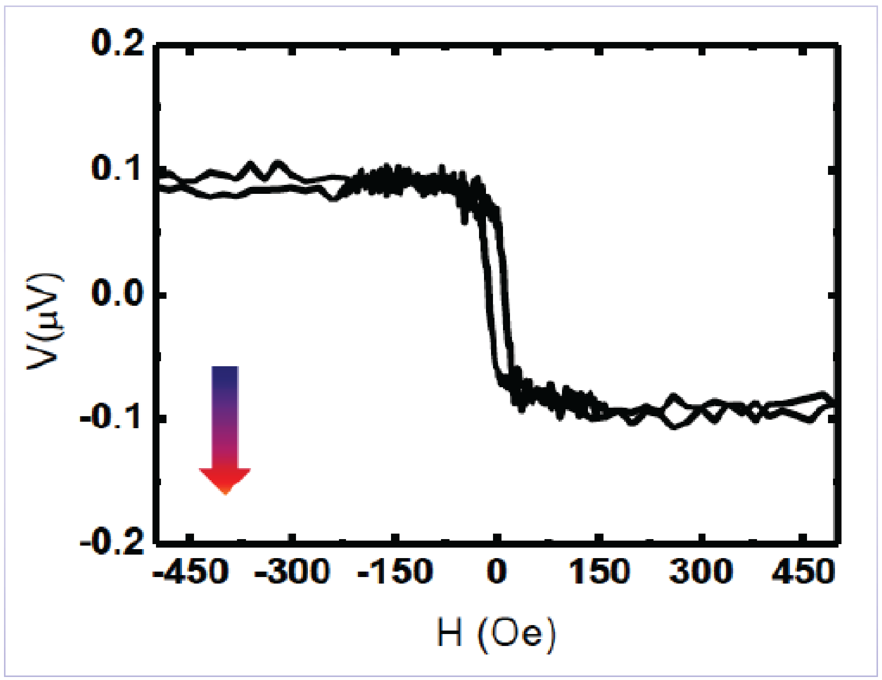

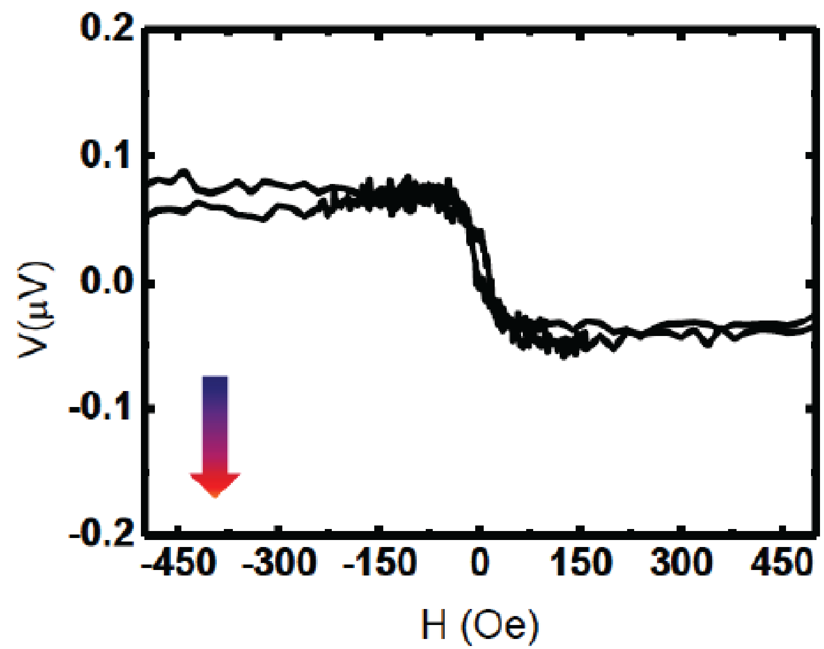

Same ANE sign everywhere with similar magnitude

Thin film on substrate: in-plane and out-of-plane gradient

Anomalous Nernst effect: sensitive detector of ΔT_z and $\nabla_z T$

$$\boldsymbol{E}_{\mathrm{ANE}} \propto \nabla_z T \times \boldsymbol{m}$$

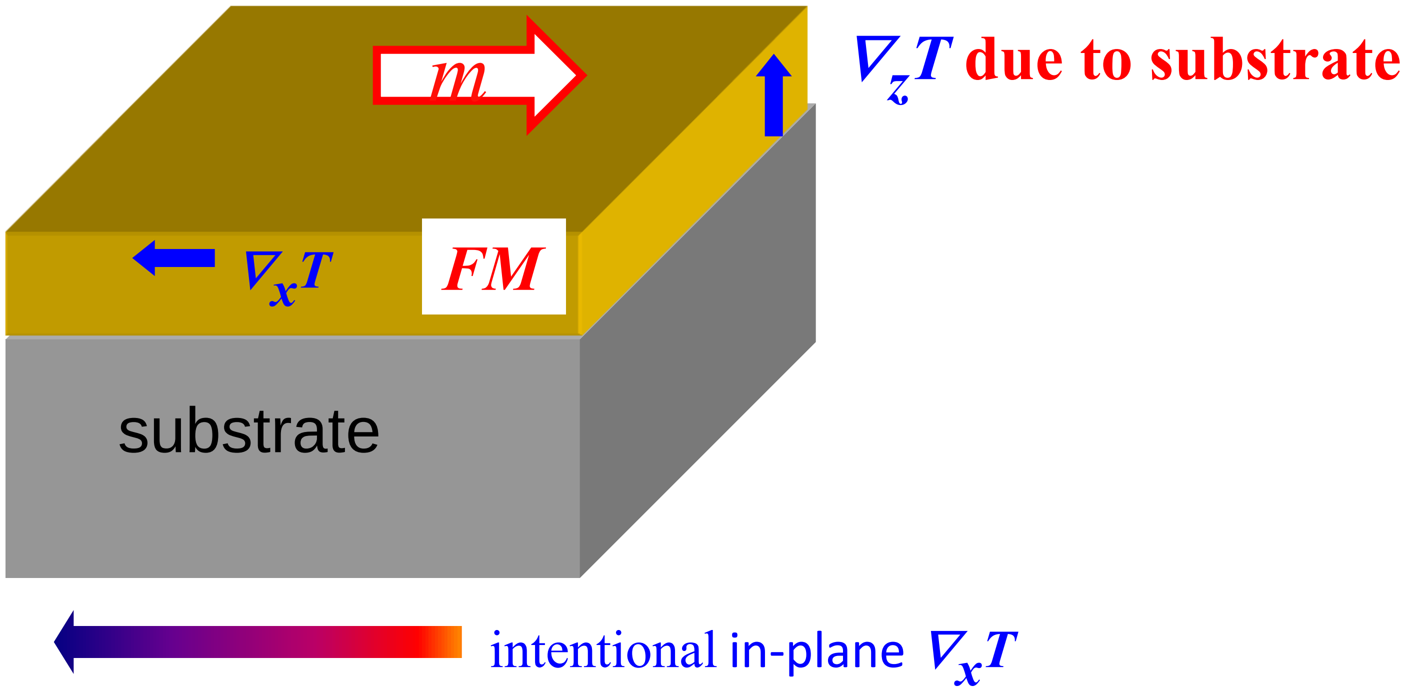

Entanglement of ANE (due to $\nabla_z T$) and SSE (due to $\nabla_x T$)

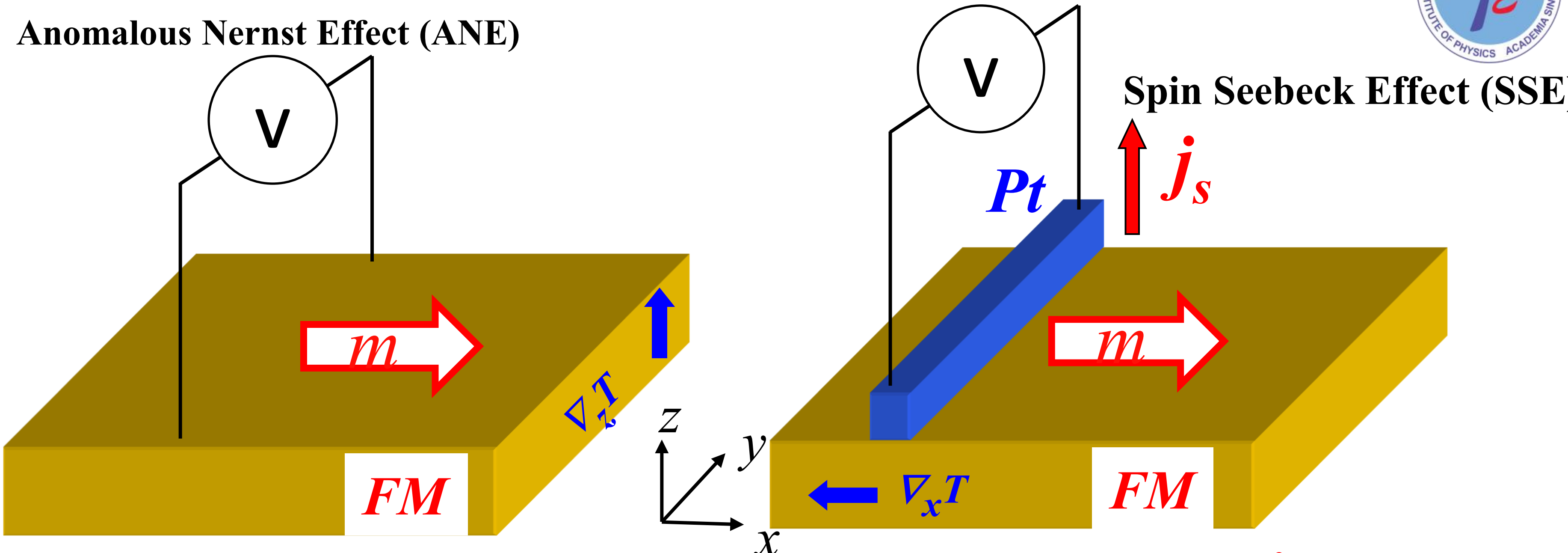

$\boldsymbol{E}_{\mathrm{ANE}} \propto \nabla_z T \times \boldsymbol{m}$

Both along y

$(\boldsymbol{E}_{\mathrm{SSE}})_{\mathrm{Pt}} \propto \boldsymbol{j}_s \times \boldsymbol{m}$

V_{ANE} and $(V_{\mathrm{SSE}})_{\mathrm{Pt}}$ **additive**, both are asymmetric in ***m (or H)***

$(V_{\mathrm{SSE}})_{\mathrm{Pt}} > V_{\mathrm{ANE}}$, one concludes SSE

If V_{ANE} unknown, $(V_{\mathrm{SSE}})_{\mathrm{Pt}}$ uncertain

If $(V_{\mathrm{SSE}})_{\mathrm{Pt}} < V_{\mathrm{ANE}}$, Any SSE ??

Can we eliminate ANE (due to $\nabla_z T$) ?

SSE in FM Metal

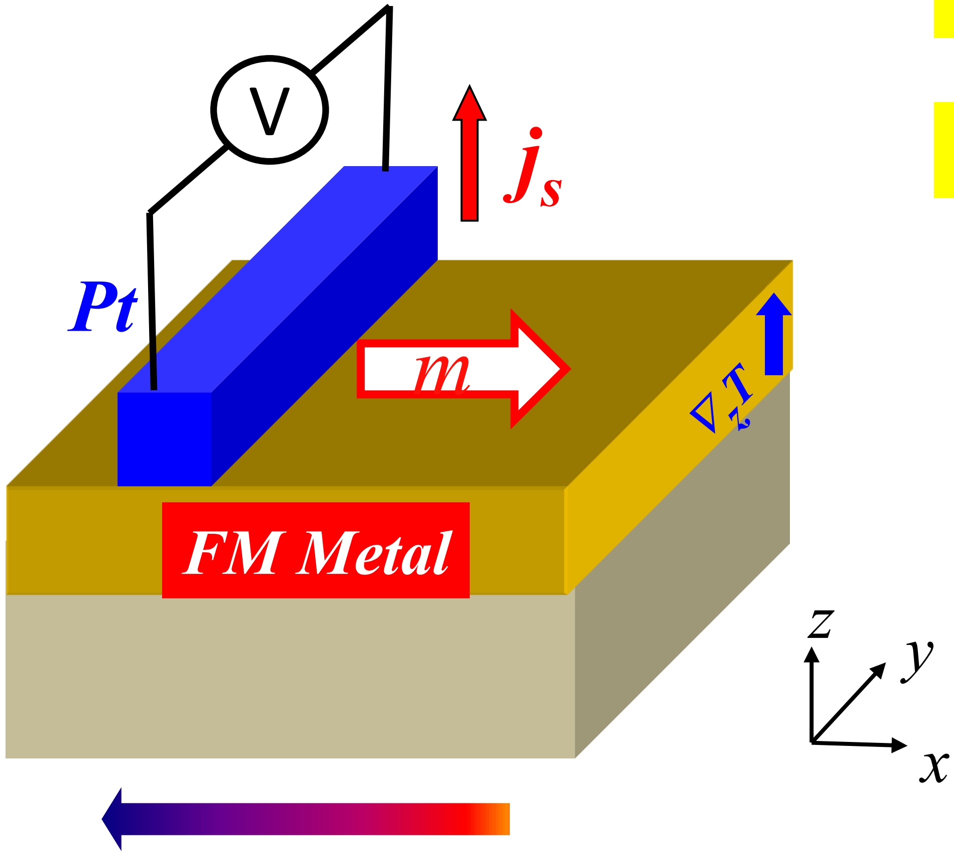

intentional in-plane $\nabla_x T$

SSE + ANE

- **Pt shorts out ANE**
- **Thermally matched substrate**

(Both have been claimed)

Does thin Pt layer short out ANE ?

Spin diffusion length of Pt ~ 5 nm

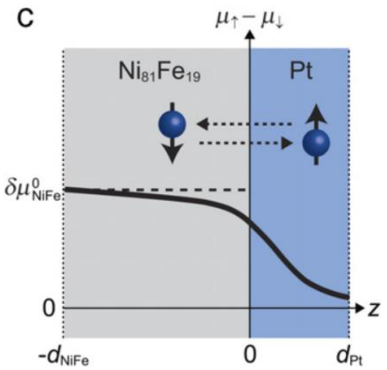

Pt layer shorts out ANE claimed in SSE studies.

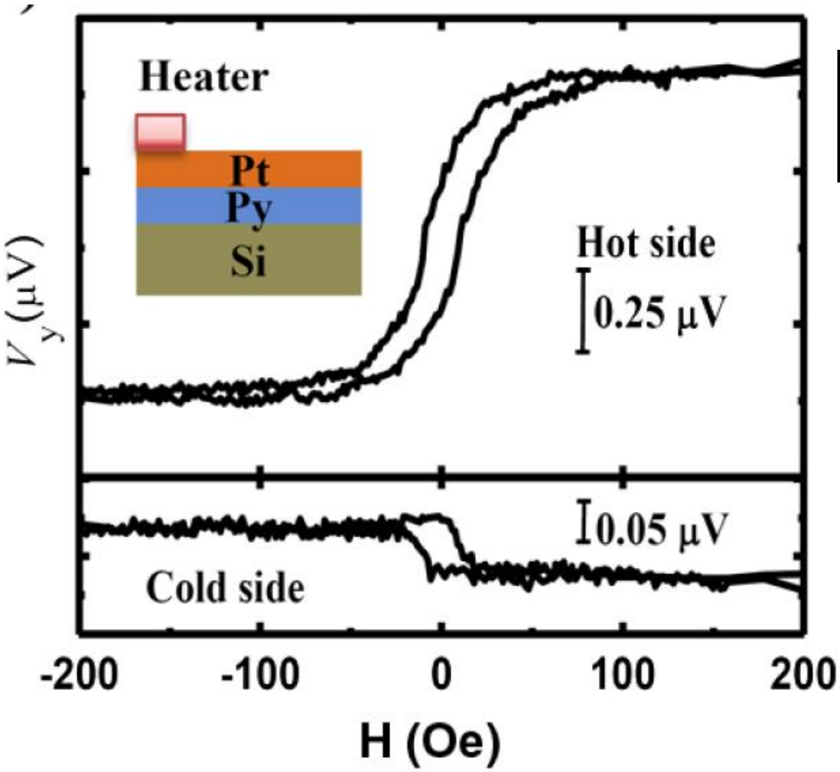

continuous
Pt 10 nm

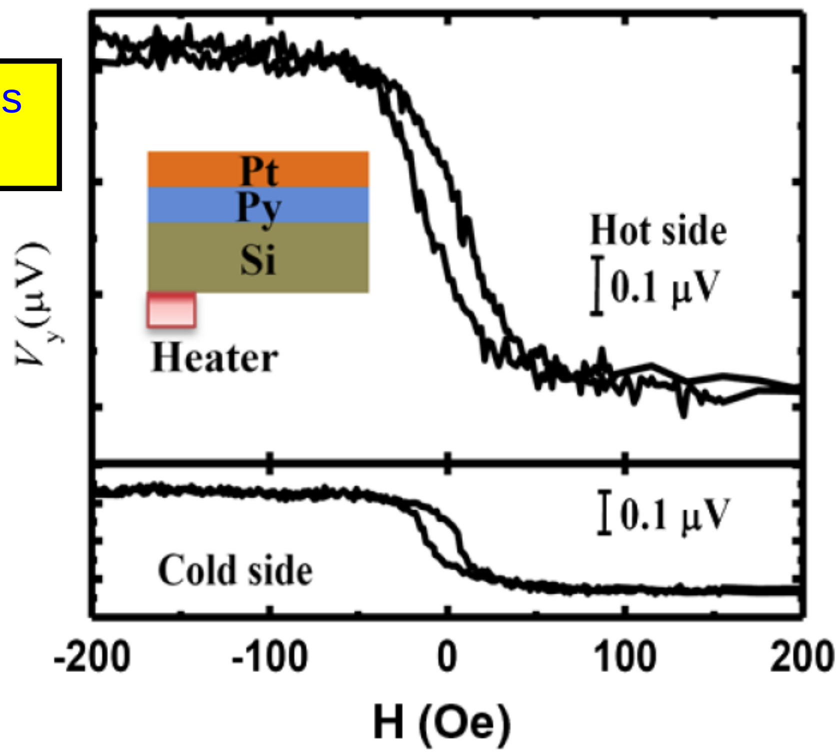

Thin Pt layer reduces, but does not eliminate ANE.

Py on different substrates

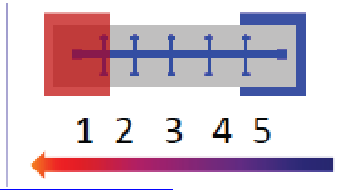

ANE and $\nabla_z T$ in every case

κ(Py)/κ(MgO) ~0.5
Py 50 nm
Heater on top of 1

κ(Py)/κ(GaAs) ~0.54
Py 50 nm
Heater on top of 1

κ(Py)/κ(Glass) ~30
Py 190 nm
Heater on top of 1

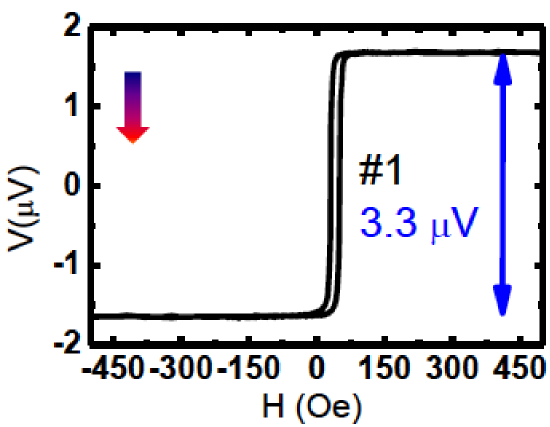

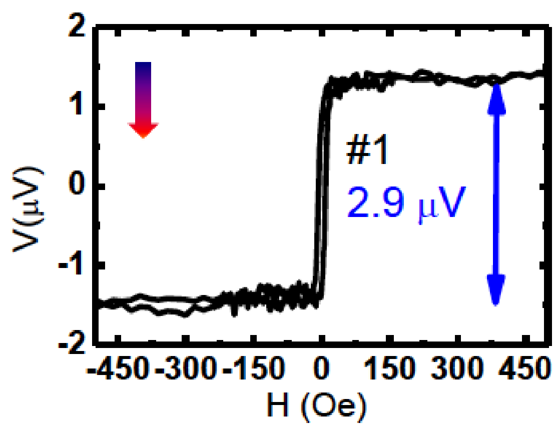

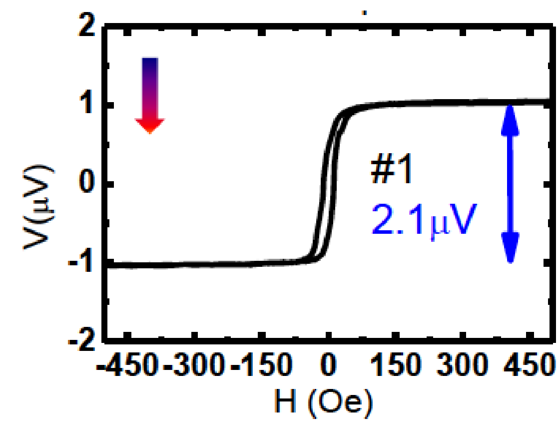

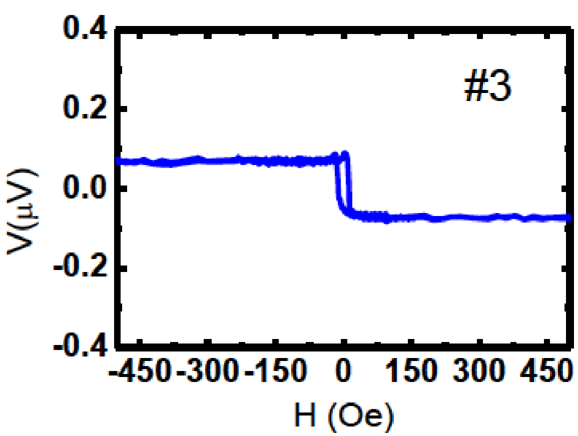

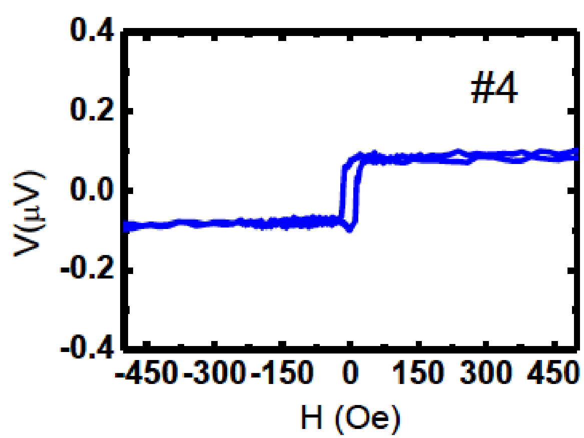

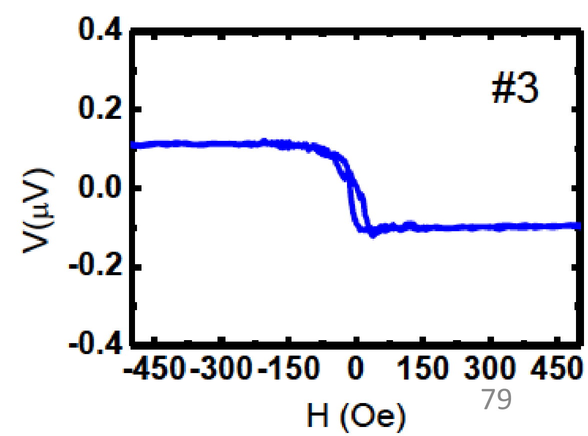

FM on different substrates

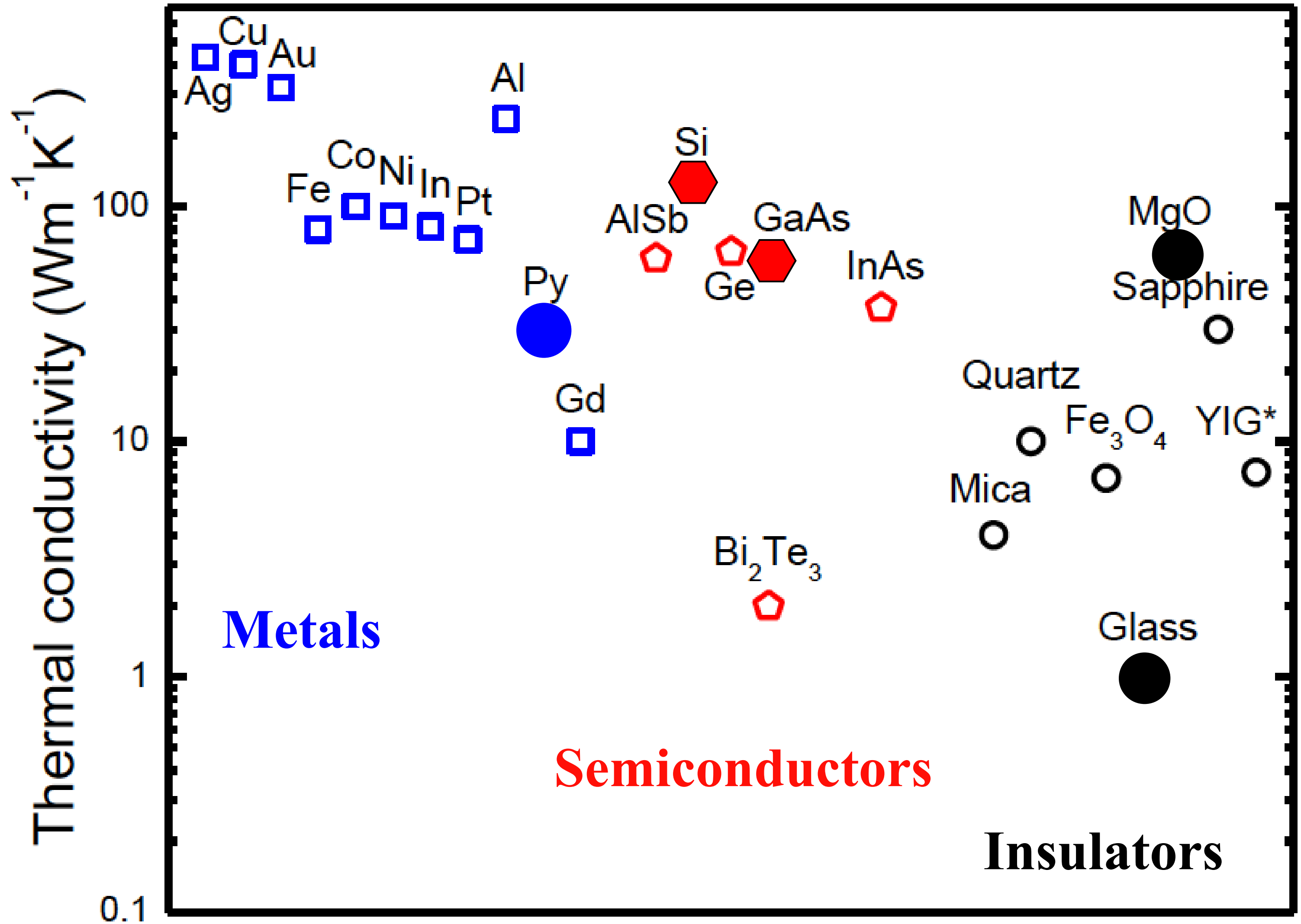

Out-of-plane $\nabla_z T$ exists in all substrates

Intrinsic spin-dependent **Longitudinal** thermal transport in **substrate-free** samples

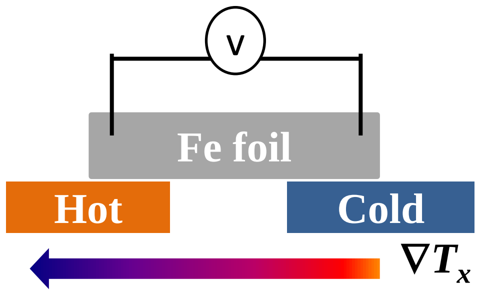

Symmetric in H !

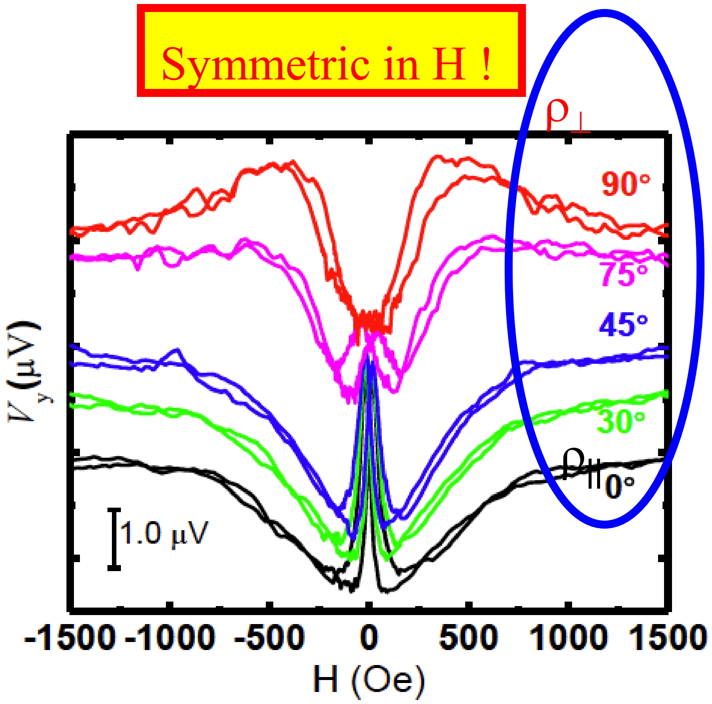

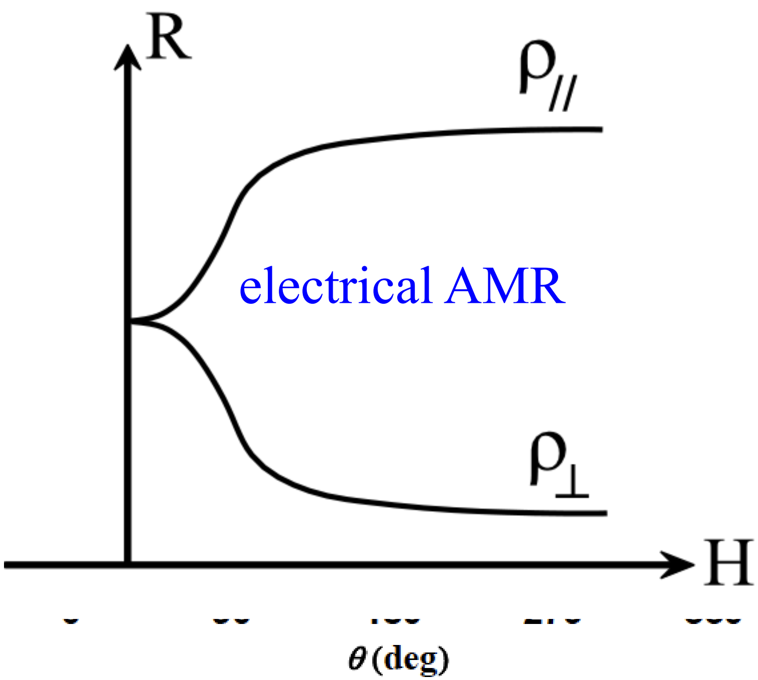

Similar field sensitivity as AMR

$\rho_\perp > \rho_{||}$ opposite to electrical AMR due to Wiedemann-Franz Law

S.D. Bader *et al*. (1991)

Intrinsic spin-dependent **Longitudinal** thermal transport in **substrate-free** samples

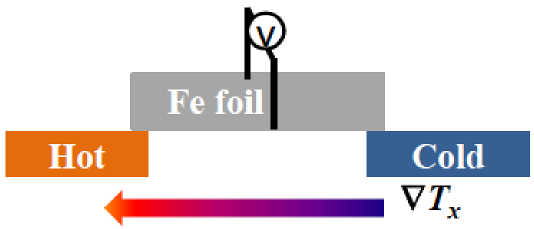

Symmetric in H !

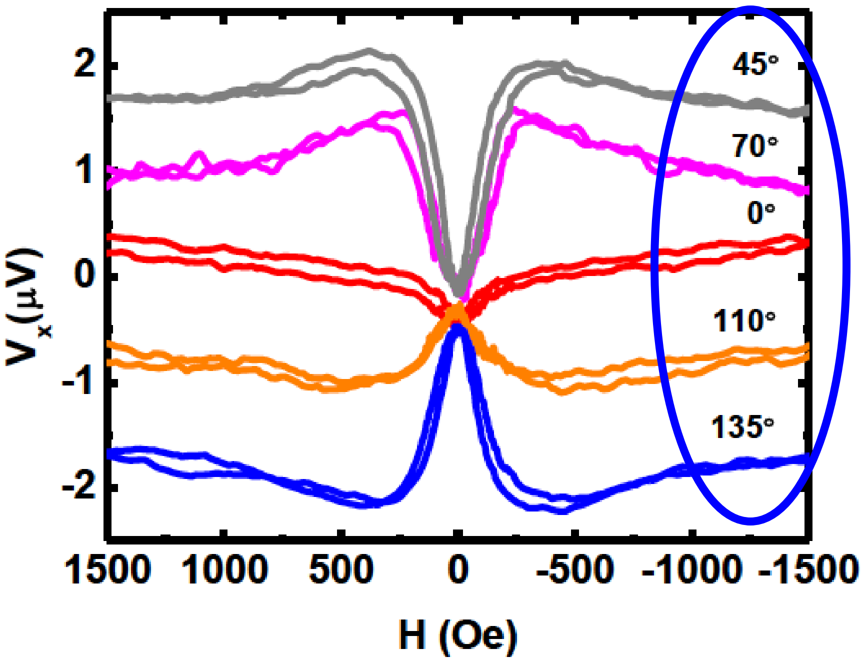

Planar Nernst Effect: sin2θ

Intrinsic spin caloritronic properties with in-plane $\nabla_x T$

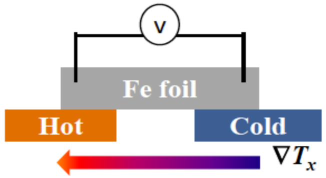

Longitudinal voltage: thermal AMR

$V_{th} = V_{th\perp} + (V_{th\perp} - V_{th||})\cos^2\theta_M$

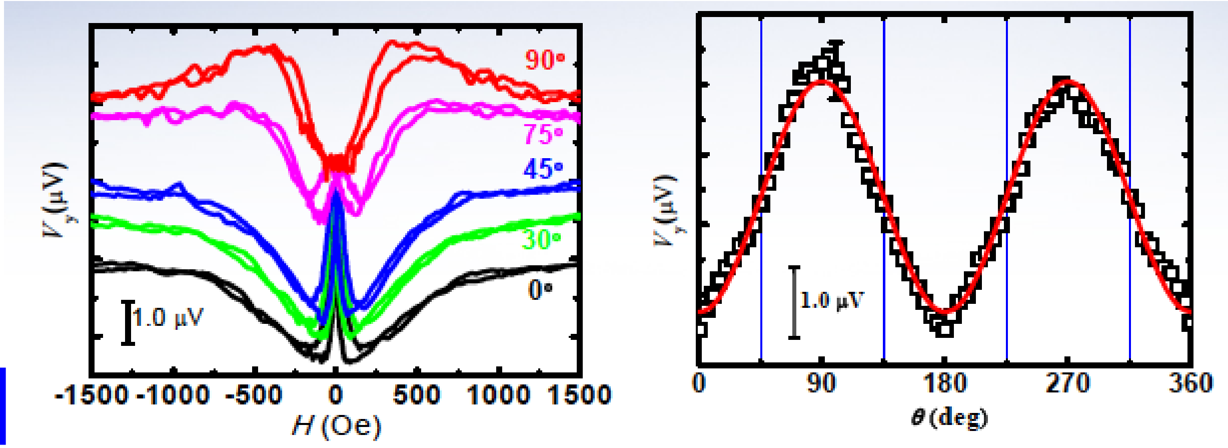

Symmetric in H !

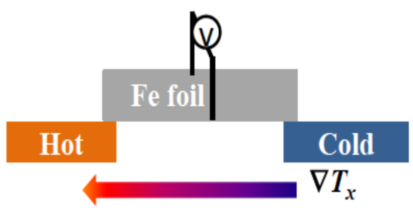

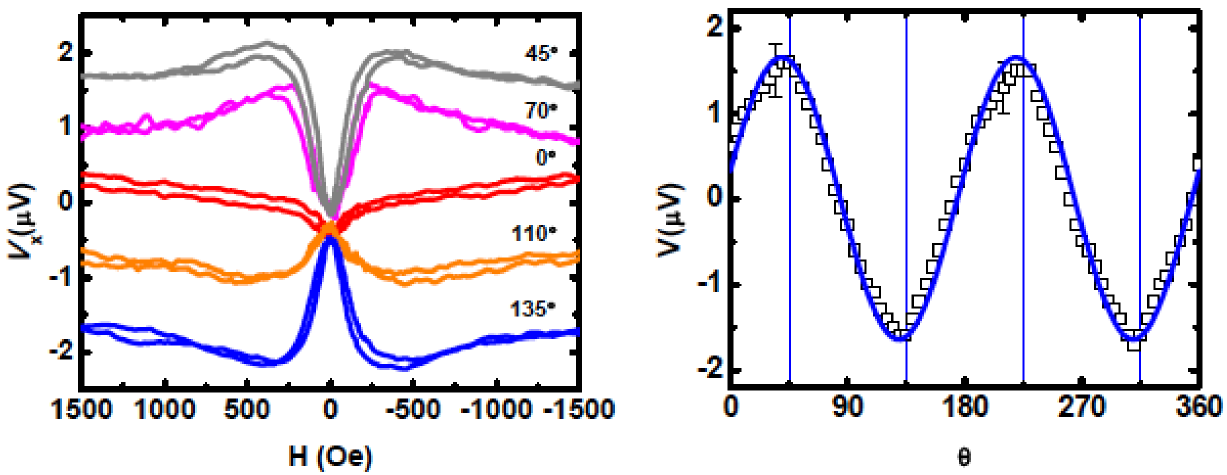

Transverse voltage: Planar Nernst effect

$\sin 2\theta_M$

Necessary Signatures of FM film with in-plane $\nabla_x T$

Summary

1. Thin film/substrate, in-plane ($\nabla_x T$) and perpendicular ($\nabla_z T$)

Spin Seebeck effect ($\nabla_x T$) with Pt

Anomalous Nernst effect ($\nabla_z T$) with or without Pt

2. V_{ANE} and $(V_{SSE})_{Pt}$ are additive

If V_{ANE} unknown, $(V_{SSE})_{Pt}$ uncertain

Intrinsic spin Seebeck effect ?

3. ANE: excellent detector of $\nabla_z T$ and ΔT_z

4. Intrinsic spin caloritronics with in-plane $\nabla_x T$ in Fe foils

Thermal AMR ($cos^2\theta$) Planar Nernst ($sin2\theta$)

Necessary conditions for in-plane $\nabla_x T$ only

Summary

Spintronics has involved

- Magnetic materials, metallic multilayers, tunnel junctions, magnetic semiconductors, and (hopefully) room temperature half metal.
- Spin dependent electron transport, spin imbalance induced charge accumulation and relaxation, which transforms into the concept of pure spin current.
- Static and dynamic properties of magnetic nanostructures.

Seebeck spin tunneling

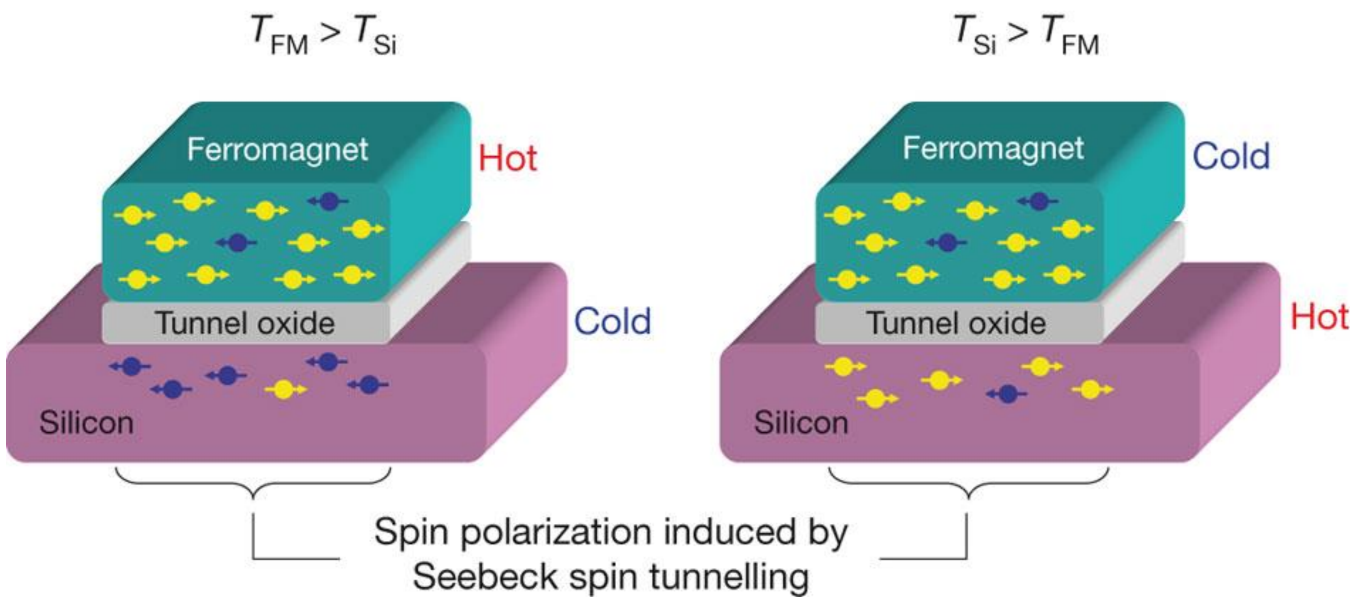

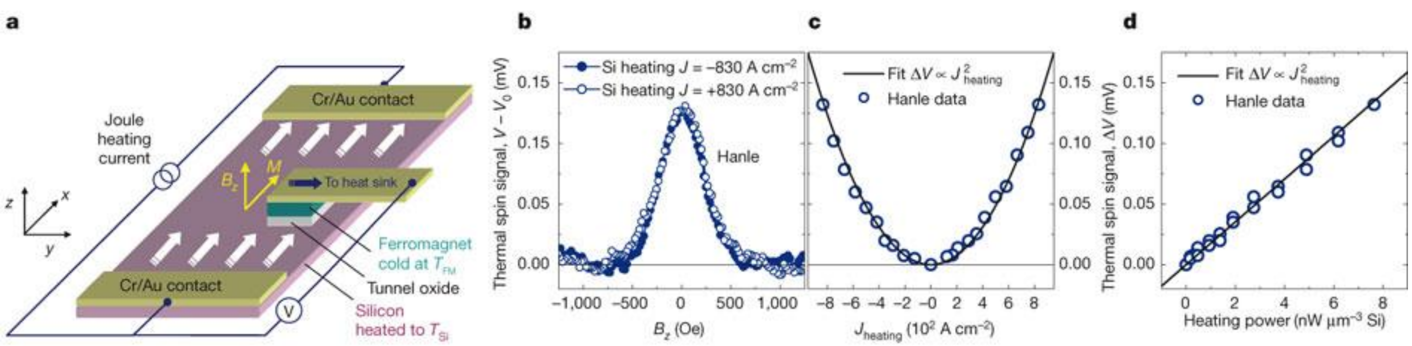

J-CL Breton *et al. Nature* **475**, 82 (2011) doi:10.1038/nature10224

Laser heating induced Spin Currents and Magnetothermal effect

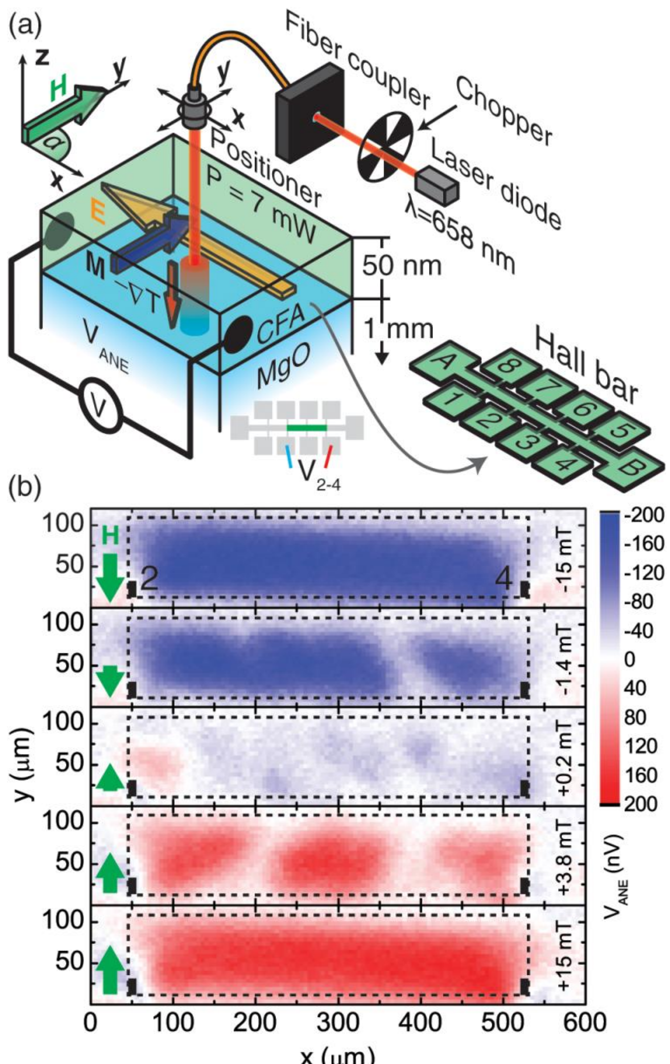

(a) The scannable laser beam generates a local temperature gradient ∇T normal to the ferromagnetic thin film plane. The dc voltage V_{ANE} which arises due to the anomalous Nernst effect depends on the local magnetization ***M*** at the position (*x*, *y*) of the laser beam. All investigated samples are patterned into 80 μm wide and 900 μm long Hall bars with contacts labeled as sketched. (b) V_{ANE} determined between contacts 2 and 4 as a function of the laser-spot position (*x*, *y*) and the external magnetic field magnitude $\mu_0 H$ in a 50 nm thick Co_2FeAl (CFA) film.

Weiler *et al.* PRL **108**, 106602 (2012)